Wind Resource Assessment in Complex Terrain: Validation and Comparison of Two Computational Fluid Dynamics Models

Master's Thesis

Faculty of Science
University of Bern

presented by

Regina Maria Daus

2015

Supervisor:

Prof. Dr. Olivia Romppainen-Martius
Institute for Geography, University of Bern and Oeschger Centre for Climate Change Research, University of Bern

Advisors:

Dr. Saskia Bourgeois Head of Wind Energy Group, Meteotest, Bern
Dr. Paul Froidevaux, Wind Energy Group, Meteotest, Bern

Abstract

Before a wind park is constructed, a site with high mean annual wind speeds in hub height has to be found. To analyse the wind resources at a potential wind park site the three-dimensional wind field has to be simulated. This task can easily be fulfilled in flat and homogeneous terrain like at offshore sites or in flat coastal regions. In countries where there is a lack of such sites, mountain peaks are the best location for wind turbines. In this inhomogeneous and sloped terrain computational fluid dynamics models that solve the Reynolds averaged Navier-Stokes equations are preferably used to simulate wind fields. These models are designed to deal with flow structures like recirculation or separation in complex terrain. To save computation time a steady state assumption is made which can cause simulation errors in complex terrain because the real flow is assumed to be highly unsteady. Very steep slopes and forested areas cause additional problems.

To address these problems computational fluid dynamics models are continuously improved. Additionally, increasing computer power allowed for finer and finer mesh resolution in the last years. This created a need for ongoing validation of the models that are used for wind resource predictions in complex topography. WindSim and Meteodyn WT are two commercial computational fluid dynamics models that both have been frequently used in terrain of medium and high complexity in the last years. They differ in some important properties like mesh generation as well as turbulence, stability and forest parametrisation and therefore produce substantial differences in predicting annual mean wind, turbulence intensity and energy yield. They have not been compared and validated systematically in very complex topography. This master thesis aims in closing this gap by comparing Meteodyn and WindSim for three potential wind park sites in the Alps and Jura in Switzerland by using mast and SODAR measurements.

Both models have proven to cope with the complex topography in general while single model runs produced non-negligible errors in predicting the mean annual wind speed. The differences between the models concerning this variable resulted for one of the wind parks in discrepancies of planning relevancy for the annual energy yield predictions. The simulation results of turbulence intensity are not comparable between the models. Modelling results showed bigger errors compared to measurements for the annual mean turbulence intensity than for the annual mean wind speed.

Additional field measurements would be valuable for validating modelling results of steep forested slopes and downstream of mountains. Alternatively the models could be compared by using the data of the frequently used boundary layer flow experiments of Bolund and Askervein Hill although these sites have a much less complex topography than can be found in the case studies of this thesis.

Contents

1. Introduction

1.1 Motivation

During the process of planning a wind park, it is necessary to assess the wind resources of a potential wind park site. This is a crucial step, as it answers the question whether the future wind park will be economically viable (Landberg *et al.* , 2003). Measuring and modelling the environmental wind field are the first steps in this process. If the wind field is known, it is possible to design an optimal wind park layout in terms of number and positioning of the turbines inside the wind park. If they are located too close to each other, lowered wind speed and enhanced turbulence intensity in the wake downstream of the wind turbines would lower total energy yield of the wind park (Emeis, 2013).
The growing demand for wind energy and the lack of offshore sites in some countries (e.g. Switzerland) brought attention to mountainous regions with high wind speeds. Draxl and Mayr (2011) showed that wind parks in the Alps might produce even more energy per year and wind turbine than offshore parks.
In the complex topography of the Alps different wind field investigation methods are needed than in flat and homogeneous terrain. As the flow separates from the surface in steep topography, models which integrate the linearised Navier-Stokes equations to save computation time (e.g. WA^{s}P described in Troen (1990)) are not appropriate (Barthelmie *et al.* , 2007, 2009; González *et al.* , 2014). In complex terrain, wind fields should preferably be simulated with computational fluid dynamics (CFD) models instead (Brower, 2012). These models consider flow separation and recirculation processes. Most CFD models can be divided in two groups. The first are Large Eddy Simulations (LES) which resolve the bigger turbulent eddies and parametrise smaller ones on a temporal and spatial scale. The second solve the Reynolds averaged Navier-Stokes (RANS) equations which seek a steady state solution. Sanderse *et al.* (2011) and Probst and Cárdenas (2010) state that RANS CFD models are the first choice when it comes to wind resource assessment in complex terrain because they are less computational time intensive than LES CFD models. As RANS CFD models (in the following only called CFD models) do not capture the temporal evolution of the flow, the validation of model results is necessary especially when unsteady flow structures like vortices in recirculation zones are expected.

1.2 State of Research

There exists a huge variety of CFD models with different boundary conditions, numerical schemes, turbulence parametrisations and wake models. Politis *et al.* (2012) found wide differences for wind field predictions of wind park sites in different CFD models. In the Bolund Experiment, field data was used for a blind comparison of 57 microscale flow models including

40 RANS CFD models, eight linear models, and five LES CFD models (Bechmann *et al.* , 2011). In general, the group of RANS CFD models performed best in predicting speed-up factors (ratio of the simulated wind speed to a reference wind speed) and turbulent kinetic energy. However, they still showed non-negligible errors. These results show the necessity of ongoing validation and comparison of CFD models to find a model that is best suited for applications in mountainous topography.

Although CFD models are designed for the use in complex terrain there are not many studies that show as steep slopes and big height differences as can be found at potential wind park sites in Switzerland. The sparsely vegetated test site in Bechmann *et al.* (2011) can hardly be called complex as it is only several meters higher than the surrounding terrain. In Eidsvik (2005), Castro *et al.* (2008), Leroy (1999) and Gobbi and Dorweiler (2012) the performance of CFD models is validated with the help of measurements at and around a hill that is approximately $100m$ higher than its environment. In an environment with comparable complexity El Kasmi and Masson (2010) evaluate the performance of two CFD turbulence closure schemes. Politis *et al.* (2012) compare simulations of two CFD solvers in a large wind park in Spain. Although located in much more complex terrain than the before mentioned test sites, the surrounding environment of this wind park, it cannot compete with the complexity of sites in the Alps or Jura.

Studies for the CFD model WindSim performed in more complex environments are described in Cattin *et al.* (2002), Bourgeois *et al.* (2009) and Bourgeois *et al.* (2010). A comparison to results of other CFD models in the same area would be interesting.

1.3 Objectives

In this master thesis the commercial CFD models Meteodyn WT (thereafter called Meteodyn; (meteodyn.com)) and WindSim (windsim.com), which are designed for wind field simulation, energy yield estimation and wind park layout optimization are compared and validated for different potential wind park sites in Switzerland. Three sites with very complex topography have been analysed with WindSim by the Bernese company Meteotest between 2008 and 2014. For all case studies long-term corrected short-term field measurements of $10min$ mean wind speed (v) and wind direction (dd) for at least two different locations at different heights is available. One of the data sets can be used as the climatology to scale the model and the second to validate the results of the simulation ("cross checking"). This procedure allows to address the first question:

1. Is Meteodyn capable of reproducing mean long-term corrected measurements of the wind speed (v_{mean})?

Furthermore the three dimensional fields of the mean annual wind speed (v_{moy}) and the mean annual turbulence intensity (TI_{moy}) as well as the expected mean annual energy yield ($Prod_{moy}$) at the position of the wind turbines are simulated in Meteodyn and compared to WindSim results. To decide which model is more suitable for wind assessment in complex terrain the following questions are addressed:

2. Which model does better reproduce v_{mean}?

3. How large are the differences in the simulated two-dimensional fields of v_{moy} and TI_{moy} between Meteodyn and WindSim?

4. How large are the differences in $Prod_{moy}$ between Meteodyn and WindSim and If so, how can they be explained?

As the models use different turbulence closure schemes it is expected that the two-dimensional fields of the mentioned variables will differ especially in regions of complex topography like steep slopes or in valleys.
In a further step, the thermal stability adjustment and the forest model of Meteodyn are tested. This raises two additional questions:

5. Do the simulation results improve if the stability adjustment option in Meteodyn is used?

6. Do the simulation results improve if the forest model of Meteodyn is used?

2. The Physics of CFD Models

2.1 Reynolds Averaged Navier-Stokes Equations

CFD models integrate the mass conservation equation and RANS equations (Eq. 2.1 and 2.2) for each cell of a three-dimensional grid by using site independent vertical wind profiles at the inlet boundaries of the computational domain. In Equation 2.1 and 2.2 incompressibility, and steady state conditions are assumed and the Coriolis force is neglected.

$$\frac{\partial U_i}{\partial x_i} = 0 \tag{2.1}$$

$$U_j \frac{\partial U_i}{\partial x_j} = -\frac{1}{\rho}\frac{\partial P}{\partial x_i} + \frac{\partial}{\partial x_j}\left(\nu\left(\frac{\partial U_i}{\partial x_j} + \frac{\partial U_j}{\partial x_i}\right) - \left(\overline{u_i' u_j'}\right)\right) \tag{2.2}$$

U_i, U_j, u_i' and u_j' for $i = j = 1, 2, 3$ denote the means and fluctuations of the wind components in x, y and z-direction of a Cartesian coordinate framework. P, ν and ρ are the Reynolds averaged mean pressure, kinematic viscosity and density of the air. Reynolds averaging encompasses time averaging after the decomposition of each variable into a temporal mean an a fluctuating component (Stull, 1988). As the typical computational domain in wind resource assessment has a side length in the order of kilometre and the smallest turbulent eddies have a size in the order of millimetre, resolving them would be not affordable in terms of computation time. Therefore the turbulent fluxes of Equation 2.2 have to be parametrized in CFD models (Launder and Spalding, 1974).

To save CPU-resources often a turbulence scheme based on a hypothesis formulated by Boussinesq in 1877 is used to model turbulent fluxes. He stated that turbulence depends on the derivative of the mean velocity and the turbulent viscosity (ν_T) (Sanderse *et al.* , 2011) (Eq. 2.3). The latter describes the viscosity of turbulently flowing fluids. It is much higher than the molecular viscosity in laminarly flowing fluids due to the enhanced friction between moving molecules.

$$\overline{u_i' u_j'} = -\nu_T \left(\frac{\partial U_i}{\partial x_j}\right) \tag{2.3}$$

The so called k-ϵ turbulence closure models use this approach. In WindSim and Meteodyn two variants of the model are used. They are discussed in Section 2.2 and 2.3 respectively.

2.2 One Equation $k - \epsilon$ Turbulence Closure

Based on Arritt (1987) and Yamada (1983), Hurley (1997) introduced additional to Equations 2.1 and 2.2 one more conservation equation to model ν_T in Equation 2.3 Meteodyn (2012). As one additional equation is introduced to calculate the turbulent fluxes in Equation 2.3, this approach is named one equation $k - \epsilon$ turbulence closure scheme. The additional equation is the conservation equation for turbulent kinetic energy (k), which is dependent on the reduction

of k by dissipation (ϵ). It reads

$$\frac{\partial}{\partial x_i}(U_i k) = \frac{\partial}{\partial x_i}\left(\frac{\nu_T}{\sigma_k}\frac{\partial k}{\partial x_i}\right) + P_k - \epsilon \quad \text{with} \quad \begin{cases} P_k = \nu_T\left(\frac{\partial U_i}{\partial x_j} + \frac{\partial U_j}{\partial x_i}\right)\frac{\partial U_j}{\partial x_j} \\ \nu_T = \sqrt{k}L_T \end{cases} \tag{2.4}$$

where P_k gives the production of k. The expression for ϵ can be found in Meteodyn (2012). The first term on the right hand and left hand side of the equation are the divergence and the molecular diffusion of k respectively. σ_k is an empirical constant and L_T is the turbulent length scale which is dependent on the flux Richardson number. Its equation is described in Meteodyn (2012). It gives the size of the eddies in a turbulent flow, which transport most of the energy (Wyngaard, 2010). The one equation $k-\epsilon$ turbulence closure scheme has proven to produce fairly good results for the flow over a hill (Hurley, 1997). It is used in Meteodyn.

2.3 Two Equation $k-\epsilon$ Turbulence Closure

Jones and Launder (1972) propose a two equation turbulence closure scheme also based on the Boussinesq hypothesis to close the system of Equations 2.1-2.2. Different to the one equation turbulence closure scheme in Meteodyn (2012), they assume that ν_T in Equation 2.3 can be expressed by an empirical constant c_ν, k and ϵ (Eq. 2.5).

$$\nu_T = \frac{c_\mu k^2}{\epsilon} \tag{2.5}$$

To calculate k and ϵ two new conservations equations are solved (Eq. 2.6 and 2.7).

$$\frac{\partial}{\partial x_i}(U_i k) = \frac{\partial}{\partial x_i}\left(\frac{\nu_T}{\sigma_k}\frac{\partial k}{\partial x_i}\right) + P_k - \epsilon \quad \text{with} \quad P_k = \frac{\nu_T}{2}\left(\frac{\partial U_i}{\partial x_j}\frac{\partial U_j}{\partial x_i}\right)^2 \tag{2.6}$$

$$\frac{\partial}{\partial x_i}(U_i \epsilon) = \frac{\partial}{\partial x_i}\left(\frac{\nu_T}{\sigma_\epsilon}\frac{\partial \epsilon}{\partial x_i}\right) + c_{\epsilon 1}\frac{\epsilon}{k}P_k - c_{\epsilon 2}\frac{\epsilon^2}{k} \tag{2.7}$$

The first term at the left hand side of Equation 2.7 is the advection of ϵ. The terms at the right hand side are the turbulent diffusion, the production and the destruction of ϵ. c_ν, $c_{\epsilon 1}$, $c_{\epsilon 1}$, σ_k and σ_ϵ are empirical constants that have been adjusted by many authors to different flow types and environments. Some examples are Yakhot *et al.* (1992), Yakhot and Orszag (1986) and Gravdahl (1998). For the constants as cited in Launder and Spalding (1974) Equations 2.6 and 2.7 are called the "standard $k-\epsilon$ model". It is used in many CFD models and can also be chosen in WindSim. Discussions of this model and comparisons to others can be found in Bechmann *et al.* (2011), Sumner *et al.* (2010), Eidsvik (2005), Stathopoulos (2002), Kim and Patel (2000) and Hurley (1997).

While consuming less computation time, two equation $k-\epsilon$ models have been proven to nearly produce the same results for mean variables as the full second order turbulence closure scheme in Equations 2.1 and 2.2 (Ayotte, 2008).

3. WindSim and Meteodyn

The CFD models Meteodyn and WindSim are used to simulate the wind conditions of three potential wind park sites in Switzerland. Although the models are designed for the same tasks they differ in some aspects. The most important model settings of Meteodyn and WindSim are described in this chapter. Table 3.1 gives an overview of the differences between the models which are discussed. For more details about the features in this table and explanations about the equations see the accordingly named sections.

Tab. 3.1: Summary of differences between Meteodyn and WindSim discussed in Chapter 3. Details about the listed features are given in the accordingly named sections.

Feature	**Meteodyn**	**WindSim**
Computational Mesh	one mesh per wind direction sector	one mesh for all directions
Turbulence Closure	one equation $k-\epsilon$ closure	standard two equation $k-\epsilon$ closure
Wake Model		
wind speed reduction:	Park/Jensen model (Katic *et al.* , 1986) with	
	$c_k = 0.5TI_{rotor}$	$c_k = 0.5 \ln\left(\frac{z_{hub}}{z_0}\right)^{-1}$
additional turbulence:	complete Frandsen model (Frandsen, 2007)	
Inlet Wind Profiles		
$z < z_s$	$u = \left(\ln\left(\frac{z}{z_0}\right) - \Psi\left(\frac{z}{L}\right)\right)\frac{u_*}{\kappa}$	$u = \frac{u_*}{\kappa}\ln\left(\frac{z}{z_0}\right)$
$z > z_s$	$u = u_g - (u_g - u_{zs})\frac{\ln\left(\frac{z_h}{z}\right)}{\ln\left(\frac{z_h}{z_s}\right)}$	$u = 10ms^{-1}$
Atmospheric Stability	stability classes 0-9	adjustment option not used
Forest Model	activated for several runs	model not activated

3.1 Physical Equations

The version of the RANS equations (Eq. 2.1 and 2.2), which is implemented in Meteodyn neglects viscous forces. The turbulent fluxes are modelled by the one equation $k-\epsilon$ turbulence closure scheme which is described in Section 2.2 (Meteodyn, 2012).
In WindSim the full set of Equations 2.1 and 2.2 is solved in the model. For this thesis the standard (two equation) $k-\epsilon$ turbulence closure scheme of Launder and Spalding (1974) is chosen.

3.2 Computational Domain

In Meteodyn the computational domain is restricted by the parameter *radius* which is set by the user. The extents of the input land surface roughness and topography data sets are given by circles with $1.2 radius\sqrt{2.0} + 2000m$ and $1.2 radius\sqrt{2.0}$, respectively. For each wind

direction sector a square of side length $2.0 radius 1.2\sqrt{2.0}$ is defined, which gives the extent of the computational mesh. A square with side length $0.7 radius$ describes the maximum possible extent of the two-dimensional output data sets. The computational mesh is generated in two steps. First, the surface grid is built as a two-dimensional Cartesian grid, which gets finer near the position of wind turbines, measurement locations, and inside the "mapping area" (in this case the area of the planned wind park). This grid is expanded towards the upper boundary by getting coarser according to a vertical expansion coefficient defined by the user. The horizontal grid lines follow the terrain heights near the surface. This effect decays towards the upper boundary. Near the surface, the vertical grid lines and the terrain following grid lines in x- and y-direction built spiky, elongated grid cells (trapezoidals). As this could result in computational divergence above steep topography, the user can specify the orthogonality factor. With the help of this factor it can be assured that the vertical grid lines are almost orthogonal to the sloped surface (Meteodyn, 2012, 2015) and the grid cells are rather cubical than trapezoidal.
In WindSim the wind field is first run for the "base area", where the cell size expands by moving away from the centre. The resulting wind profiles are used as the inlet profiles for a nested area with finer resolution ("refinement area"). The cells in the refinement area have a minimum side length of $25m$ in x- and y-direction, which expands up to $100m$ in the base area. The rate of horizontal expansion of the cells is determined by the additive length to resolution ratio. The height distribution factor allows the user to adjust the ratio between the heights of the lowest and topmost cells. In difference to Meteodyn, WindSim only uses one computational mesh for all wind direction sectors. Details about the generation of the computational mesh can be found in WindSim (2013).

3.3 Wake Model

The wake is the region of reduced v and intensified TI in the lee of a wind turbine or any other obstacle (Christiansen and Hasager, 2005). Following this definition, the wake effect is simulated by a model for the wind speed reduction and the added turbulence due to the wind turbines.
In this master thesis, for the former, a modified version of the Park or Jensen model, which was developed by Katic *et al.* (1986) was chosen in Meteodyn. It calculates the wind speed reduction coefficient (c_{wake}) in a conical volume in a distance x downstream of the wind turbine depending on the wake decay coefficient (c_k), the rotor diameter (d_{rotor}) and the turbine thrust coefficient (c_t) (Eq. 3.1).

$$c_{wake} = \frac{u_{downwind}}{u_{upwind}} = 1 - \left(1 - \sqrt{1 - D}\right) \left(\frac{d_{rotor}}{d_{rotor} + 2 c_k x}\right)^2 \quad \text{with} \quad c_k = 0.5 TI_{rotor} \tag{3.1}$$

c_k is dependent on the turbulence intensity at the position of the rotor (TI_{rotor}) of the wind turbine that generates the wake. To calculate the turbulence in the wake the complete Frandsen model of Frandsen (2007) was chosen. It estimates the added TI as a function of c_t, the distance to the wind turbine and D (Meteodyn, 2015)
For the wind speed reduction in WindSim the same model as in Meteodyn is chosen but with $c_k = 0.5 \ln\left(\frac{z_{hub}}{z_0}\right)^{-1}$ in Equation 3.1, where z_{hub} is the hub height of a wind turbine. To calculate the additional turbulence in the wake region the complete Frandsen model of Frandsen (2007) is implemented in WindSim (WindSim, 2013).

3.4 Boundary Conditions

Modelling wind fields in a CFD model involves two steps named "directional computation" and "scaling". They are explained in Section 6.1. In the directional computation, for the incoming vertical wind profiles at the lateral boundaries of the Meteodyn model domain, a logarithmic function based on Monin-Obukhov similarity theory and findings of Dyer and Hicks (1970) are assumed for the surface layer. The height of the surface layer (z_s) is defined as 10% of the ABL height (z_h) (Meteodyn, 2015). The equation for the profiles is given in Table 3.1. The integrated dimensionless shear function (Ψ) varies according to Equation 3.2. L denotes the Obukhov length, which is used in Monin-Obukhov theory to describe turbulence produced by buoyant forces. Its formula is given in Meteodyn (2015). u_* is the friction velocity that is a measure of the shear stress (Stull, 1988).

$$\begin{aligned}
&\text{for } 0 < L < 3000 \quad && \Psi\left(\frac{z}{L}\right) = -5\frac{z}{L} \\
&\text{for } L = 0 && \Psi\left(\frac{z}{L}\right) = 2\ln\left(\frac{1+x}{2}\right) + \ln\left(\frac{1+x^2}{2}\right) - 2\tan^{-1}(x) + \frac{\pi}{2} \quad \text{with} \quad a = \left(1 - 16\frac{z}{L}\right)^{0.25} \\
&\text{for } L > 3000 && \Psi\left(\frac{z}{L}\right) = 0
\end{aligned} \tag{3.2}$$

Above the surface layer Equation 3.3 is used instead, where u_{z_s} is the wind speed at the top of the surface layer.

$$u = u_g - (u_g - u_{zs})\frac{\ln\left(\frac{z_h}{z}\right)}{\ln\left(\frac{z_h}{z_s}\right)} \tag{3.3}$$

Towards the upper boundary the wind speed approaches the geostrophic wind velocity (u_g), which is given by Equation 3.4.

$$\left(\frac{u_g}{u_*}\right)^2 = \left(\ln\left(\frac{z_h}{z_0}\right) - A_2\right)^2 + B_2^2 \tag{3.4}$$

A_2 and B_2 are functions depending on $\frac{z}{L}$. They can be found in Garratt (1999). At ground level, a momentum sink term is implemented in Equations 2.2. It is proportional to z_0 and the thermal stability (Meteodyn, 2012).
In WindSim the inlet vertical wind profile inside the ABL (up to $z = 500m$) is described by the logarithmic wind profile (Tab. 3.1) in the base area. For $z > 500m$ the profile has a constant value of $u = 10ms^{-1}$. At the lower boundary, a wall function is applied to simulate the turbulent flow near the ground (Gravdahl, 1998). This is necessary, because $k - \epsilon$ turbulence closure schemes underestimate the viscous forces near rough surfaces (Launder and Spalding, 1974).

3.5 Atmospheric Stability

As in Meteodyn the conservation equation for heat is not implemented, it is not possible to directly simulate atmospheric stability. To take into account impacts of the thermal stratification on turbulence and vertical wind profiles anyway, the user can alter L and thereby the inlet vertical wind profiles (Tab. 3.1 and Eq. 3.3) with the help of the stability class. Table 3.2 lists

the values of L belonging to each class.

Tab. 3.2: Thermal stability class as implemented in Meteodyn and corresponding values of L.

thermal stability class	**Monin-Obukhov length**	**thermal stratification**
0	-80	very unstable
1	-500	unstable
2	10000	near neutral
3	1500	slightly stable
4	800	stable
5	500	stable
6	300	stable
7	200	stable
8	130	very stable
9	30	very stable

To adjust the model to local atmospheric stability conditions, WindSim also offers the possibility to alter inlet vertical wind profiles by altering L (WindSim, 2013). This feature did not produce good results in former simulations performed by Meteotest so it was not activated for this master thesis.

3.6 Forest Model

In Meteodyn, the height of the forest is calculated as $z_f = c_u z_0$ where c_u is a parameter set by the user. In case that z_f exceeds half of the height of a cell, the forest model is activated for this cell and a momentum sink term is implemented in Equation 2.2. The sink term is proportional to the surface drag coefficient (c_D) which is altered according to a forest density class chosen by the user. The activation of the forest model also results in different formulations for ϵ and $\frac{1}{l}$ in Equations 2.4. For details the reader is referred to Meteodyn (2015).
In WindSim, a forest model is implemented, too. It was decided not to activate it because it did not yield good results in past work of Meteotest.

4. Case Studies

The wind park sites are chosen in a way that an alpine and prealpine site, a site in the Swiss Jura as well as areas of different afforestation are represented. Figure 4.1 shows the approximate locations of the three wind parks.

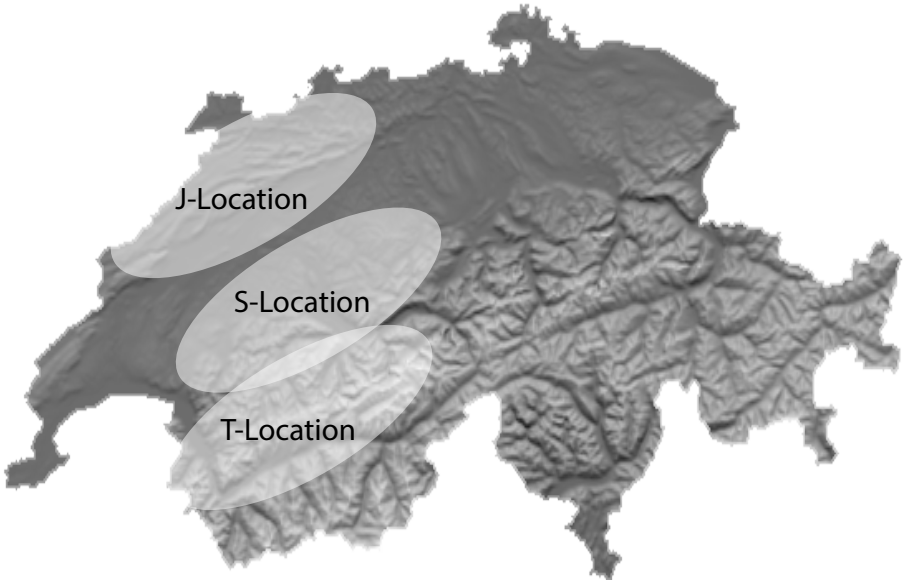

Fig. 4.1: Approximate locations of the three wind park sites on a topographic map of Switzerland.

To classify the complexity of the terrain a modified ruggedness index (RIX) of Bowen and Mortensen (1996) was calculated. It gives the percentage of area with a slope bigger than 18.0° in a radius of $3500m$ around a wind turbine instead of 13.5° as used in the original paper. As the wind parks consist of several wind turbines, which are distributed over an elongated area, RIX is calculated for the joint area of the circles with radius $3500m$ around each wind turbine of the wind park.

Tab. 4.1: RIX, topographical area and terrain height range for each wind park in the base area

wind park	**topographical area**	**RIX (%)**	**terrain height range (m)**
T-Location	Alps	74.4	370–3223
S-Location	Prealps	46.3	437–2702
J-Location	Jura	20.2	427–1603

Table 4.1 gives RIX of the wind parks as well as the topographical area and the range of the terrain height in the base area defined in Tables 4.2, 4.5 and 4.8. In Gobbi and Dorweiler (2012) a site is classified as complex if $RIX > 30\%$.

4.1 T-Location

4.1.1 Site Description

Near [redacted] (Valais, Switzerland) a wind park with six wind turbines is planned. Figure 4.2 shows a satellite image, where the extent of the base and refinement area as defined in the WindSim simulation is indicated by the big and small rectangles, respectively.

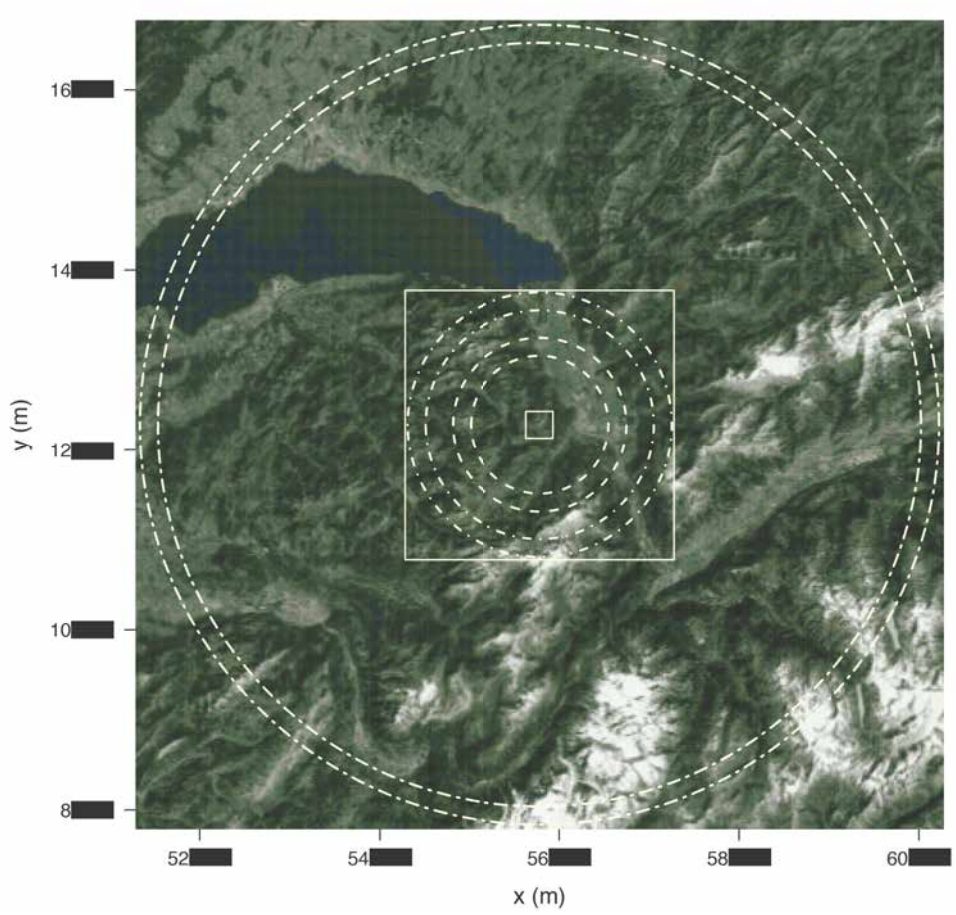

Fig. 4.2: Satellite image of the T-Location site. The small and big rectangles give the extent of the refinement and base area, respectively. The three pairs of circles indicate the size of the topography and roughness data sets in Meteodyn for three different sizes of *radius* as given in Table 4.4 (Google and DigitalGlobe, 2015).

The three pairs of circles show the size of the topography and roughness data sets for three different values of *radius* (compare Tab. 4.4). The formula for the radius of the circles and the extent of the rectangles is given in Table 4.2.

Tab. 4.2: Extent of base and refinement area as defined in WindSim and extent of topography and roughness input data sets, which are considered in Meteodyn for the T-Location wind park in Swiss Grid coordinates. The values for *radius* are given in Table 4.4.

WindSim base area x-range (m) y-range (m)	**WindSim refinement area** x-range (m) y-range (m)	**Meteodyn input data extent** centre x|y (m) radius (topography, roughness)(m)
54[redacted]–57[redacted] 10[redacted]–13[redacted]	55[redacted]–55[redacted] 12[redacted]–12[redacted]	55[redacted]|12[redacted] $1.2\sqrt{2}radius$, $1.2\sqrt{2}radius + 2000$

In Figure 4.3 the roughness lengths (z_0) and height contour lines of the refinement area with the position of the wind turbines and measurement devices are visualized.

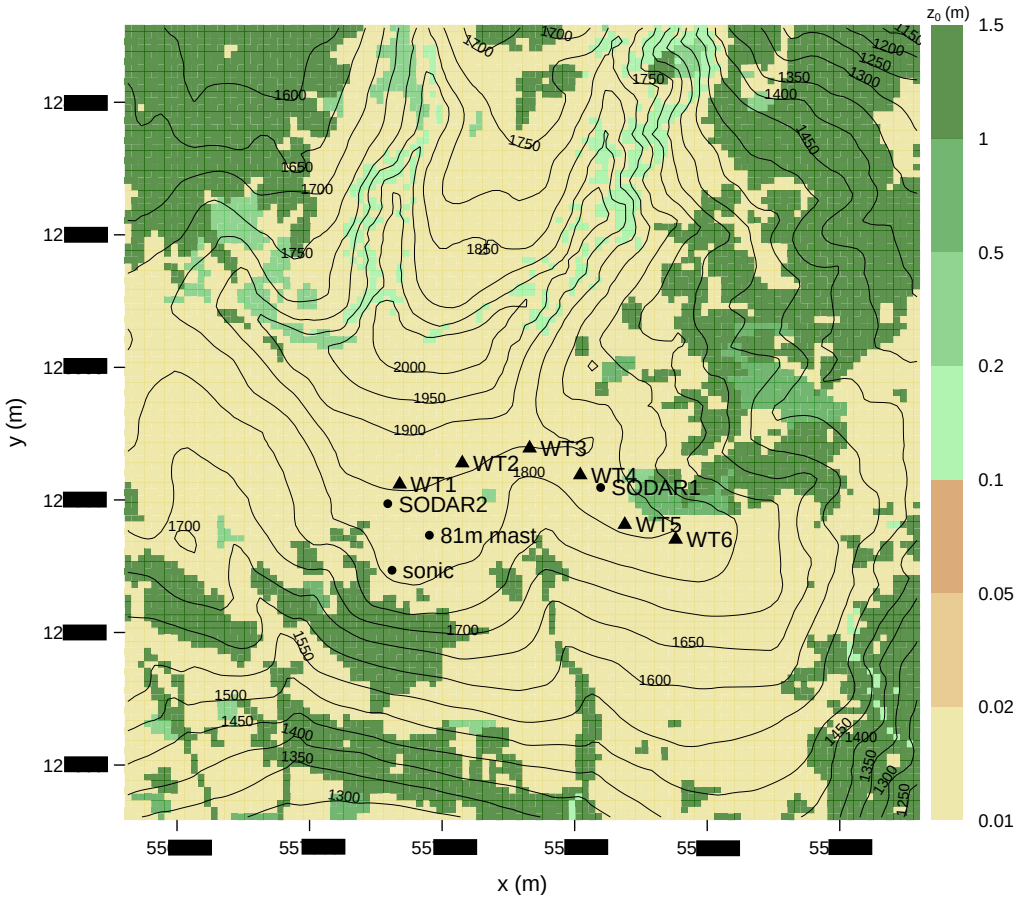

Fig. 4.3: z_0 in m (shaded) with black height contour lines with an equidistance of $50m$ of the refinement area of the T-Location wind park. Positions of measurement devices and wind turbines (named WT) are indicated with circles and triangles, respectively

The surface cover classes behind the roughness lengths are described in Table A.1 in the appendix. A satellite image of the site can also be found there (Fig. A.2). The coordinates of the wind turbines and measurement devices are given in Table 4.3.

Tab. 4.3: Swiss Grid x- and y-coordinates and height a.s.l. of wind turbines and measurement devices in the T-Location wind park (Koller *et al.* , 2014).

label	**x (m)**	**y (m)**	**height a.s.l (m)**
81m mast	55[redacted]	12[redacted]	1838
SODAR1	55[redacted]	12[redacted]	1839
SODAR2	55[redacted]	12[redacted]	1847
sonic	55[redacted]	12[redacted]	1814
WT1	55[redacted]	12[redacted]	1855
WT2	55[redacted]	12[redacted]	1887
WT3	55[redacted]	12[redacted]	1845
WT4	55[redacted]	12[redacted]	1825
WT5	55[redacted]	12[redacted]	1803
WT6	55[redacted]	12[redacted]	1783

The site for the future wind park is located on a plane south of the mountain Pointe de Bellevue. Between the wind turbines there are almost no trees or other obstacles. North of wind turbine 6 (WT6) and south of WT1 and WT2 there is forest. The terrain is slightly ascending between WT6 and WT2 and is descending between WT2 and WT1. Figure A.3 in the appendix shows panorama photos of the site. With $RIX = 74.4\%$ and a difference of more than $2800m$ between lowest and highest point in the base area, the site has very complex terrain (Tab. 4.1). Details about the project can be found in Koller *et al.* (2014).

4.1.2 Meteodyn Runs

In Meteodyn four model runs are performed for the T-Location wind park. Table 4.4 summarizes the most important model settings.

Tab. 4.4: Summary of Meteodyn model settings for the five runs of the T-Location case study. Explanations can be found in the text.

run	**sectors**	**radius (m)**	**forest model**	**stability**	**c_h**	**sectorwise settings**	**maximum smoothing (occurrence)**
T1	12	4525	no	2	1.01	same	3 (12)
T2	30	7500	yes	2	1.10	different	1 (7)
T3	30	7500	no	2	1.20	different	1 (7)
T4	30	25000	no	2	1.10	same	1 (30)

In run T1 a small value for *radius* is chosen to make a small value for the horizontal grid expansion factor (c_h) possible (small values for c_h result in a finer grid and therefore enhance computation time). This resulted in convergence problems which is why the smoothing parameter (ranging from 0 to 5) had to be set to 3. The number in brackets gives the occurrence of the maximum smoothing parameter where the highest possible occurrence is the number of calculated wind direction sectors (for details see Section 6) which is also given in Table 4.4. For run T2, *radius* is set to $7500m$ and the forest model is switched on. The forest density was set to normal for the whole data set of roughness lengths. c_h has to be set higher to ensure convergence in the whole area. It is tested in run T3 if a low resolution ($c_h = 2$) would result in worse cross checking results than a high resolution. Run T4 was ran by Bértrand Crouzille (Meteodyn, Nantes) on a high performance computer to test the influence of the size of the input roughness and topography data. The runs are sorted chronologically and also mirror a learning progress.

4.2 S-Location

4.2.1 Site description

At [redacted], a hill range in the canton Fribourg, a wind park consisting of two groups of wind turbines is planned. In Figure 4.4, the extent of the base and refinement area of the simulation in WindSim is indicated by the big and small rectangles. The small and big circles with dashed and dotted-dashed lines show the size of the topographical and roughness data considered for

the CFD simulation in Meteodyn for two different values of *radius* (compare Table 4.7). These extents are defined in Table 4.5.

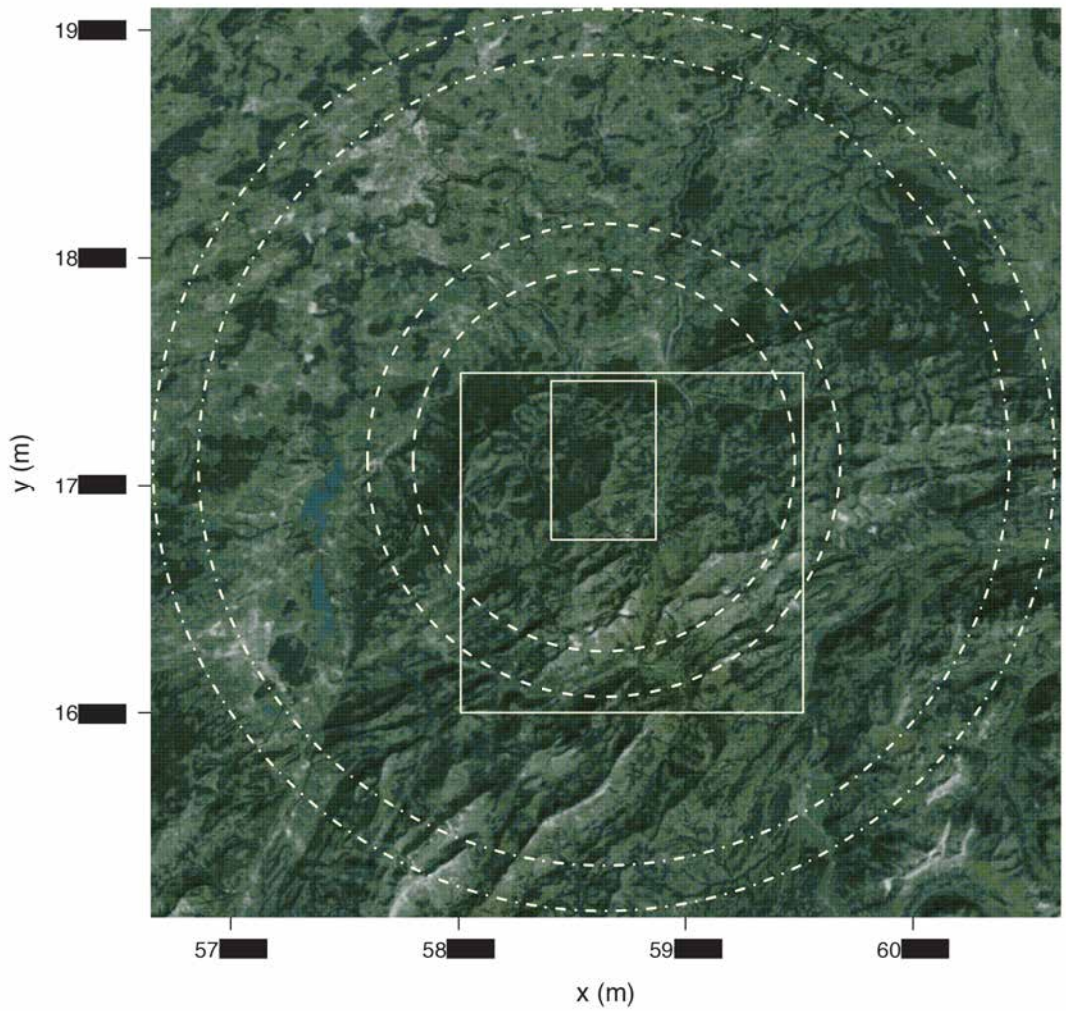

Fig. 4.4: Satellite image of the S-Location site. The small and big rectangles give the extent of the refinement and base area. The two pairs of circles indicate the size of the topography and roughness data sets in Meteodyn for two different sizes of *radius* as given in Table 4.7 (Google, 2015a).

Tab. 4.5: Extent of base and refinement area as defined in WindSim and extent of topography and roughness input data sets, which are considered in Meteodyn for the S-Location wind park in Swiss Grid coordinates. The values for *radius* are given in Table 4.7

WindSim base area	**WindSim refinement area**	**Meteodyn topography extent**
x-range (m)	x-range (m)	centre x|y (m)
y-range (m)	y-range (m)	radius (topography, roughness)(m)
58[redacted]–59[redacted]	58[redacted]–58[redacted]	58[redacted]|17[redacted]
16[redacted]–17[redacted]	16[redacted]–17[redacted]	$1.2\sqrt{2}radius$, $1.2\sqrt{2}radius + 2000$

In Figure 4.5 z_0 and height contour lines of the refinement area with the position of the wind turbines and measurement devices can be seen. A satellite image of the same area is shown in Figure A.4. The coordinates of the wind turbine sites and measurement devices are given in Table 4.6.

Five wind turbines are supposed to be installed in the northern part of S-Location at heights

between 1520m and 1589m a.s.l. Four more wind turbines are planned for the southern area of the mountain at heights between 1596m and 1620m a.s.l.

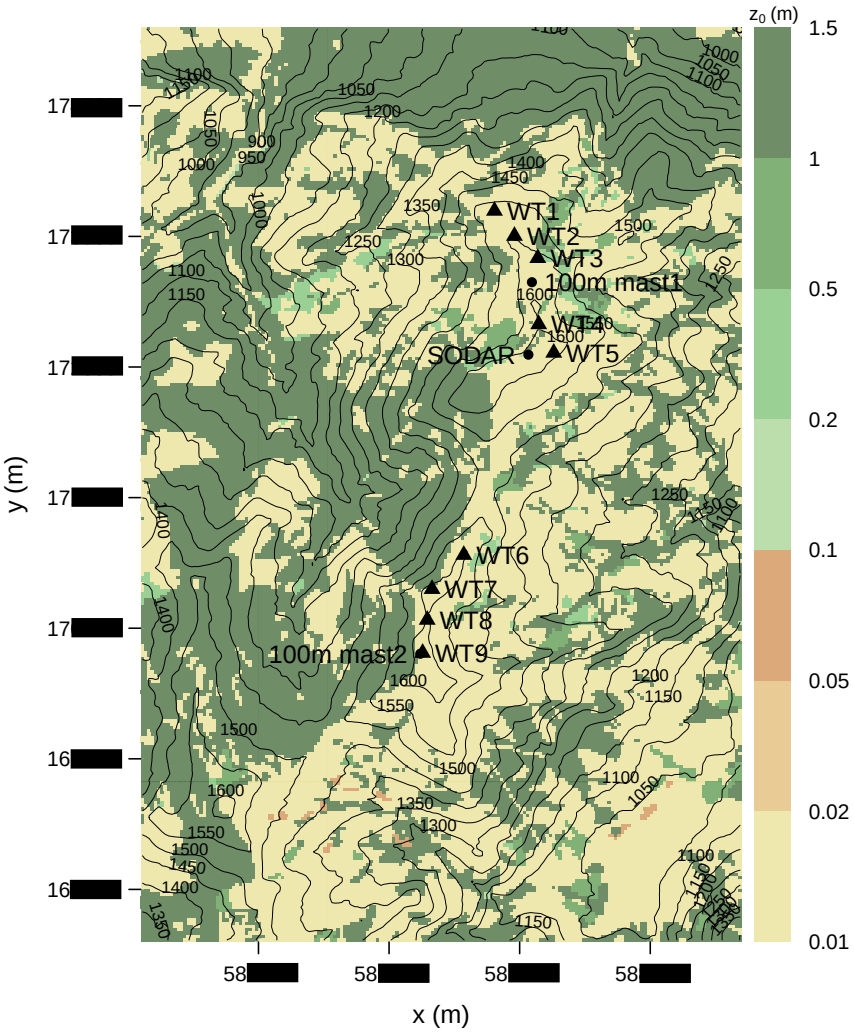

Fig. 4.5: z_0 in m (shaded) with black height contour lines in 50m steps of the refinement area of the S-Location wind park. Positions of measurement devices and wind turbines are indicated with circles and triangles, respectively.

Tab. 4.6: Swiss Grid x- and y-coordinates and height a.s.l. of wind turbines and measurement devices in the S-Location wind park (Dierer *et al.* , 2008).

label	**x (m)**	**y (m)**	**height a.s.l. (m)**
100m mast1	58[redacted]	17[redacted]	1576
100m mast2	58[redacted]	16[redacted]	1604
WT1	58[redacted]	17[redacted]	1520
WT2	58[redacted]	17[redacted]	1546
WT3	58[redacted]	17[redacted]	1557
WT4	58[redacted]	17[redacted]	1589
WT5	58[redacted]	17[redacted]	1612
WT7	58[redacted]	17[redacted]	1596
WT7	58[redacted]	17[redacted]	1605
WT8	58[redacted]	17[redacted]	1600
WT9	58[redacted]	16[redacted]	1620

A conifer forest can be found $100m$ away from the positions of WT5–WT9 on the western flank of S-Location. On the eastern flank, only single trees or smaller groups of trees grow in greater distance from the wind turbines. Around WT1–WT4 there are several smaller forested areas at a distance of approximately $100m$-$200m$. In the appendix, panorama photographs of both wind turbine sites at S-Location can be found (Fig. A.5 and A.6). With $RIX = 46.3\%$ and a height difference of $2265m$, the S-Location wind park site has a less complex terrain than the T-Location wind park site (Tab. 4.1). Dierer *et al.* (2008) give more details about the S-Location wind park site.

4.2.2 Meteodyn Runs

Table 4.7 gives an overview of the most important settings of the six Meteodyn runs.

Tab. 4.7: Summary of Meteodyn model settings for the six runs of the S-Location case study. Explanations can be found in the text.

run	**sectors**	**radius (m)**	**forest model**	**stability**	**c_h**	**sectorwise settings**	**maximum smoothing (occurrence)**
S1	12	4950	no	2	1.01	same	5 (12)
S2	12	10500	no	2	1.10	different	5 (1)
S3	30	10500	yes	2	1.10	different	5 (3)
S4	12	10500	yes	2	1.10	different	5 (1)
S5	12	10500	yes	2	1.10	different	5 (2)

Run S1 was performed with a small *radius* to get a roughness and topography input data set of approximately the same size as the WindSim base area. As the centre of the refinement and base area in WindSim are different it was not possible to define the roughness circle such that it lies completely inside the base area without shrinking it a lot (Fig. 4.4). For the other runs *radius* was enhanced to test if the wind fields alter. In runs S3-S5 the forest model was activated. In S3 and S4 the forest density was set to normal for the whole data set of roughness lengths. In run S5 the forest density was set to high for CORINE class 25 and to low for classes 16 and 29 (see Table A.1). All other classes were assigned with normal forest density. As it was not possible to get convergent solutions for some wind direction sectors the maximum smoothing of 5 was used for several sectors in all S-Location runs.

4.3 J-Location

4.3.1 Site description

[redacted] is a pass between [redacted] and [redacted] in the canton of Bern (Switzerland). Near the pass, a wind park project with eight turbines is planned at the mountains [redacted] and [redacted] which belong to the hill range [redacted]. In Figure 4.6, the extent of the base and refinement area of the simulation in WindSim is indicated by the big and small rectangles. The small and big circles give the size of the topography and roughness data considered for the CFD simulations in Meteodyn. These extents are defined in Table 4.8. Figure 4.7 shows z_0 of the refinement area with the position of the wind turbines and measurement

devices. A satellite image of the same region can be found in the appendix (Fig. A.7). The coordinates of the wind turbines are given in Table 4.9. They are distributed over an area with many single trees and groups of a few trees.

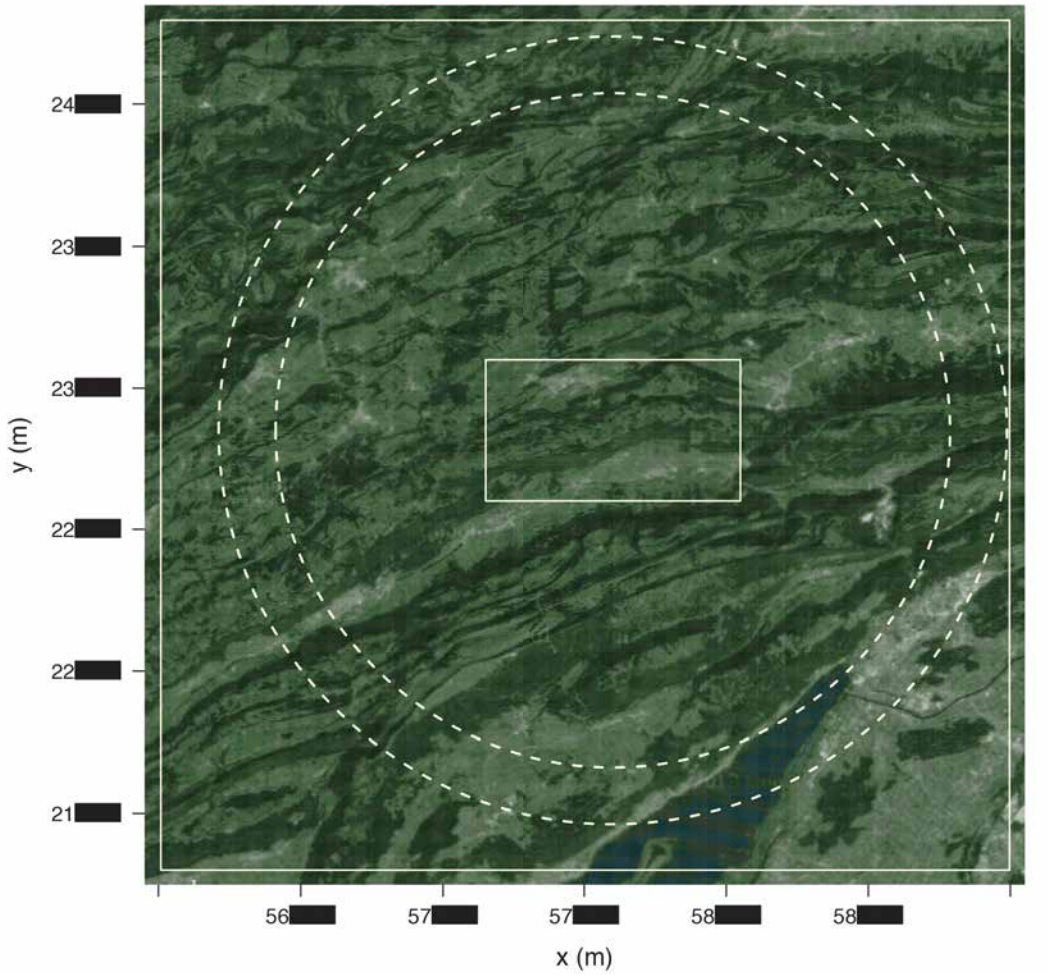

Fig. 4.6: Satellite image of the J-Location wind park site. The big and small rectangles give the extent of the base and refinement area, respectively. The big and small circles show the extent of the roughness and topography input data sets, respectively. (Google, 2015b).

The panorama photos in the appendix (Fig. A.8 and A.9) illustrate the landscape around the wind park. WT2–WT8 are located at terrain heights of around $1100m$ a.s.l. WT1 will be installed about $100m$ higher than the others. West of WT1 at a $2000m$ distance, the terrain is further ascending up to about $1300m$ a.s.l. North and south of the wind park there is a forest of higher density.

Tab. 4.8: Extent of base and refinement area as defined in WindSim and the extent of the topography and roughness input data sets, which are considered in Meteodyn for the J-Location wind park in Swiss Grid coordinates. For the J-Location wind park $radius = 7000m$ in all runs.

WindSim base area	**WindSim refinement area**	**Meteodyn topography extent**
x-range (m)	x-range (m)	centre x|y (m)
y-range (m)	y-range (m)	radius (topography, roughness) (m)
56[redacted]–59[redacted]	57[redacted]–58[redacted]	57[redacted]|27[redacted]
21[redacted]–24[redacted]	22[redacted]–23[redacted]	$1.2\sqrt{2}radius$, $1.2\sqrt{2}radius + 2000$

The J-Location wind park lies in the Swiss Jura. With $RIX = 20.2\%$ and a height difference of $1176m$ the least complex terrain of all case studies presented in this master thesis (Tab. 4.1). According to the definition of Gobbi and Dorweiler (2012) this terrain would not even be classified as complex. For more details about the J-Location wind park site the reader is referred to Koller and Bourgeois (2011).

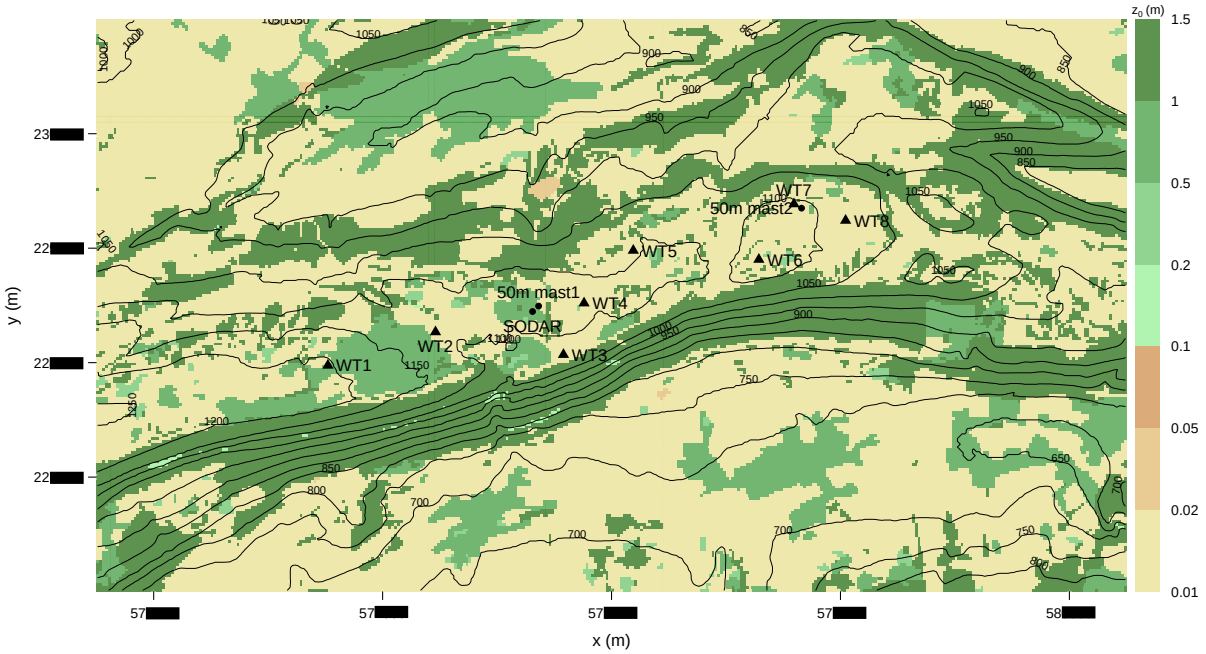

Fig. 4.7: z_0 in m (shaded) with black height contour lines in $50m$ steps of the refinement area of the J-Location wind park. Positions of measurement devices and wind turbines are indicated with circles and triangles, respectively.

Tab. 4.9: Swiss Grid x- and y-coordinates and height a.s.l. of wind turbines and measurement devices in the J-Location wind park (Koller and Bourgeois, 2011).

label	**x** (m)	**y** (m)	**height a.s.l.** (m)
50m mast1	57[redacted]	22[redacted]	1115
50m mast2	57[redacted]	22[redacted]	1112
SODAR	57[redacted]	22[redacted]	1115
WT1	57[redacted]	22[redacted]	1203
WT2	57[redacted]	22[redacted]	1113
WT3	57[redacted]	22[redacted]	1085
WT4	57[redacted]	22[redacted]	1107
WT5	57[redacted]	22[redacted]	1097
WT6	57[redacted]	22[redacted]	1119
WT7	57[redacted]	22[redacted]	1106
WT8	57[redacted]	22[redacted]	1087

4.3.2 Meteodyn Runs

In Table 4.10 an overview of the model settings of the J-Location Meteodyn runs is given. The variable *radius* is the same in all runs. For run J1 four stability classes are used. For run J2 and J3 stability class 6 is not used because it was assumed that such a high class cannot

occur at this site very often. The reasons for this assumption are discussed in Section 8.7. Run J3 is performed with the highest possible resolution by setting c_h to 1.01 which resulted in convergence problems for some wind direction sectors. That is why the maximum smoothing factor is higher in this run.

Tab. 4.10: Summary of Meteodyn model settings for the six runs of the J-Location case study. Explanations can be found in the text.

run	**sectors**	**radius (m)**	**forest model**	**stability**	**c_h**	**sectorwise settings**	**maximum smoothing (occurrence)**
J1	12	7000	no	0, 2, 4, 6	1.10	different	1 (1)
J2	12	7000	yes	0, 2, 5	1.10	different	1 (6)
J3	12	7000	no	0, 2, 4	1.01	different	5 (2)

5. Input Data for CFD Models

5.1 Topography

The topographical data sets for the CFD simulations of the three wind parks were cut from the digital height model of Switzerland with $25m$ resolution (DHM25). It is assumed that the accuracy of DHM25 compared to reality is between $2m$ and $8m$ (Swisstopo, 2005). The extent of the data sets for the T-Location, S-Location, and J-Location case studies are given in Tables 4.2, 4.5, and 4.8. The topography of the T-Location area, that was not covered by DHM25 because it is located in France, is taken from the Shuttle Radar Topography Mission (SRTM) data provided by the Consortium for Spatial Information of the Consultative Group for International Agricultural Research (CGIAR-CSI) (Jarvis *et al.* , 2008).

5.2 Surface Roughness

The roughness input data set was built with the help of land use information, which was transferred to roughness lengths according to BMUB (2002) by Meteotest. For areas in Switzerland the digital landscape model with a scale of 1:25000 (VECTOR25) documented in Swisstopo, 2007 was used as the land use data set. It classifies objects into 155 different classes where 48 belong to natural and agricultural structures like lakes, forests or fields. For areas outside of Switzerland the Coordinated Information of the Environment (CORINE) land cover raster data base (CLC2006) with 44 land cover classes and a resolution of $100m$ described in Büttner *et al.* (2012) is used instead. CLC2006 is freely available at eea.europa.eu. The surface cover classes occurring in the used cuts and their roughness lengths are listed in Table A.1 in the appendix.

5.3 Wind Measurements

All measurement campaigns and data correction procedures described in this section were performed by Meteotest or were provided by customers of Meteotest.

5.3.1 T-Location

At the T-Location wind park site, measurements were conducted at four different sites as documented in Koller *et al.* (2014). The coordinates of the locations of the measurement devices can be found in Table 4.3. A 81m mast carried anemometers at $40m$, $60m$ and $82m$ height above ground (a.g.) to measure $1s$ values of wind speed (v). Additionally it was equipped with wind vanes, a hygro-thermic sensor and an air pressure sensor to measure $1s$ values of v, wind direction (dd), air pressure (p), air Temperature (T_a), and relative humidity (RH). Some of the devices were heated to prevent measurement errors during icing conditions. An overview of the equipment of the 81m mast is described in Table A.2 in the appendix. The $1s$ values were used

to calculate $10min$ means from 14$^{\text{th}}$ March 2012 to 18$^{\text{th}}$ May 2014. For the resulting time series, Pearson correlation was performed with the long-term (at least 10 years without gaps) hourly and daily data from some nearby meteorological stations to find a station to correct the short-term measurements at the wind park site. The World Meteorological Organisation (WMO) station Plaffeien was chosen to calculate long-term corrected measurements $v_{mast,c}$ as its wind speed data showed the highest correlation with the T-Location measurements. This was done by multiplying the mast measurements $v_{mast,m}$ by a factor that is calculated as the fraction of the mean wind speed as measured by the WMO station during the long period ($v_{WMO,m}$) to the mean wind speed measured at the same station but during the period of the mast measurements ($v_{WMOt,m}$)(Eq. 5.1).

$$v_{mast,c} = v_{mast,m} \frac{v_{WMO,l}}{v_{WMO,m}} \tag{5.1}$$

The correction was done, because the measured time series are too short to give reliable information about the long-term wind conditions of the site. Additionally a AQ500 SODAR of AQSystem was installed between the 17$^{\text{th}}$ December 2013 and the 3$^{\text{rd}}$ April 2014 as well as from 4$^{\text{th}}$ April 2014 to 16$^{\text{th}}$ May 2014 at the sites SODAR1 and SODAR2.

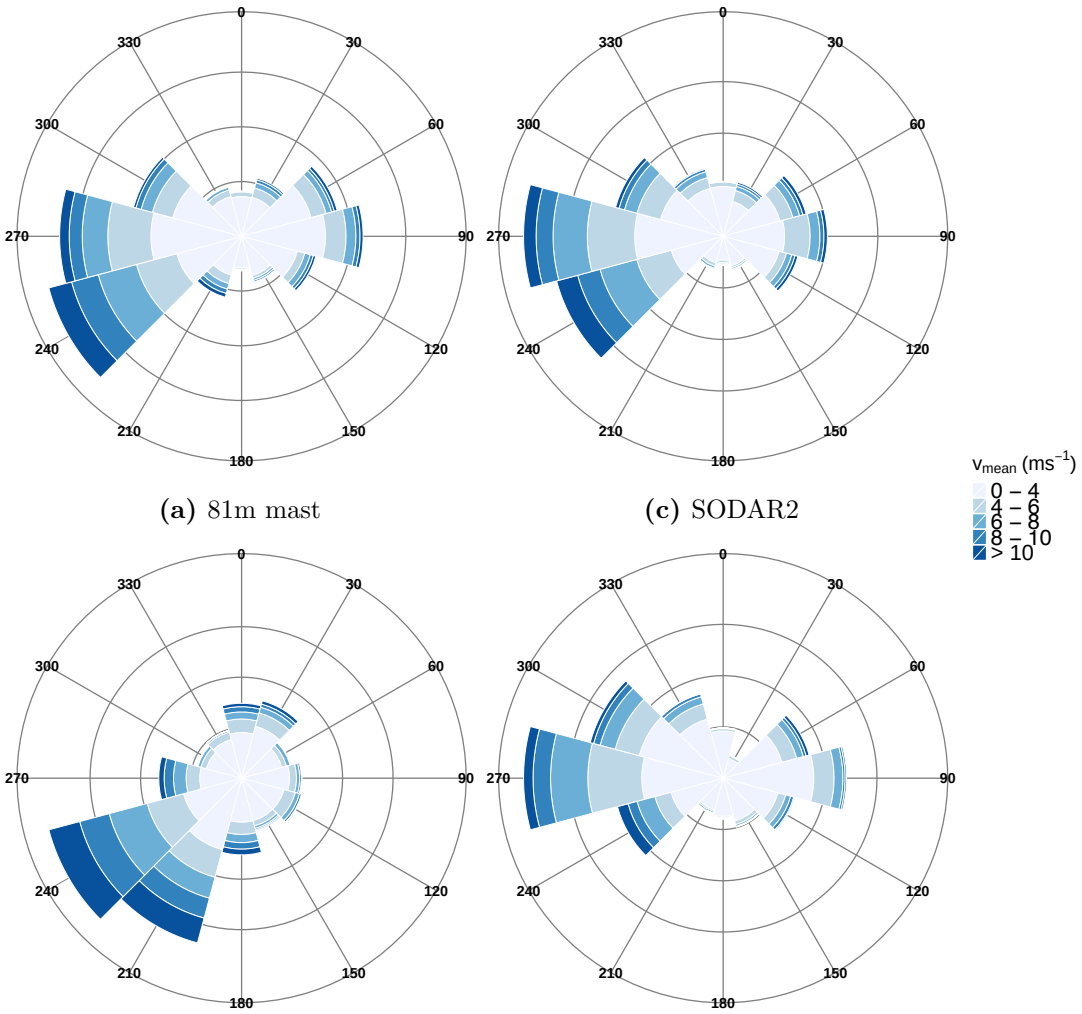

(a) 81m mast **(c)** SODAR2

(b) SODAR1 **(d)** sonic

Fig. 5.1: Wind roses of the long-term corrected $10min$ means of v of four different measurement devices at the T-Location wind park site as reported in Koller *et al.* (2014). The grey circles indicate frequency margins in 5% steps.

From that campaign $10min$ mean values of v are available at steps of $5m$ between $50m$ and $200m$ a.g. at both positions. Another data set was measured by a Gill Instruments WindMaster sonic anemometer at $37m$ a.g. on an electricity mast for the period of 17^{th} January to 18^{th} May 2014. The measurements at the sites SODAR1, SODAR2 and sonic are also long-term corrected. Figure 5.1 (a) visualizes the long-term corrected $10min$ means of v of the 81m mast in $82m$ a.g. as a wind rose.

Winds predominantly came from south-westerly directions during the measurement period. Especially high values of more than $6.0ms^{-1}$ blew from this direction. This is not surprising as the position of the 81m mast was shielded by the higher terrain north of the mast. The wind roses of the SODAR1 and SODAR2 (fig. 5.1 (b) and (c) are valid for $80m$ height above ground. The wind rose of the sonic anemometer is valid for $37m$ a.g. (Fig. 5.1 (d)). The wind pattern of SODAR2 looks similar to the one of the 81m mast. The SODAR1 and 81m mast wind rose differ especially for winds coming from the west (270°) and south-west (210°). The sonic anemometer showed less frequent wind from south-westerly directions (240°) because it was located in the wind shadow of a forest.

In Table 5.1 the corrected mean annual wind speed in reference height at the locations of the measurement devices can be found. For simplicity, they are thereafter called v_{mean}. Table 5.1 also gives the reference height, the shape (k) and scale parameters (A) of a Weibull distribution that was fitted to the corrected time series. Weibull distributions are often used to describe skewed data as wind speed measurements. v_{mean} is with $4.4ms^{-1}$ and $4.0ms^{-1}$ lower at the position of the SODAR1 and SODAR2 measurements than at the position of the 81m mast although the measuring height is lower. v_{mean} of the sonic time series is $3.6ms^{-1}$.

Tab. 5.1: v_{mean}, Weibull parameter k and A for different measurement stations and reference heights at the T-Location wind park site.

station	**height (m a.g.)**	**v_{mean} (ms^{-1})**	**k (–)**	**A (ms^{-1})**
81m mast	82	3.9	1.26	4.0
SODAR1	80	4.4	1.27	4.6
SODAR2	80	4.0	1.36	4.4
sonic	37	3.6	1.28	3.7

5.3.2 S-Location

At S-Location two masts (100m mast1 and 100m mast2) of $100m$ height were installed. $10min$ means of v and dd are available between 19^{th} July and 10^{th} November 2007 in $66m$, $86m$ and $100m$ a.g. The measurement equipment of 100m mast1 is described in detail in Table A.3 in the appendix. The 100m mast2 has nearly the same settings. Its equipment specifications can be found in Dierer *et al.* (2008). The coordinates of all measurement sites can be found in Table 4.6. Figures 5.2 (a) and (b) show the long-term corrected wind roses in $100m$ height at the position of 100m mast1 and 100m mast2. The measurements in $100m$ height of 100m mast1 and 100m mast2 were corrected with the help of data from the WMO station Le Moléson using Equation 5.1. The SODAR data were not corrected and are therefore not used as input climatology for the simulation in Meteodyn and WindSim. The predominant wind direction is 240° at both measurement positions in Figure 5.2.

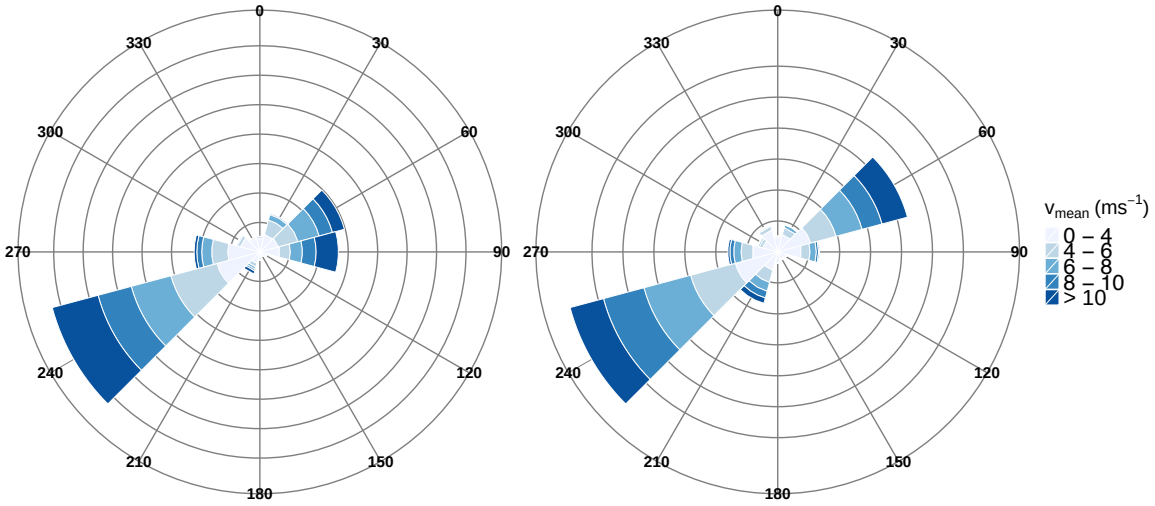

(a) 100m mast1 **(b)** 100m mast2

Fig. 5.2: Wind roses of the the long-term corrected $10min$ means of v of the two measurement devices at the S-Location wind park site as reported in Dierer *et al.* (2008). The grey circles indicate frequency margins in 5% steps.

Wind is blowing more often from the north-east (60°) at the 100m mast2 than at the 100m mast1. Table 5.2 reports the corrected v_{mean} and its reference height as well as the k and A value of a fitted Weibull distribution of the wind roses use as scaling climatologies for the CFD models. At 100m mast1 at $100m$ a.g., a higher value of v_{mean} was measured than at 100m mast2.

Tab. 5.2: v_{mean}, Weibull parameter k and A for different measurement stations and reference heights at the S-Location wind park site.

station	**height (m a.g.)**	**v_{mean} (ms^{-1})**	**k (–)**	**A (ms^{-1})**
100m mast1	100	6.0	1.63	6.7
100m mast2	100	5.6	1.74	6.3

5.3.3 J-Location

In the J-Location wind park area three measurement campaigns were performed. The coordinates of the devices' positions and the height of the measurements that were used to run the CFD models are listed in Table 4.9. The 50m mast1 was installed in the western part of the area and the 50m mast2 stand in the eastern part. The devices on the 50m mast1 are described in Table A.4. The equipment on the 50m mast2 had similar settings and the specifications can be found in Koller and Bourgeois (2011). The $10min$ means of v and dd are available between 1st July 2009 and 1st November 2010 for both masts at $31.5m$, $39.5m$, and $47.1m$ ($47.2m$ for the 50m mast2) a.g. The measurements of the winter period at the 50m mast1 had to be corrected with measurements of the 50m mast2 due to icing conditions that caused errors. Details about the correction procedure can be found in Koller and Bourgeois (2011). Near to the 50m mast1 an AeroVironment miniSODAR 4000F was installed that measured v and dd in $10m$ steps between $20m$ and $150m$ a.g. The data was used to extrapolate the wind measurements of the 50m mast1 at $47.1m$ height up to $100m$. The sensors at $47.2m$ height of the 50m mast2 were extrapolated

up to $50m$ height. The short term measurements of the two masts were adjusted with the help long-term data of the WMO station at Napf by using Equation 5.1. The resulting wind roses are shown in Figure 5.3.

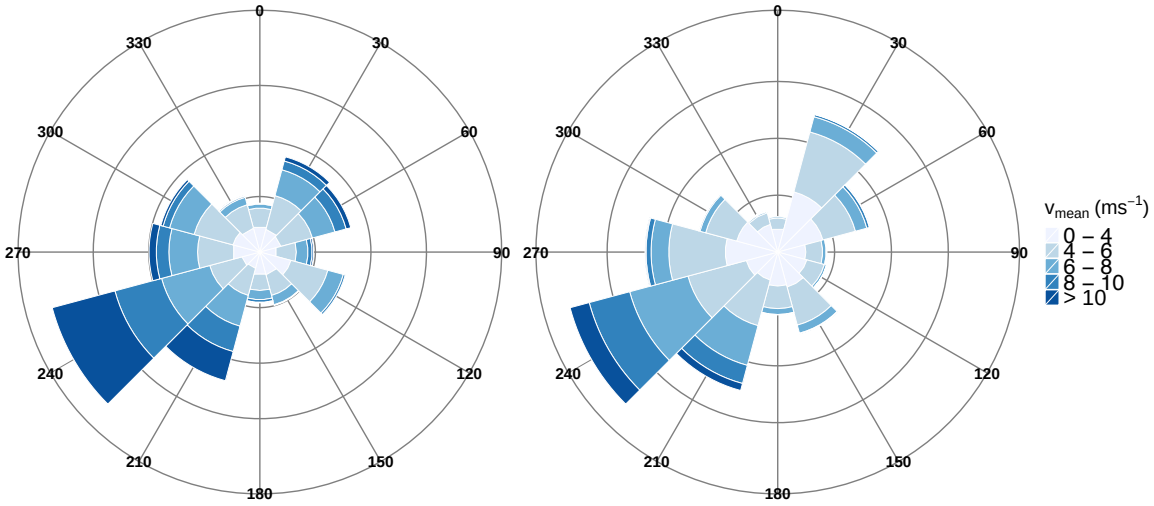

(a) 50m mast1 **(b)** 50m mast2

Fig. 5.3: Wind roses of the long-term corrected $10min$ means of v of the two measurement devices at the J-Location wind park site as reported in Koller and Bourgeois (2011). The grey circles indicate frequency margins in 5% steps.

Both wind roses show a similar wind pattern where most of the time, the wind came from south-westerly directions (240°). At the 50m mast2 the frequencies of 30°, 270°, and 210° were a bit higher than at the 50m mast1. As expected frequencies of high wind velocities of $v > 10ms^{-1}$ are more frequent in the extrapolated 100m wind rose (50m mast1). As can be seen in Table 5.3, the extrapolated value for v_{mean} in $100m$ a.g. for the 50m mast1 is higher than v_{mean} of the 50m mast2 at $50m$ a.g., as expected. In the same table the k and A values of a fitted Weibull distribution are listed for the two wind roses.

Tab. 5.3: v_{mean}, Weibull parameter k and A for different measurement stations and reference heights at the J-Location wind park site.

station	**height (m a.g.)**	**v_{mean} (ms^{-1})**	**k (–)**	**A (ms^{-1})**
50m mast1	100	6.1	1.89	6.6
50m mast2	50	4.8	2.02	5.3

5.4 Power and Thrust Curves of Wind Turbines

Power and thrust curves are needed to calculate wake effects and $Prod_{moy}$ at the position of the wind turbines. These data are provided by turbine manufacturers. In Koller *et al.* (2014), Dierer *et al.* (2008), and Koller and Bourgeois (2011) several wind turbine types were tested for the three wind parks. For this master thesis only the turbine types that produced the highest values for $Prod_{moy}$ are used. Their thrust and power curves are visualized in Figure 5.4.

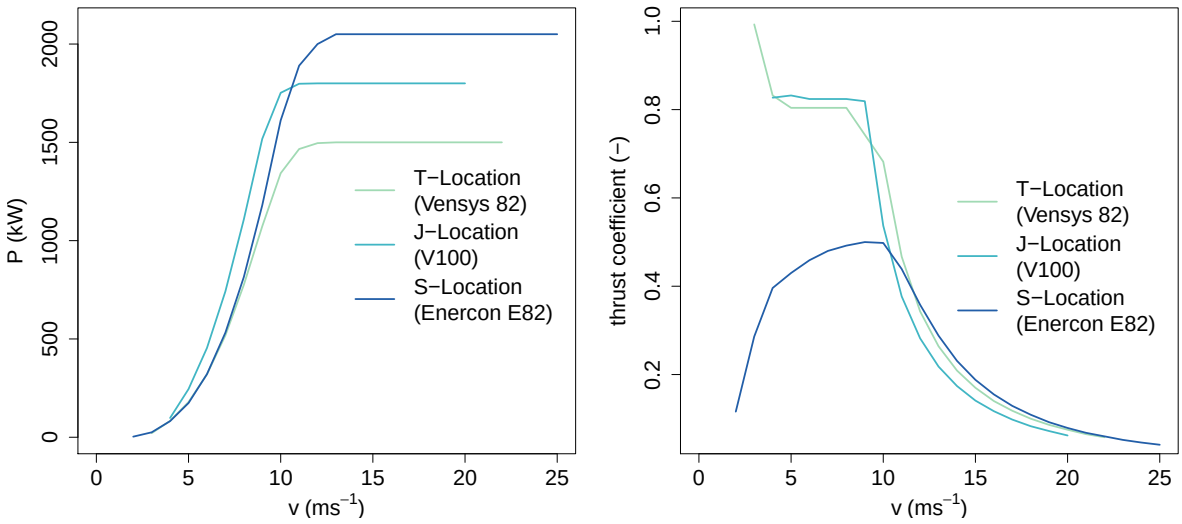

Fig. 5.4: Power (a) and thrust curve (b) for the wind turbine types used in the T-Location, S-Location and J-Location wind park. The curves start and end at cut-in and cut-off velocities.

The wind turbine types have different cut-in and cut-off velocities (starting and ending point of the curves in Figure 5.4). They give the value for v that is needed to start the movement of the rotor blades and the threshold at which the turbines are stopped to prevent them from getting damaged. The power curve gives the power (P) generated at each value for v. P increases with v. The thrust curve gives the thrust coefficient which is a measure for the thrust force. The thrust force is the resultant of the lift force and the drag force that act perpendicular and parallel to the flow streaming around the rotor blade (Quaschning, 2013). These forces let the wind turbine rotate. The wake model of a CFD model needs the thrust coefficients to calculate the production of turbulence and consumption of momentum in the wake that is induced by the rotor blades. As the thrust coefficient gets lower with higher values of v, the impact on energy yields for each turbine are lower for highwind speeds than for low ones.

6. Methods

6.1 Modelling of Wind Fields

The wind fields of three potential wind park sites in Switzerland are modelled for twelve or 36 wind direction sectors in Meteodyn ("directional computation"). This is done by defining site independent vertical wind profiles for the incoming flow for each sector. The result of the directional computation is a speed-up factor (s_c) for each grid cell in the computational domain, which is dependent on roughness and terrain structures. For each wind park site different model runs are performed to analyse the variability of the modelled results. Long-term corrected measurements of Dierer *et al.* (2008), Koller and Bourgeois (2011), and Koller *et al.* (2014) are used to adjust the results of the directional computation to local wind conditions in the CFD model ("scaling"). The scaling is done by using reference climatologies to calculate the two-dimensional fields of v_{moy} and TI_{moy} at different heights with the help of s_c. Equation 6.1 explains how this is done for v_{moy} in each grid cell.

$$v_{moy} = s_c v_{mean} \tag{6.1}$$

v_{mean} is fed into the model at the position of the measurement site. At this position s_c is 1.0 by definition. With the help of power and thrust curves for several wind turbine types as well as the position and height of the planned wind turbines, $Prod_{moy}$ can be calculated for the turbines of the wind parks.
The same procedure has already been performed in WindSim for the same wind park sites by Dierer *et al.* (2008), Koller and Bourgeois (2011), and Koller *et al.* (2014). They modelled wind fields for twelve wind direction sectors for all wind park sites. The results of their work are used in this master thesis. For the S-Location wind park $Prod_{moy}$ has been recalculated in WindSim.

6.2 Cross Checking

A CFD model can be validated and assessed by a procedure called cross checking. Thereby, long-term corrected wind measurements ("climatologies") from at least two different sites are compared to simulated values. That means that the directional computation is first scaled by the first climatology and compared to the values of the second climatology at the measuring position of the second climatology and the other way round.

6.3 Meteodyn Calibration: Atmospheric Stability

As no measurements of atmospheric stability were taken during the field campaigns, two stability calibration methods are used to fit modelled results to measured data.

First, the model is run for different stability classes where all wind direction sectors get the same stability class. The vertical wind profiles of each stability class simulated by the model are compared to the measured profiles to decide which stability class reproduces measurements the best. Secondly, different stability classes are set for each wind direction sector. To find the best combination of stability classes directional means of v for different stability classes are compared to measured directional means.
The stability calibration costs a lot of computation time. Therefore the simulations of the T-Location and S-Location case studies are only performed for the stability class 2 (near neutral). For the J-Location runs the stability classes 0, 2, 4, 5 and 6 are used.

6.4 Meteodyn Calibration: Forest Model

The forest model can be deactivated by setting $c_r = 0$. For some runs of all case studies it is activated with $c_r = 20$. For one of the J-Location and T-Location case studies the forest density was set to normal for the whole data set of roughness lengths. It is expected that the surrounding forests at the S-Location wind park site might have a big influence on the wind fields at the site. Therefore, different forest density classes are defined for different CORINE surface cover classes. Details can be found in Section 4.2.2.

6.5 Comparison of Vertical Wind Profiles

The different Meteodyn runs were evaluated by comparing the modelled mean vertical wind profiles v_{moy} to the mean climatologies v_{mean} at three different heights ($40m$, $60m$ and $82m$ for T-Location; $66m$, $86m$ and $100m$ for S-Location and $30m$, $40m$ and $50m$ for J-Location). For the T-Location case study also measured (TI_{mean}) and modelled (TI_{moy}) mean vertical profiles of the turbulence intensity are compared . TI_{mean} is calculated as $\frac{\sigma_{v_{10min}}}{v_{10min}}$ from the $10min$ means and the $10min$ standard deviations time series for all $v > 10ms^{-1}$. Details about the calculation of TI_{moy} in Meteodyn and WindSim can be found in Section 6.6.

6.6 Comparison of WindSim and Meteodyn

The fields of v_{moy} (all case studies) and TI_{moy} (only T-Location) as well as $Prod_{moy}$ at the position of the wind turbines simulated by Meteodyn and WindSim are compared and differences are calculated. In WindSim TI_{moy} is evaluated from Equation 6.2 (WindSim, 2013). In Meteodyn it is given by Equation 6.3 (Meteodyn, 2015).

$$TI_{moy} = \frac{\sqrt{\frac{4}{3}k}}{\sqrt{u^2+v^2}}100\% \qquad (6.2) \qquad\qquad TI_{moy} = \frac{\sqrt{k}}{\sqrt{u^2+v^2+w^2}}100\% \qquad (6.3)$$

It is assumed that for an annual mean w_z can be neglected. Therefore TI_{moy} results of WindSim are divided by $\sqrt{\frac{4}{3}}$ to make Meteodyn and WindSim TI_{moy} results comparable. Furthermore TI_{moy} is evaluated for $v_{mean} > 10ms^{-1}$ in Meteodyn. The WindSim help facility does not report such a threshold. Furthermore, k is calculated differently in Meteodyn and WindSim (see Sections 2.2 and 2.3). Therefore comparisons of the turbulence intensity between Meteodyn and WindSim can only be made with caution.

7. Results

7.1 T-Location

7.1.1 Cross Checking

Table 7.1 lists the results of the cross checking for the WindSim run and Meteodyn runs T1–T4 of the T-Location case study. The second column gives v_{mean} at four positions at the reference heights $82m$, $80m$, $80m$ and $37m$ a.g. They are calculated from the long-term corrected time series described in Section 4.1. The other columns of the upper and lower part of the table show modelled values by using one of the four reference climatologies to scale WindSim and Meteodyn.

Tab. 7.1: Annual mean wind speed in ms^{-1} at four different locations at the T-Location site as measured and simulated by the Meteodyn runs T1-T4 and WindSim (WS) where the 81m mast, SODAR1, SODAR2 and the sonic mast served as the reference climatology in Meteodyn, respectively. The wind speeds are given for $82m$, $80m$, $80m$ and $37m$.

position	**measured**	**81m mast (ms^{-1})**					**SODAR1 (ms^{-1})**				
		WS	T1	T2	T3	T4	WS	T1	T2	T3	T4
81m mast	3.9	–	–	–	–	–	3.9	4.2	4.8	5.4	4.3
SODAR1	4.5	4.2	4.2	4.3	4.2	4.2	–	–	–	–	–
SODAR2	4.1	3.9	3.8	3.6	3.7	3.7	3.9	4.1	4.6	5.3	4.2
sonic	3.6	3.4	3.7	3.4	3.5	3.5	3.5	4.0	4.3	5.1	3.9
		SODAR2 (ms^{-1})					**sonic (ms^{-1})**				
		WS	T1	T2	T3	T4	WS	T1	T2	T3	T4
81m mast	3.9	4.1	4.2	4.4	4.4	4.3	4.1	3.8	4.3	4.5	4.0
SODAR1	4.5	3.6	4.4	4.9	4.7	4.5	4.3	3.9	4.9	5.4	4.2
SODAR2	4.1	–	–	–	–	–	4.1	3.7	4.1	4.0	3.9
sonic	3.6	3.6	4.1	3.8	3.9	3.9	–	–	–	–	–

Table 7.2 lists differences between the measured and modelled Meteodyn and WindSim v_{mean} of Table 7.1 as absolute values and relative to measurements. Values which are marked red indicate the smallest difference for each measuring position and reference climatology. WindSim showed 14 times out of 24 the smallest difference, followed by Meteodyn runs T1 and T4 with six times and T2 and T3 with four times out of 24. This shows that WindSim better matched measured values than Meteodyn. The largest difference of $-1.5ms^{-1}$ was produced by Meteodyn run T3. Using the 81m mast and sonic climatologies as the reference climatologies resulted in slightly lower differences than using SODAR2 and SODAR1 climatologies (five, four and three times lowest difference).

Tab. 7.2: Differences between measured and modelled Meteodyn values in Table 7.1 as absolute value and in percent of measured value at the T-Location site. The smallest difference is marked red for each position and reference climatology

position		**81m mast**					**SODAR1**				
		WS	T1	T2	T3	T4	WS	T1	T2	T3	T4
81m mast	ms^{-1}	–	–	–	–	–	0.0	−0.3	−0.9	−1.5	−0.4
SODAR1		0.3	0.3	0.2	0.3	0.3	–	–	–	–	–
SODAR2		0.2	0.3	0.5	0.4	0.4	0.2	0.0	−0.5	−1.2	−0.1
sonic		0.2	−0.1	0.2	0.1	0.1	0.1	−0.4	−0.7	−1.5	−0.3
81m mast	%	–	–	–	–	–	0.0	−7.7	−23.2	−38.5	−10.3
SODAR1		6.7	6.7	4.4	6.7	6.7	–	–	–	–	–
SODAR2		4.9	7.3	12.2	9.8	9.8	4.9	0.0	−12.2	−29.3	−2.4
sonic		5.6	−2.8	5.6	−2.8	2.8	2.8	−11.1	−19.4	−41.7	−8.3

		SODAR2					**sonic**				
		WS	T1	T2	T3	T4	WS	T1	T2	T3	T4
81m mast	ms^{-1}	−0.2	−0.3	−0.5	−0.5	−0.4	−0.2	0.1	−0.4	−0.6	−0.1
SODAR1		0.9	0.1	−0.4	−0.2	0.0	0.2	0.6	−0.4	−0.9	0.3
SODAR2		–	–	–	–	–	0.0	0.4	0.0	0.1	0.2
sonic		0.0	−0.5	−0.2	−0.3	−0.3	–	–	–	–	–
81m mast	%	−5.1	−7.7	−12.8	−12.8	−10.3	−5.1	2.0	−10.3	−15.5	−2.6
SODAR1		20.0	13.2	−8.9	−4.4	0.0	4.4	13.3	−8.9	−20.0	6.7
SODAR2		–	–	–	–	–	0.0	9.8	0.0	2.4	4.9
sonic		0.0	−13.9	−5.6	−8.3	−8.3	–	–	–	–	–

7.1.2 Vertical Wind Profiles

Figures 7.1 (a) and (b) show measured and modelled (Meteodyn runs T1–T4) mean vertical wind and TI profiles of the 81m mast. The horizontal black lines show the standard deviation of v_{mean} and TI_{mean} at $40m$, $60m$ and $82m$ a.g. TI_{mean} is calculated from $v_{mean} > 10ms^{-1}$ because in Meteodyn TI is calculated in the same way. All modelled vertical wind profiles match the measured ones relatively well. Meteodyn run T1 best fits v_{mean} at $40m$ and $60m$ a.g. At $82m$ a.g. modelled and measured values are the same, because the reference climatology feeds into the model at this position (Fig. 7.1).

Profiles of TI_{mean} are better reproduced between $60m$ and $82m$. The measured $40m$ value ($TI_{mean} = 18.9\%$) is underestimated by an absolute value of 5.5% by run T4, which is a relative error of 29.1%. Only the value of run T1 (15.3%) lies inside the one standard deviation range at this height. This is a relative error of 19.0%. At $60m$ a.g. run T2 with $TI_{mean} = 14.7\%$ is closest to the measured value of 14.9% which is a relative error of only 1.3%. At $82m$ a.g. it is run T4 with $TI_{mean} = 14.3\%$ that fits the measured value of 13.9% best. The relative error is −2.9%. The whole profile is best reproduced by run T1 because it captured the negative slope between $60m$ and $82m$ and showed the lowest difference in $40m$ a.g.

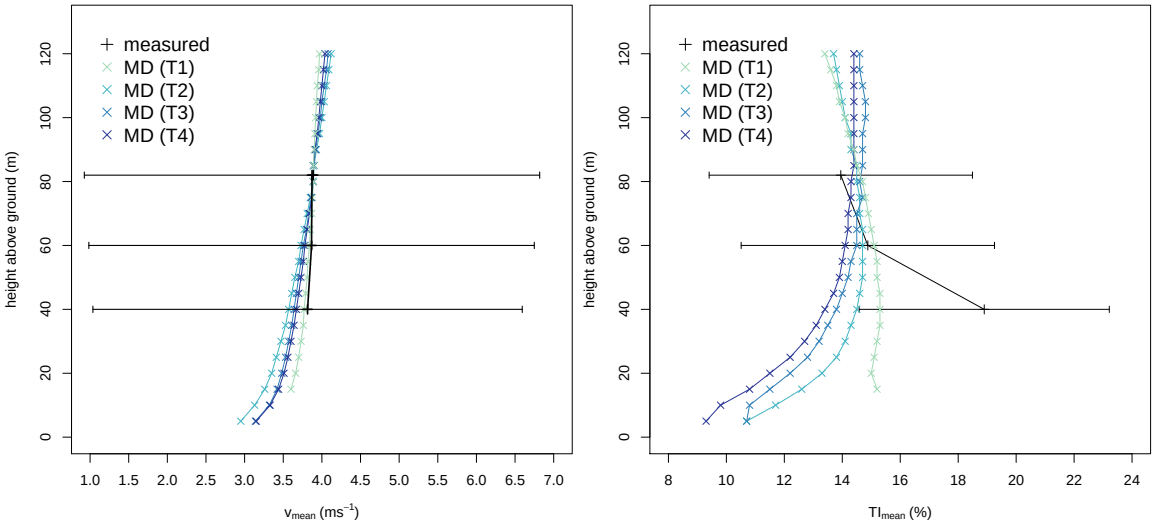

(a) **(b)**

Fig. 7.1: Vertical profiles of v_{mean} at $40m$, $60m$ and $82m$ a.g. and v_{moy} in $5m$ steps between $5m$ and $120m$ a.g (a) and TI_{mean} for $v_{mean} > 10ms^{-1}$ and TI_{moy} (b) as measured and simulated by Meteodyn runs T1–T4 at the 81m mast. The SODAR1, SODAR2 and sonic climatologies were used as the reference climatologies.

7.1.3 Two-dimensional Fields

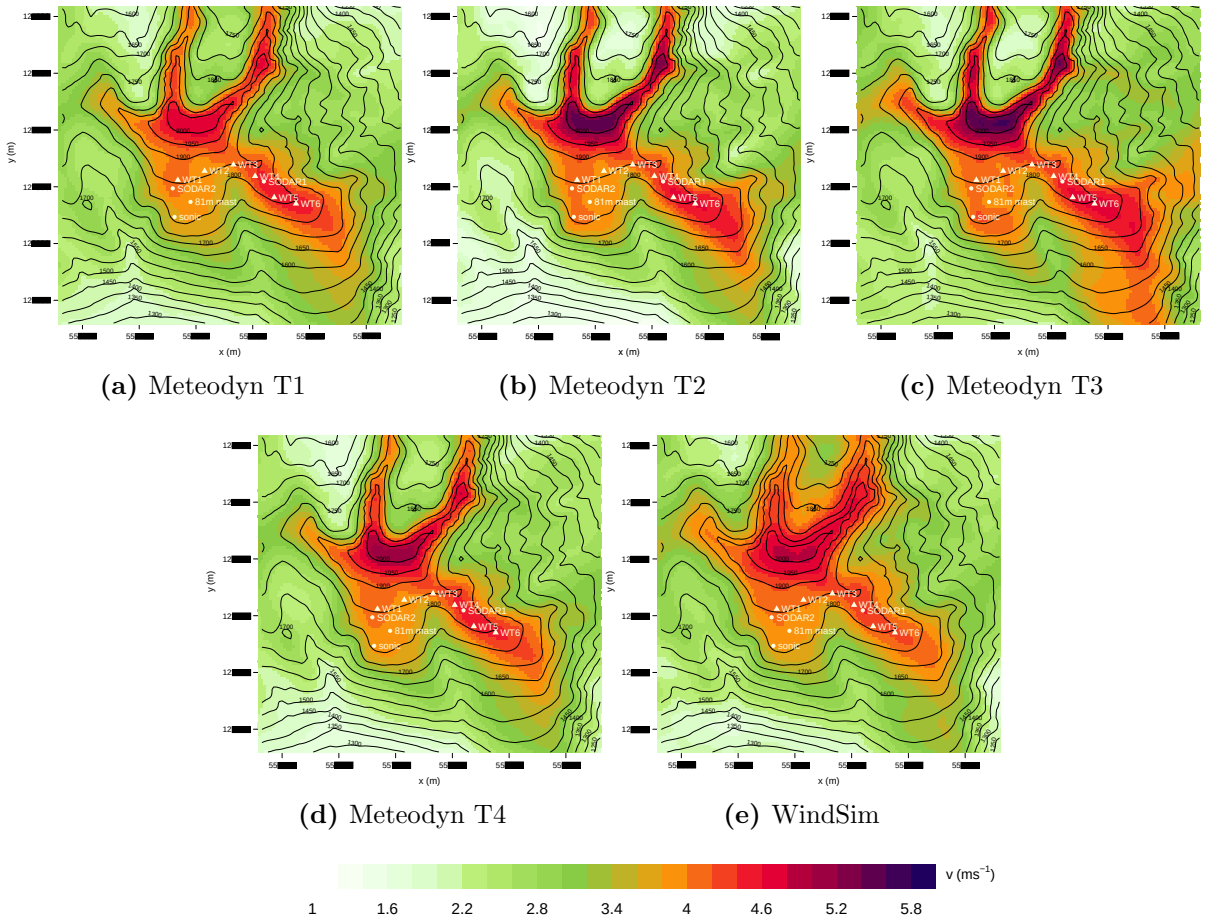

(a) Meteodyn T1 **(b)** Meteodyn T2 **(c)** Meteodyn T3

(d) Meteodyn T4 **(e)** WindSim

Fig. 7.2: v_{moy} in ms^{-1} at $80m$ a.g. for the refinement area of the T-Location wind park as simulated by Meteodyn runs T1-T4 (a-d) and WindSim (e) (shaded). Triangles and circles indicate the position of wind turbines and measuring sites, respectively. The black lines are height contour lines with an equidistance of $50m$.

Figure 7.2 shows v_{moy} at $80m$ a.g. for the refinement area of the T-Location wind park. Figures (a)–(d) show Meteodyn runs T1-T4. Figure 7.2 (e) is the wind field as simulated by WindSim. At the mountain peak north of the wind park, the highest values for v_{moy} are simulated in both models.

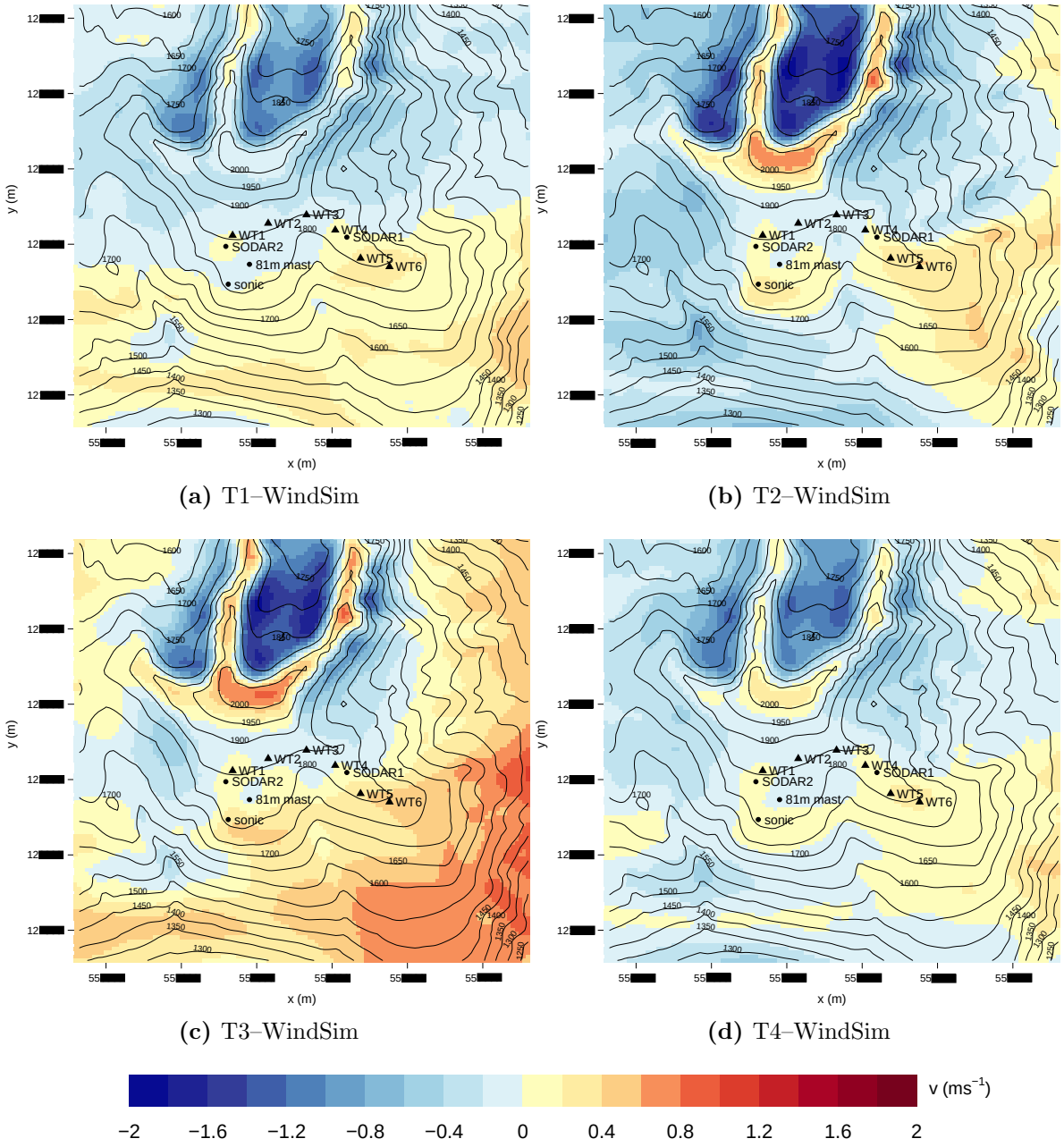

(a) T1–WindSim **(b)** T2–WindSim

(c) T3–WindSim **(d)** T4–WindSim

Fig. 7.3: Differences of v_{moy} in ms^{-1} calculated as Meteodyn–WindSim at $80m$ a.g. of the refinement area of the T-Location wind park (shaded). Each figure shows the differences between one of the Meteodyn runs T1-T4 and WindSim. Triangles and circles indicate the position of wind turbines and measuring sites, respectively. The black lines are height contour lines with an equidistance of $50m$.

The lowest values can be found in the south western region of the refinement area. It lies around $700m$ lower than the mountain peak and is partly covered with forest (compare Fig. 4.3). Although the maxima and minima are located in the same region in all Meteodyn runs and also the WindSim run, their values differ.

Table 7.3 lists the minimum, maximum and mean of v_{moy} calculated over all cells of Figure 7.2.

Meteodyn run T3 and WindSim show the lowest minimum values for the T-Location wind park ($1.3ms^{-1}$). Runs T2 and T3 simulate the highest maximum values ($5.6ms^{-1}$). The mean is highest and lowest in runs T3 and T2 respectively.

Tab. 7.3: Minimum, maximum and mean of v_{moy} and TI_{moy} in the refinement area of the T-Location wind park as simulated in Meteodyn runs T1–T4 and the WindSim run.

statistic	$\boldsymbol{v_{moy}}$ $\boldsymbol{(ms^{-1})}$					$\boldsymbol{TI_{moy}}$ **(%)**				
	WS	T1	T2	T3	T4	WS	T1	T2	T3	T4
minimum	1.3	1.5	1.3	1.6	1.5	15.9	10.0	9.1	10.0	7.4
maximum	4.8	4.8	5.6	5.6	5.1	40.0	26.6	39.4	39.3	22.6
mean	3.1	3.0	2.8	3.2	2.9	27.0	16.7	22.1	18.9	15.0

Figure 7.3 shows the differences between v_{moy} fields of the four Meteodyn runs and WindSim. The lowest negative difference is located in the luv of the mountain peak for all Meteodyn runs. The location of the highest positive difference has different locations in the Meteodyn runs.

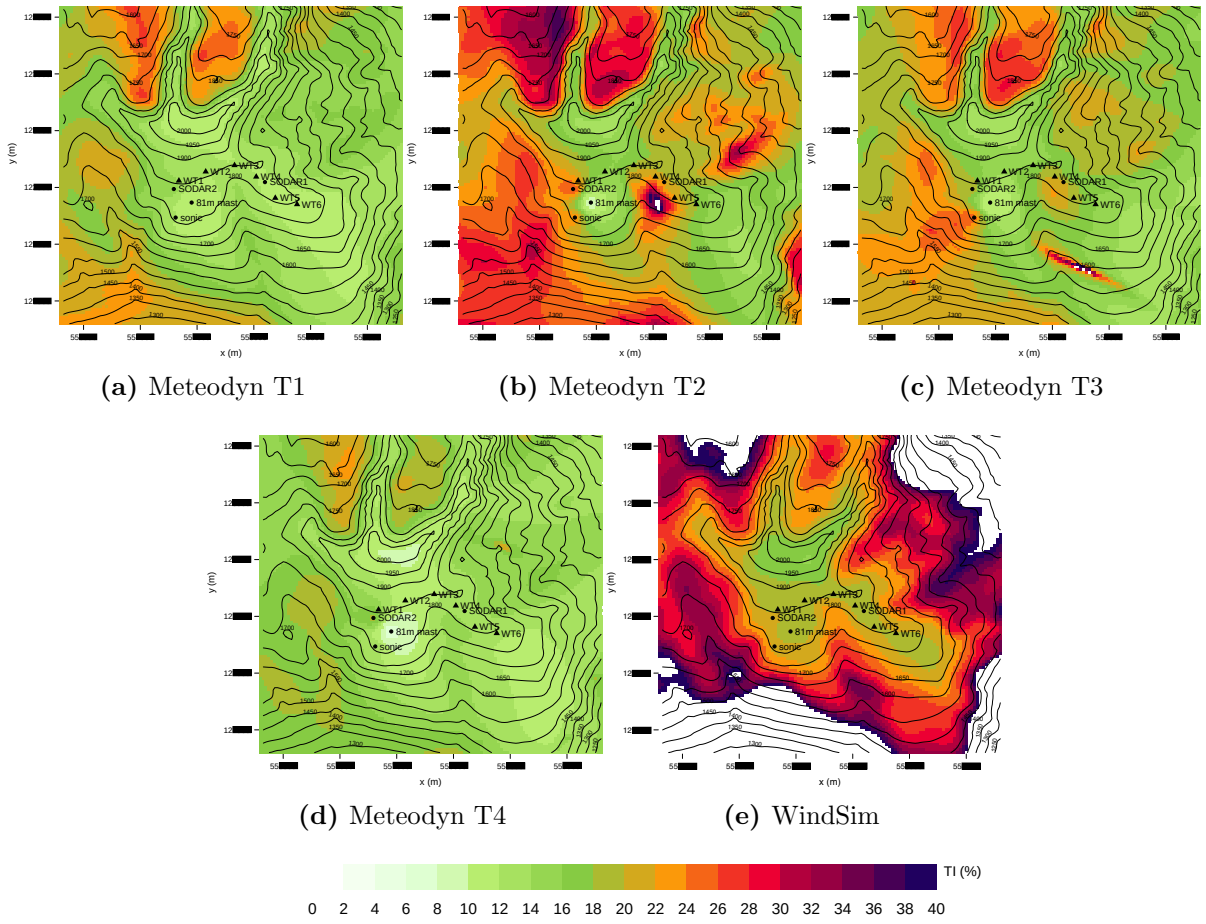

(a) Meteodyn T1 **(b)** Meteodyn T2 **(c)** Meteodyn T3

(d) Meteodyn T4 **(e)** WindSim

Fig. 7.4: TI_{moy} in % at $80m$ a.g. for the refinement area of the T-Location wind park site as simulated by Meteodyn runs T1-T4 (a-d) and WindSim (e) (shaded). The triangles and circles indicate the position of the wind turbines and measuring sites, respectively. The black lines are height contour lines with an equidistance of $50m$.

The minima and maxima for differences between the Meteodyn runs and WindSim can be found in the appendix (Tab. A.5). To be able to interpret these differences the reader has to know

that the wind energy that is available for extraction by wind turbines is proportional to the third power of the wind speed. A detailed discussion can be found in Section 8.2.
In Figures 7.4 (a)–(d) TI_{moy} fields of the four Meteodyn runs are visualized. Figure 7.4 (e) shows corrected WindSim TI_{moy}. Before the correction the results showed values of up to 200.6% in the outer regions of the refinement area where v_{moy} was low. Therefore it was decided to remove values where $TI_{moy} > 40\%$ for WindSim and Meteodyn simulations because findings in literature and measurements suggest that higher values are unlikely to occur. A detailed discussion can be found in Section 8.6.

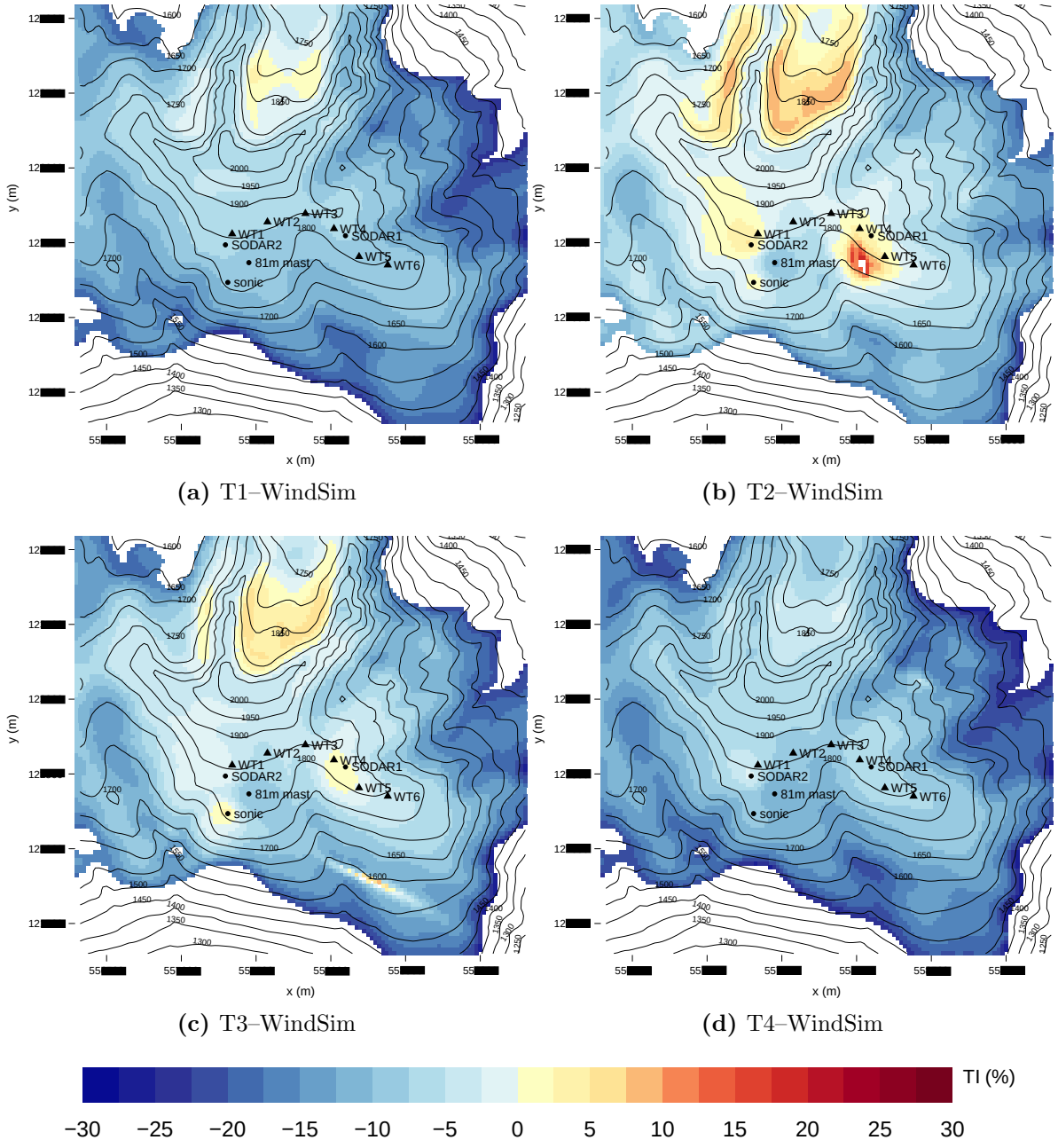

(a) T1–WindSim **(b)** T2–WindSim

(c) T3–WindSim **(d)** T4–WindSim

Fig. 7.5: Differences of TI_{moy} in % calculated as Meteodyn–WindSim at $80m$ a.g. for the refinement area of the T-Location wind park site (shaded). Each figure shows the differences between one of the Meteodyn runs T1-T4 and WindSim. The triangles and circles indicate the position of the wind turbines and measuring sites, respectively. The black lines are height contour lines with an equidistance of $50m$.

The minimum, maximum and mean values of TI_{moy} in the refinement area are listed in Table

7.3. The threshold of 40% is reached in Meteodyn runs T2 and T3 but for fewer cells. In general, Meteodyn runs show lower TI_{moy} than WindSim. The lowest minimum and highest maximum are found in Meteodyn run T4 and WindSim (7.4% and 40.0%). The mean was lowest and highest in Meteodyn run T4 and WindSim with 15.0% and 27.0% respectively. There are large differences of up to 30.0% among the Meteodyn runs especially in the trough north of the mountain peak, in the trough located in the north western and south western area and between 81m mast and WT5. At the mountain peak, around the 81m mast and in the south eastern area, the Meteodyn runs show similar TI_{moy}. Differences between the Meteodyn runs and the WindSim simulation are big as can be seen in Figure 7.5 and Table A.5. Differences between T1 and T4 and WindSim are smallest in the trough north of the mountain. This is also the region where Meteodyn runs T1, T2 and T3 show higher TI_{moy} than WindSim. The biggest negative and positive differences reported in A.5 do not occur at the same positionin all Meteodyn runs. To interpret the differences it has to be know that a value of 2% more or less of TI_{moy} could result in the choice of a different turbulence class for the wind turbines. This is discussed in more detail in 8.6.

7.1.4 Energy Production

$Prod_{moy}$ for the T-Location wind park is calculated as the sum of $Prod_{moy}$ for each wind turbine. Values between $12656 MWhy^{-1}$ (T1) and $13235 MWhy^{-1}$ (T3) are found for the Meteodyn runs without wake effect. WindSim predicts $12066 MWhy^{-1}$ for $Prod_{moy}$ without wake effect.

Tab. 7.4: Predicted $Prod_{moy}$ in Meteodyn runs T1–T4 and WindSim and differences calculated as Meteodyn–WindSim.

		WS	**T1**	**T2**	**T3**	**T4**
$Prod_{moy}$ no wake	**($MWhy^{-1}$)**	12 066	12 656	13 118	13 235	12 819
$Prod_{moy}$ wake		11 064	11 362	11 956	11 843	11 587
difference no wake		–	590	1052	1169	753
difference wake		–	298	892	780	523

This results in a difference of $590 MWhy^{-1}$ and $1169 MWhy^{-1}$. For comparison: an average European household has an electricity demand of approximately $5 MWhy^{-1}$ (Bertoldi *et al.* , 2012). The wake effect is larger in all Meteodyn runs compared to WindSim. This resulted in lower differences with wake effect between the Meteodyn runs and WindSim (Tab. 7.4).

7.1.5 Summary

Section 7.1.1 showed that WindSim best reproduces measurements of v_{mean}. Among the Meteodyn runs, run T1 and T4 performed best. In Section 7.1.2 it is shown that in Meteodyn run T1, modelled profiles of v_{mean} and TI_{mean} best fit measured profiles. Therefore it can be concluded that the model configuration of run T1 was the best at the T-Location site among the Meteodyn runs, although the topography and roughness input data are small and the forest model was not activated. The reason for the good results of run T1 might be the small grid spacing at this site (see Tab. 4.4).

7.2 S-Location

7.2.1 Cross Checking

Table 7.5 lists the results of the cross checking for WindSim and Meteodyn runs S1–S5 in the S-Location case study. The second column gives the mean long-term corrected wind speed at $100m$ a.g. for the 100m mast1 and 100m mast2. The third column shows v_{mean} at $100m$ a.g. at the position of the 100m mast1 where the climatology of the 100m mast2 was used to scale the directional computation in WindSim. Columns four to eight show respective Meteodyn values. The last six columns list v_{mean} at $100m$ a.g. at the position of the 100m mast2 as simulated in WindSim and Meteodyn runs S1–S5. Here the climatology of the 100m mast2 was used to scale the model.

Tab. 7.5: Annual mean wind speed at $100m$ a.g. at two different locations of the S-Location site as measured and simulated by Meteodyn runs S1-S5 and WindSim, where the measurements at $100m$ a.g. of the 100m mast1 and the 100m mast2 served as the reference climatologies in Meteodyn.

position	**measured**	**100m mast1 (ms^{-1})**						**100m mast2 (ms^{-1})**					
		WS	S1	S2	S3	S4	S5	WS	S1	S2	S3	S4	S5
100m mast1	6.0	–	–	–	–	–	–	5.4	5.5	6.3	5.9	6.0	6.0
100m mast2	5.6	6.0	6.2	5.5	5.9	5.6	5.7	–	–	–	–	–	–

The long-term corrected measured mean wind speed values at the 100m mast1 and 100m mast2 are $6.0ms^{-1}$ and $5.7ms^{-1}$. The modelled values of WindSim are $0.6ms^{-1}$ lower and $0.4ms^{-1}$ higher as can be seen in Table 7.6. The five Meteodyn runs range between $5.5ms^{-1}$ (S1) and $6.3ms^{-1}$ (S2) for v_{mean}. The differences between the simulated and measured values of WindSim and Meteodyn are given in Table 7.6.

Tab. 7.6: Differences between measured and modelled values of WindSim and Meteodyn runs in Table 7.5 as absolute value and in percent of measured values at the S-Location site.

position		**100m mast1**						**100m mast2**					
		WS	S1	S2	S3	S4	S5	WS	S1	S2	S3	S4	S5
100m mast1	ms^{-1}	–	–	–	–	–	–	0.6	0.6	−0.2	0.1	0.0	0.0
100m mast2		−0.4	−0.6	0.1	−0.4	0.0	−0.1	–	–	–	–	–	–
100m mast1	%	–	–	–	–	–	–	10.0	10.0	−3.3	1.7	0.0	0.0
100m mast2		−7.1	−10.7	1.9	−7.1	1.9	−1.4	–	–	–	–	–	–

7.2.2 Vertical Wind Profiles

Figure 7.6 shows the simulated vertical wind profiles of Meteodyn runs S1–S5 between $5m$ and $120m$ a.g. in green and blue colours at the 100m mast1 (a) and the 100m mast2 (b). The black line gives the long-term corrected v_{mean} at $66m$, $86m$ and $100m$ a.g. at the same positions. The horizontal lines indicate the standard deviation of the time series. The profiles of the different runs show smaller differences at the 100m mast1 than at the 100m mast2. At the 100m mast1

the difference between run S1 and run S2 is less than $1.0ms^{-1}$ at all heights. At the 100m mast2 there is a difference of more than $1.5ms^{-1}$ in $20m$ a.g. and less than $1.0ms^{-1}$ in $110m$ a.g. between run S1 and S4. At the 100m mast1 the profiles of runs S1 and S2 do not match the measured profile while the others reproduce it relatively well. At the 100m mast2 all simulated profiles have a smaller vertical gradient of v_{mean} than the measured profile. Runs S2, S5 and S6 match the measured profile better than run S1 and S3 at that mast. The profiles of runs S1 and S2 are almost constant down to $15m$ a.g. while the other four show a difference of around $2ms^{-1}$ for v_{mean} between $5m$ and $120m$ a.g. at the 100m mast2. The profiles of runs S5 and S6 are similar for both masts. All simulated profiles lie inside the range of the standard deviation of the measured profile. Summing up, it can be said that Meteodyn performed good in predicting profiles of v_{mean}.

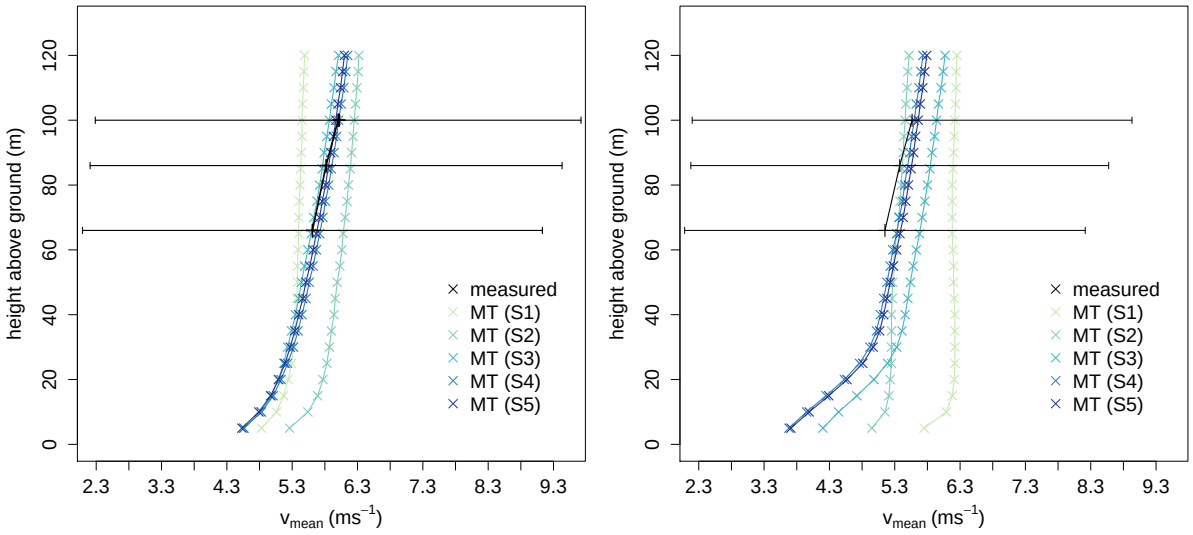

(a) 100m mast1 **(b)** 100m mast2

Fig. 7.6: Vertical wind profiles as measured (with one standard deviation whiskers) and simulated by Meteodyn runs S1–S5 at the 100m mast1 where the 100m mast2 climatology was the reference (a) and 100m mast2 where 100m mast1 climatology was the reference (b).

7.2.3 Two-dimensional Fields

In Figure 7.7 v_{moy} at $100m$ a.g. for the refinement area of the S-Location wind park is visualized. Figures 7.7 (a)–(d) show Meteodyn runs S1-S4. Run S5 shows a similar wind field as run S4 and can be found in the appendix (Fig. A.10 (a)). Figure 7.7 (e) is the wind field as simulated by WindSim. The highest values for v_{mean} are simulated at the two mountains where the wind turbines are located and at another lower mountain in the south west of the refinement area. The lowest values can be found in the forested valley in the north western part of the area.

Tab. 7.7: Minimum, maximum and mean values of v_{mean} in the refinement area of the S-Location wind park as simulated in the Meteodyn runs S1–S5 and the WindSim run.

statistic	**WS**	**S1**	**S2**	**S3**	**S4**	**S5**
minimum (ms^{-1})	1.0	1.6	1.0	0.8	0.8	0.8
maximum (ms^{-1})	6.3	5.9	6.2	6.3	6.2	6.2
mean (ms^{-1})	3.6	3.8	3.7	3.2	3.1	3.1

Table 7.7 lists the minimum, maximum and mean of v_{mean} calculated over all cells of the refinement area of the S-Location wind park as simulated in the Meteodyn runs S1–S5 and WindSim. Meteodyn runs S3, S4 and S5 show with $0.8ms^{-1}$ the lowest minimum values for the S-Location wind park. Meteodyn run S3 and WindSim simulate with $6.3ms^{-1}$ the highest maximum values. The mean calculated for the S-Location refinement area was highest in Meteodyn run S1 and lowest in runs S4 and S5.

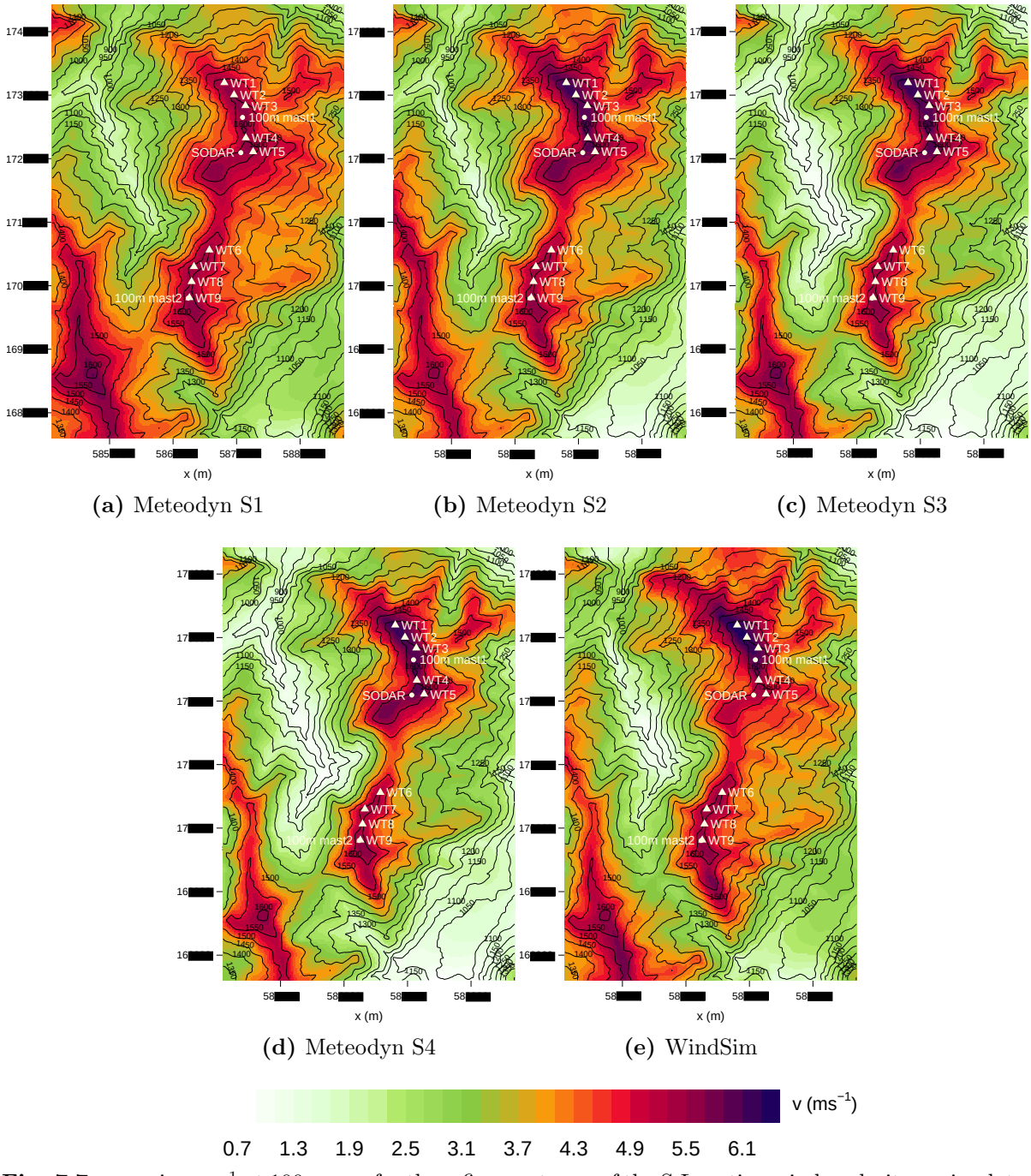

(a) Meteodyn S1 **(b)** Meteodyn S2 **(c)** Meteodyn S3

(d) Meteodyn S4 **(e)** WindSim

Fig. 7.7: v_{moy} in ms^{-1} at $100m$ a.g. for the refinement area of the S-Location wind park site as simulated by Meteodyn runs S1-S4 (a-d) and WindSim (e) (shaded). Triangles and circles indicate the position of wind turbines and measuring sites, respectively. The black lines are height contour lines with an equidistance of $50m$.

Figure 7.8 gives the differences between v_{moy} fields of the Meteodyn runs S1-S4 and the WindSim run. The same figure for Meteodyn run S5 shows again a similar pattern as run S4 and can

be found in the appendix (Fig. A.10 (b)). The position of highest and lowest maximum and minimum differences is similar for Meteodyn runs S3, S4 and S5 but different in Meteodyn runs S1 and S2. The values of these maxima and minima are given in the appendix (Tab. A.6).

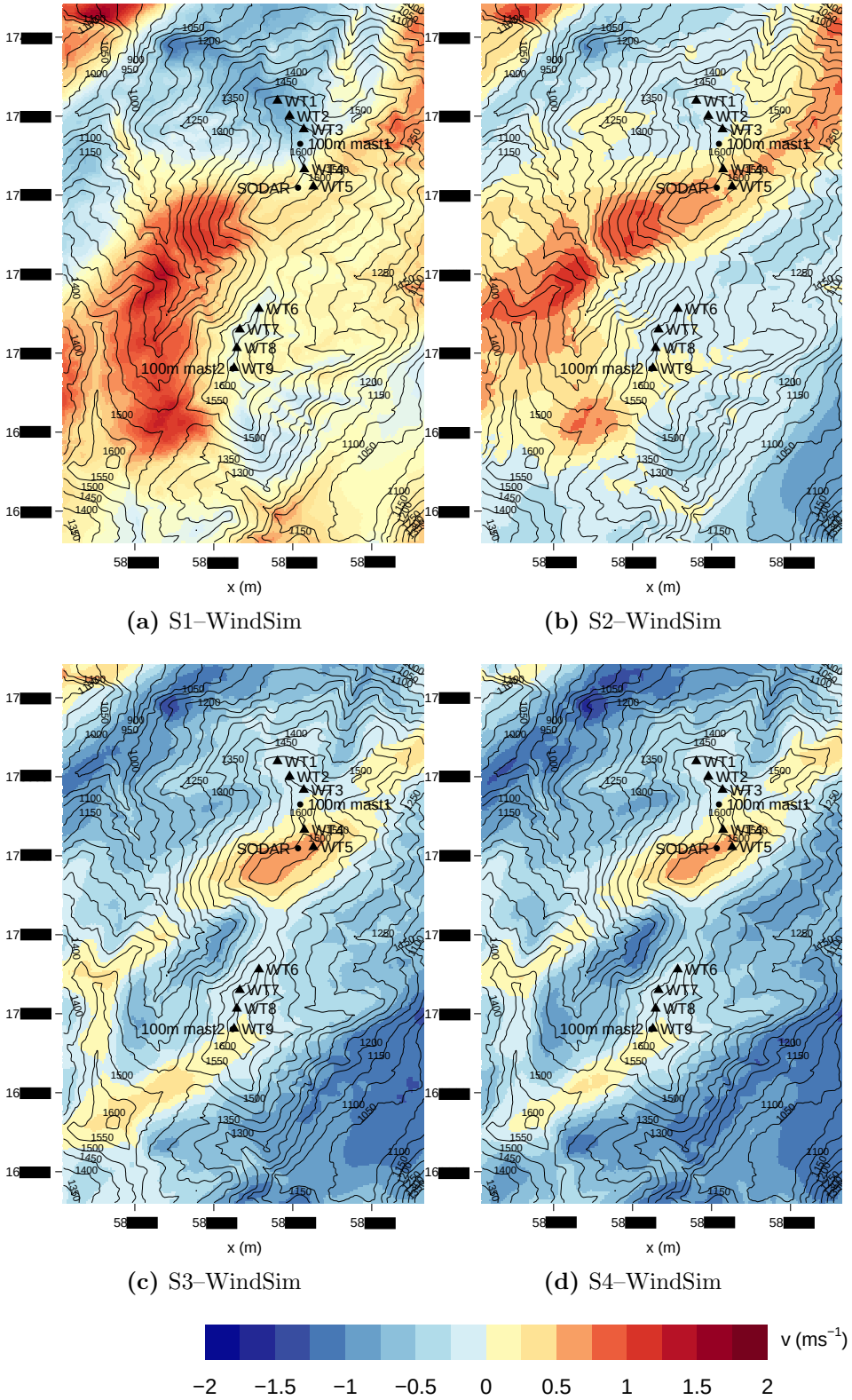

(a) S1–WindSim **(b)** S2–WindSim

(c) S3–WindSim **(d)** S4–WindSim

Fig. 7.8: Differences of v_{moy} in ms^{-1} calculated as Meteodyn–WindSim at $100m$ a.g. for the refinement area of the S-Location wind park (shaded). Each figure shows the differences between one of the Meteodyn runs S1-S4 and WindSim.Triangles and circles indicate the position of wind turbines and measuring sites, respectively. The black lines are height contour lines with an equidistance of $50m$.

7.2.4 Energy Production

Meteodyn predictions of $Prod_{moy}$ range between $36500 MWhy^{-1}$ and $36516 MWhy^{-1}$ without wake effect. The corresponding WindSim value is with $34670 MWhy^{-1}$ smaller than in all Meteodyn runs. The differences between Meteodyn and WindSim values range between $1208 MWhy^{-1}$ and $1860 MWhy^{-1}$ for runs S5 and S3. The values of runs S4 and S5 are almost equal. The wake effect is again bigger in Meteodyn than in WindSim. Therefore, the difference between Meteodyn and WindSim with wake effect are smaller than without wake effect (Tab. 7.8).

Tab. 7.8: Predicted $Prod_{moy}$ in Meteodyn runs S1–S5 and WindSim (with and without wake effect) and differences calculated as Meteodyn–WindSim.

		WS	**S1**	**S2**	**S3**	**S4**	**S5**
$\mathbf{Prod_{moy}}$ no wake	$(MWhy^{-1})$	34 670	36 702	36 735	37 126	36 500	36 516
$\mathbf{Prod_{moy}}$ wake		34 561	35 985	36 068	36 422	35 811	35 891
difference no wake		–	2032	2065	2456	1829	1786
difference wake		–	1424	1507	1860	1250	1208

7.2.5 Summary

In Section 7.2.1 it is shown that Meteodyn run S5 best reproduces measurements of v_{mean} but also the other Meteodyn runs and the WindSim run only show small differences to measurements. Section 7.2.2 gave evidence that the activation of the forest model was responsible for the good matching of modelled and measured vertical profiles of v_{mean} in Meteodyn runs S3, S4 and S5.

7.3 J-Location

7.3.1 Meteodyn Calibration: Atmospheric Stability

Figure 7.9 shows the measured and simulated vertical wind profiles of Meteodyn runs J1 and J2 between $5m$ and $120m$ a.g. for different stability classes at the position of the 50m mast1 ((a) and (c)) and 50m mast2 ((b) and (d)). The horizontal black lines show the standard deviation of the measured time series. Corresponding profiles of Meteodyn run J3 are similar to run J1 (without stability class 6). They can be found in the appendix (Fig. A.11). In general, at the 50m mast1 measurements are matched slightly better than at the 50m mast2 between $30m$ and $50m$. The measured value at $100m$ height is almost $1.0 ms^{-1}$ (run J2) and more than $1.0 ms^{-1}$ (run J1) higher than the simulated values. The profiles of run J2 better reproduce the measured values than the profiles of run J1 at both masts. The difference in v_{mean} between $5m$ and $30m$ a.g. is smaller for run J1 (about $1.5 ms^{-1}$ at the 50m mast1 and $2.0 ms^{-1}$ at the 50m mast2) than for run J2 (about $2.0 ms^{-1}$ at 50m mast 1 and $2.5 ms^{-1}$ at 50m mast 2). The profiles of the highest stability class are closest to the measured profiles in all Meteodyn runs. Based on these findings, the highest stability class (6 for J1, 5 for J2 and 4 for J3) should have been chosen for the simulation of the two-dimensional fields. Whether this choice would make sense on a physical basis is discussed in Section 8.7.

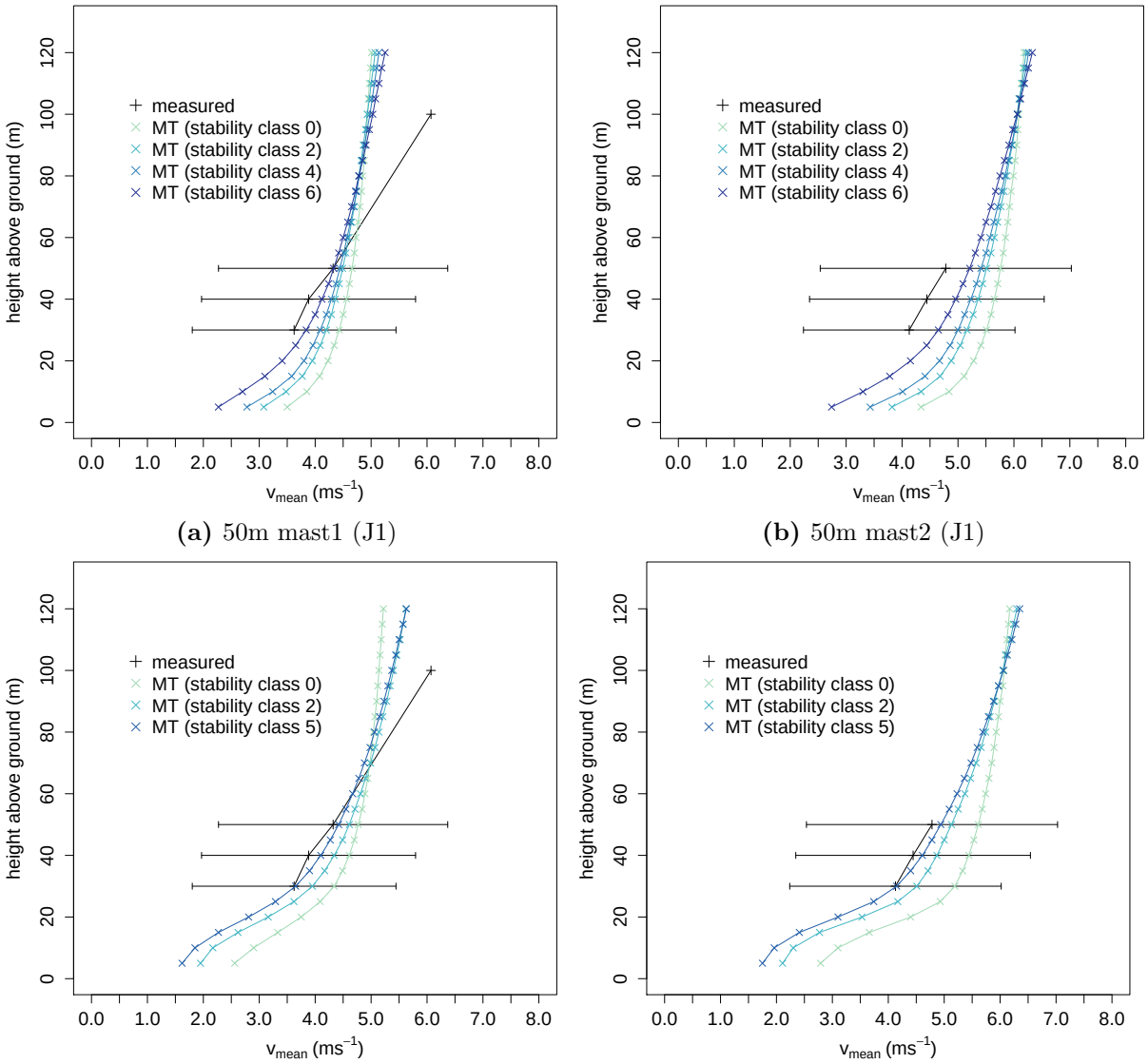

(a) 50m mast1 (J1)

(b) 50m mast2 (J1)

(c) 50m mast1 (J2)

(d) 50m mast2 (J2)

Fig. 7.9: Vertical wind profiles as measured (with one standard deviation whiskers) and simulated by Meteodyn runs J1 and J2 at the 50m mast1 where the 50m mast2 climatology was the reference (a, c) and at the 50m mast2 where the climatology of 50m mast1 was the reference (b, d).

To account for directional differences concerning the stability class, measured and simulated mean wind velocities are compared at the reference heights of the input climatologies at the 50m mast1 and 50m mast2 (Fig. 7.10 (a) and (b)).

Tab. 7.9: Stability classes for J-Location runs J1-J3 that produced the smallest difference between measured and simulated v_{mean} for each wind direction sector. The first value in each column corresponds to 50m mast1 and the second to 50m mast2. The sectors for which the chosen stability class differs at both masts is marked red.

run	30°	60°	90°	120°	150°	180°	210°	240°	270°	300°	330°	360°
J1	6|4	6|2	4|4	6|6	6|0	0|0	4|2	6|6	6|6	6|6	6|2	6|6
J2	0|0	2|2	5|5	5|5	2|5	0|0	2|5	5|5	5|0	5|5	0|2	0|0
J3	0|0	0|0	4|4	2|2	0|0	0|0	2|2	4|4	4|4	4|4	2|2	0|0

Corresponding directional plots of J1 and J3 are visualized in Figure A.12 in the appendix.

Table 7.9 lists the stability class that produced the smallest difference between measured and simulated v_{mean} for each wind direction sector and Meteodyn run at the 50m mast1 and the 50m mast2.

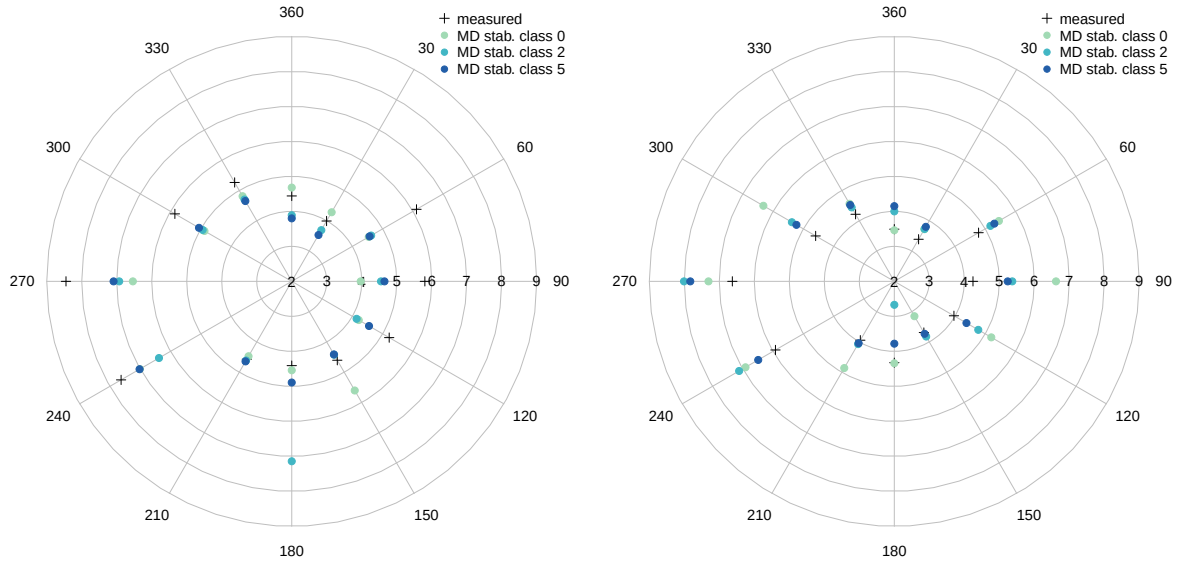

(a) 50m mast1 **(b)** 50m mast2

Fig. 7.10: Measured and simulated (Meteodyn run J2) directional mean wind speed in $100m$ a.g. at the 50m mast1 where the 50m mast2 climatology was the reference (a) and $50m$ a.g. at the 50m mast2 where the 50m mast1 climatology was the reference (b). On the x-axis the wind speed values of the grey circles are given in ms^{-1}.

The chosen stability classes are not the same at both masts for some wind direction sectors in runs J1 and J2 (red marked). Run J3 (which has a higher grid resolution) shows the same stability classes at both masts. For westerly and easterly wind directions the stability classes are higher than for northerly and southerly stability classes. A meteorological explanation for this might be that in a west to east cross-section the masts are located slightly lower than the surrounding area. This could result in less mixing of the air masses and a more stable atmosphere. Moving from north to south the masts are located higher than the surrounding area. Well mixed unstable or near neutral air can be transported towards the masts. The masts reach up to $50m$ a.g. It is expected that this effect cannot be so strong that a stable atmosphere is dominating at the mast top. In Section 8.7 it is discussed why a mean near neutral atmosphere is more likely for the J-Location wind park. For the simulation of the two-dimensional field of v_{moy} only the climatology at $100m$ at the 50m mast1 is used to scale the model. Therefore the first stability class in each column in Table 7.9 was used for runs J1–J3.

7.3.2 Cross Checking

In Table 7.10 the results of the cross checking procedure for the WindSim run and Meteodyn runs J1–J3 of the J-Location case study are listed. In Table 7.11 differences between measured and modelled Meteodyn and WindSim v_{mean} can be found. Meteodyn run J2 matches the measurements better than the WindSim run at both masts while runs J1 and J3 are worse. All model runs underestimate measurements at the 50m mast1 and overestimate the ones at 50m mast2. Measurements at the 50m mast are reproduced slightly better. The second column gives v_{mean} at $100m$ and $50m$ a.g. for the 50m mast1 and 50m mast2. In the third column v_{mean} in $100m$ and $50m$ a.g. at the position of the 50m mast1 is shown. Here the climatology of the 50m

mast2 was used to scale the directional computation results in WindSim.

Tab. 7.10: Annual mean wind speed in ms^{-1} at two different locations at the J-Location site as measured and simulated by Meteodyn runs J1-J3 and WindSim. The measurements at $50m$ a.g. of the 50m mast2 and the extrapolated values up to $100m$ from the 50m mast1 served as the reference climatology in Meteodyn respectively.

position	**measured**	**50m mast1 (ms^{-1})**				**50m mast2 (ms^{-1})**			
		WS	J1	J2	J3	WS	J1	J2	J3
50m mast1	6.1	–	–	–	–	5.4	5.1	5.5	5.0
50m mast2	4.8	5.6	5.7	5.5	5.9	–	–	–	–

Columns four to six show respective values as simulated in Meteodyn runs J1–J3. The last four columns list v_{mean} at $100m$ a.g. at the position of the 50m mast2 as simulated in WindSim and Meteodyn runs. Here the climatology of the 50m mast2 was used to scale the model.

Tab. 7.11: Differences between measured and modelled values in table 7.10 as absolute value and in percent of measured value at the J-Location site.

position		**50m mast1**				**50m mast2**			
		WS	J1	J2	J3	WS	J1	J2	J3
50m mast1	ms^{-1}	–	–	–	–	0.7	1.0	0.6	1.1
50m mast2	ms^{-1}	−0.8	−0.9	−0.7	−1.1	–	–	–	–
50m mast1	%	–	–	–	–	11.5	16.4	9.8	18.0
50m mast2	%	−16.7	−18.8	−14.6	−22.9	–	–	–	–

7.3.3 Vertical Wind Profiles

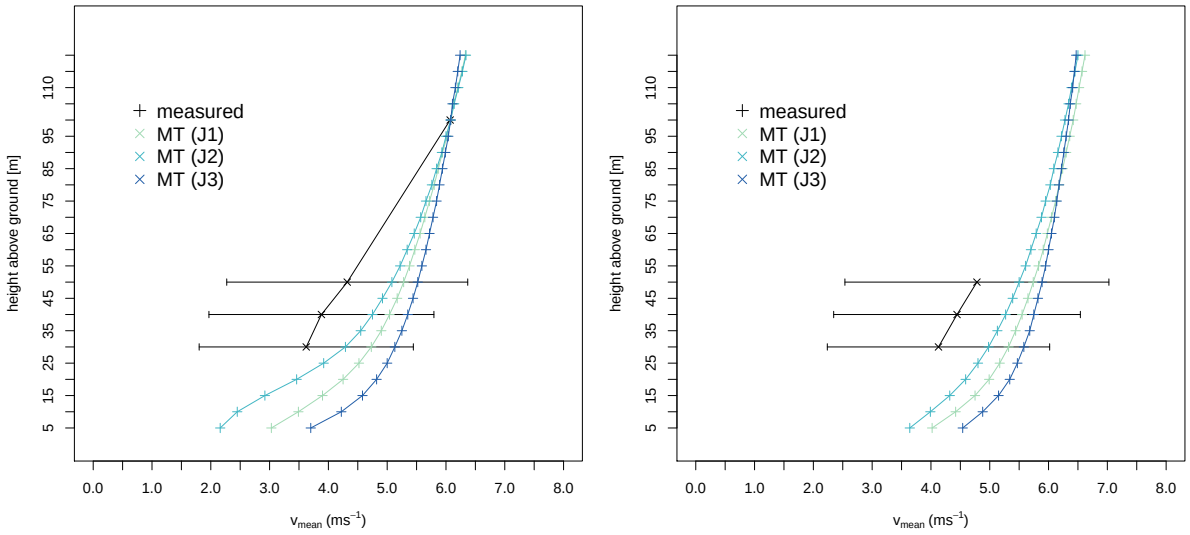

(a) 50m mast1 **(b)** 50m mast2

Fig. 7.11: Vertical wind profiles as measured (with one standard deviation whiskers) and simulated by Meteodyn runs J1–J3 at the 50m mast1 (a) and the 50m mast2 (b). The 50m mast1 climatology that was extrapolated to $100m$ a.g. was used as the reference at both masts.

Figure 7.11 shows measured and modelled (Meteodyn runs J1–J3) mean vertical wind profiles of the 50m mast1 and the 50m mast2. The measured profiles (black line) show the standard deviation for $30m$, $40m$ and $50m$ height a.g. as horizontal whiskers. None of the Meteodyn runs can reproduce the measured profiles neither at the 50m mast1 nor at the 50m mast2. Meteodyn run J2 is closest to the measured profiles. Nevertheless, all three runs still lie inside the standard deviation whiskers. The exact match of modelled and measured v_{mean} at $100m$ in Figure 7.11 cannot be accepted as successful simulation. It is nothing else than the mean of the reference climatology at its input point.

7.3.4 Two-dimensional Fields

In Figure 7.12 v_{moy} at $95m$ a.g. for the refinement area of the S-Location wind park can be seen. Figures (a)–(c) show Meteodyn runs J1-J3. Figure 7.12 (d) is the wind field as simulated by WindSim.

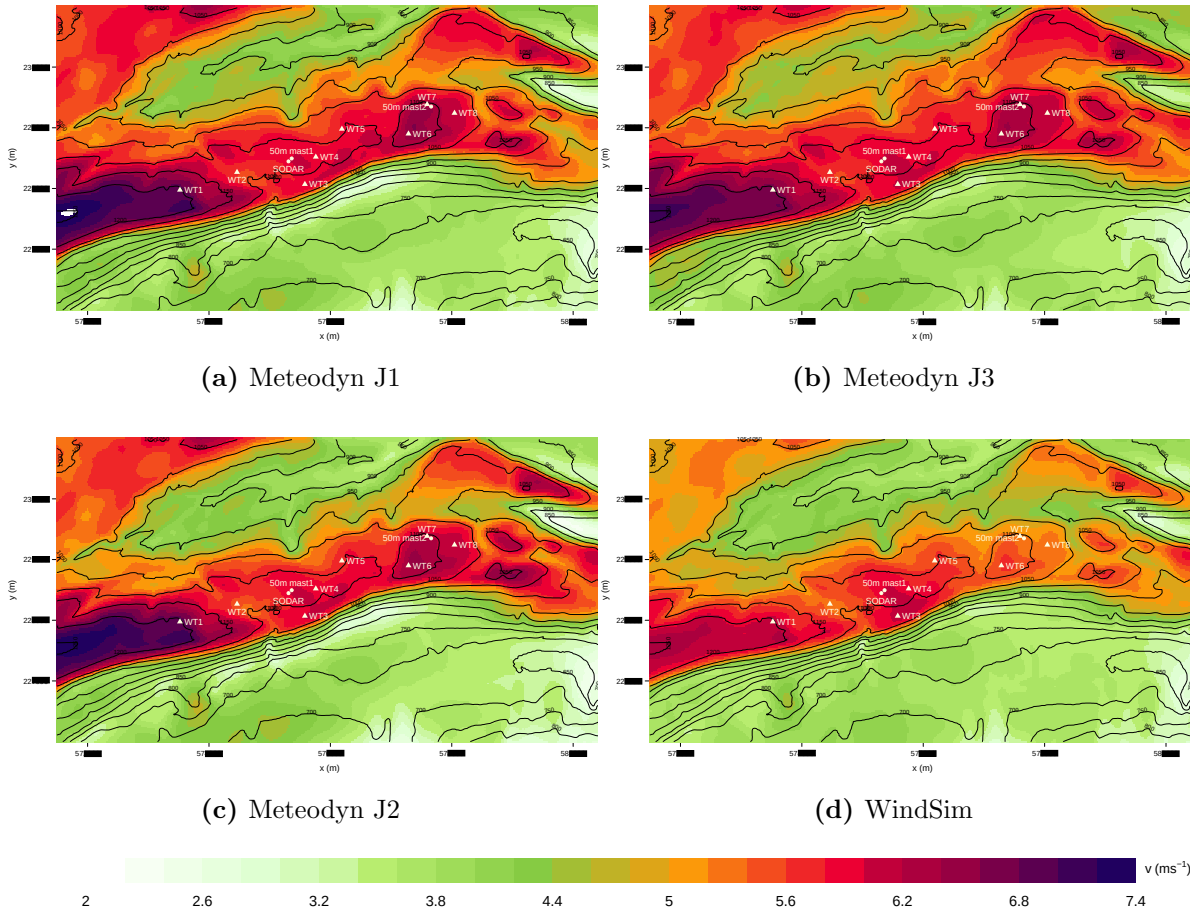

(a) Meteodyn J1 **(b)** Meteodyn J3

(c) Meteodyn J2 **(d)** WindSim

Fig. 7.12: v_{moy} in ms^{-1} at $95m$ a.g. for the refinement area of the J-Location wind park site as simulated by Meteodyn runs J1-S3 (a-d) and WindSim (e) (shaded). The triangles and circles indicate the position of the wind turbines and measuring sites, respectively. The black lines are height contour lines with an equidistance of $50m$.

The highest values for v_{mean} can be found east of WT1 in all Meteodyn runs and WindSim. The lowest values are simulated in the partly forested and much lower located region in the north western part of the refinement area. Table 7.12 lists corresponding minimum, maximum and also mean values calculated over all cells of visualized fields in Figure 7.12. Run J2 simulates

the lowest minimum values of $2.3ms^{-1}$ for the J-Location wind park. In runs J1 and J2 the highest maximum values occur with $7.4ms^{-1}$.

Tab. 7.12: Minimum, maximum and mean values of v_{mean} in the refinement area of the J-Location wind park as simulated in the Meteodyn runs J1–J3 and the WindSim run.

statistic	**WS**	**J1**	**J2**	**J3**
minimum (ms^{-1})	2.6	2.6	2.3	2.6
maximum (ms^{-1})	6.4	7.4	7.4	7.1
mean (ms^{-1})	4.4	4.8	4.7	4.9

The mean calculated for the J-Location refinement area was highest in Meteodyn run J3 and lowest in WindSim. Figure 7.13 shows the differences between v_{moy} fields of the Meteodyn runs J1-J3 and WindSim. v_{moy} was lower in all Meteodyn runs compared to WindSim for a large part of the refinement area.

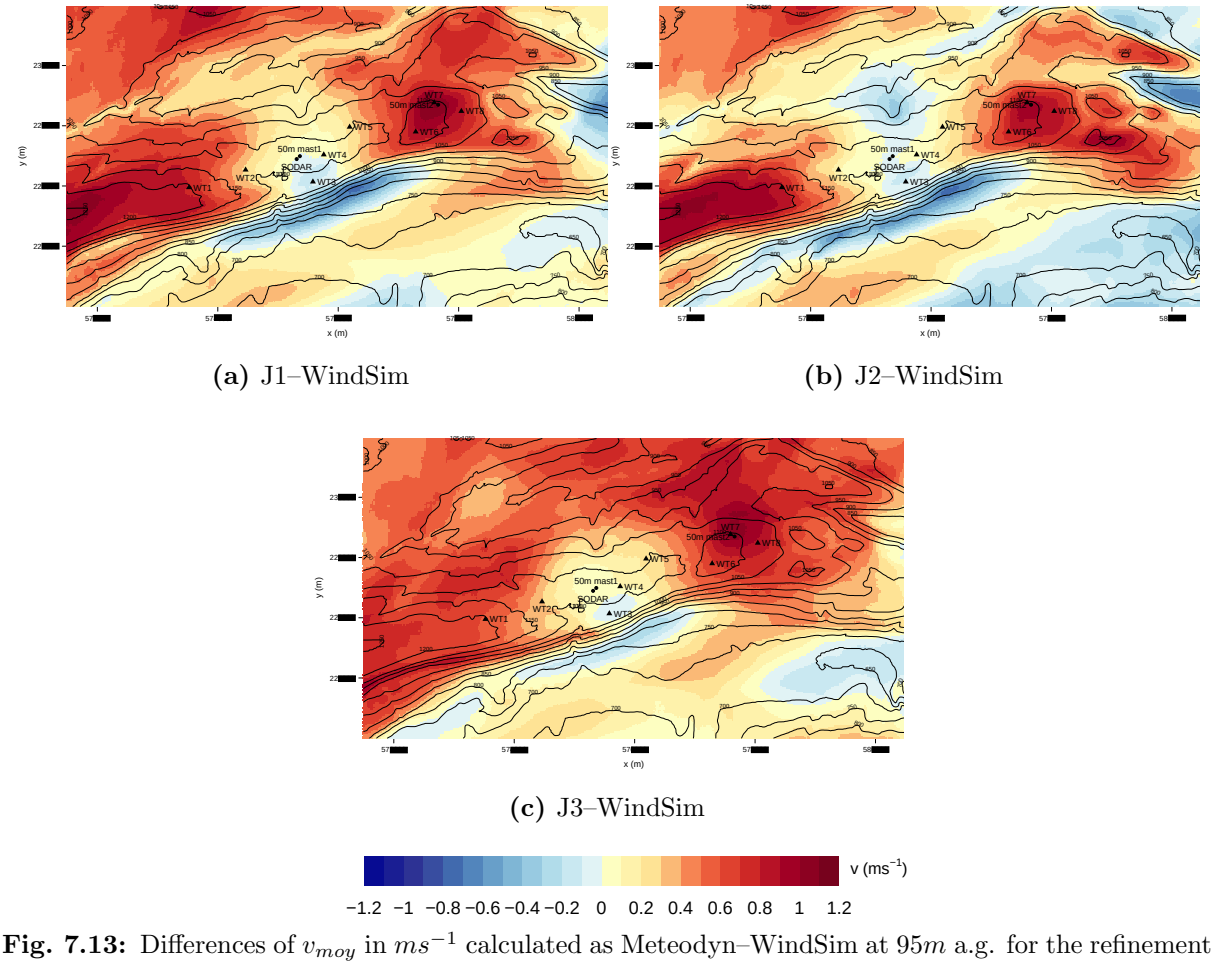

(a) J1–WindSim

(b) J2–WindSim

(c) J3–WindSim

Fig. 7.13: Differences of v_{moy} in ms^{-1} calculated as Meteodyn–WindSim at $95m$ a.g. for the refinement area of the J-Location wind park site (shaded). Each figure shows the differences between one of the Meteodyn runs J1-J3 and WindSim. The triangles and circles indicate the position of the wind turbines and measuring sites, respectively. The black lines are height contour lines with an equidistance of $50m$.

Figure 7.13 (b) shows only slight differences in most of the refinement area. In general, differences are small with values ranging between $0.2ms^{-1}$ and $-0.2ms^{-1}$ around the 50m mast1 and in

the north western area. The locations of lowest negative and highest positive difference between WindSim and the Meteodyn runs differ. Corresponding values are given in Table A.7.

7.3.5 Energy Production

Meteodyn and WindSim predictions of $Prod_{moy}$ show with values between $136 MWhy^{-1}$ (J1-WindSim) and $-603 MWhy^{-1}$ (J2-WindSim) very small differences without wake effect. As the wake effect is much higher in all Meteodyn runs than in WindSim there are differences around $-2000 MWhy^{-1}$ between $Prod_{moy}$ of Meteodyn and WindSim. WindSim and Meteodyn run J1 show the closest values (Tab. 7.13).

Tab. 7.13: Predicted $Prod_{moy}$ in Meteodyn runs J1–J3 and WindSim and differences calculated as Meteodyn–WindSim.

		WS	**J1**	**J2**	**J3**
$Prod_{moy}$ no wake	**($MWhy^{-1}$)**	39 404	39 540	38 801	39 263
$Prod_{moy}$ wake		37 949	36 044	35 550	35 674
difference no wake		–	136	−603	−141
difference wake		–	−1905	−2399	−2275

7.3.6 Summary

Meteodyn run J2 showed the smallest differences to measurements of v_{mean} although they are still relatively high (Sec. 7.3.2). It was also shown that reproducing the measured vertical profiles of v_{mean} failed (Fig. 7.11) as long as a high stability class is not chosen for all wind direction sectors (Fig. 7.9), for which there is poor meteorological justification. The better results of run J2 compared to runs J1 and J3 can be explained with the activation of the forest model (see Table 4.10).

8. Discussion

8.1 On the validity of the steady state assumption

RANS CFD models assume stationary flow fields. Based on findings of Maurizi *et al.* (1998) and Castro *et al.* (2008), Palma *et al.* (2008) raised concerns about the use of steady state models in complex topography. Recirculation evolves when a negative pressure anomaly downstream of a hill results in a reversed flow direction close to the ground. This causes production of vorticity and flow separation in the region where the down-slope flow and the reversed up-slope flow converge (Wood, 1995). Recirculating flows are highly unsteady structures which cannot be captured by RANS CFD models. When a wind turbine is located in or near to a recirculation zone, hub height wind velocities that have been predicted by RANS CFD models might be overestimated. Using methods that allow temporal flow evolution could be a better choice in this case. However, Palma *et al.* (2008) indicate that these methods (e.g. LES CFD models) are still too cost intensive for commercial use in wind energy assessment. In Bechmann *et al.* (2011) the group of LES CFD models performed worse than RANS CFD models but better than linear models in predicting speed-up factors. The simulation of the turbulent kinetic energy was almost equal in RANS and LES CFD models. The authors concluded that RANS CFD models still seem to be the best choice in wind energy assessment. For predictions of the turbulent kinetic energy they see LES CFD models as promising.
It is assumed that input climatologies and a higher grid resolution in a recirculation zone can reduce the modelling errors, which are a result of the steady state assumption. The model would be still not able to simulate the flow in this area but to adjust the mean modelled variables to measured ones.

8.2 Validity of Meteodyn v_{mean} and TI_{mean} predictions

The validity of v_{mean} can be considered from the absolute differences between measured and modelled values of the three wind parks. The five Meteodyn runs of the S-Location case study showed the lowest absolute differences of between $0.0 ms^{-1}$ and $0.6 ms^{-1}$ between measured and modelled values for v_{mean} (Tab. 7.6). In addition, the absolute differences of the T-Location case study (between $0.0 ms^{-1}$ and $1.5 ms^{-1}$ are found to be low for some runs and scaling climatologies but high for some others (Tab. 7.2). Furthermore, the J-Location case study showed relatively high absolute differences of between $0.6 ms^{-1}$ and $1.1 ms^{-1}$ for all Meteodyn runs (Tab. 7.11). These findings are somewhat unexpected as the J-Location site has the least complex terrain of the three sites. Therefore it could be assumed that Meteodyn should have less problems in reproducing measured v_{mean}. One explanation might be that there are steep forested slopes south of the J-Location wind park that resulted in wind field errors (Fig. 4.7). However, this is uncertain as there are no measurements in this region to confirm this statement. To understand

the meaning of these differences the reader has to keep in mind that the main task of a wind resource assessment CFD model is to estimate mean annual wind conditions at hub height to predict wind energy yields. Therefore the modelling errors can be interpreted in two ways.
First of all, the strength of the impact on the energy yield depends on the wind turbine type. If predicted mean wind speeds at a site are relatively low and near the cut in velocity of the chosen wind turbine type, a rather small prediction error can have a strong impact on predicted energy yields (Moreno *et al.* , 2003). If the mean wind speed is underestimated this could lead to no wind energy production at all during many hours of the year and the predicted energy yield will be largely underestimated. The wind park planner might decide not to build the park. If on the other hand it is overestimated, the turbine might operate more often in the prediction than in reality meaning the turbine might not be economically viable. In this case a small modelling error could have a big financial impact for wind park owners. To decide on the validity of the simulation results it would be necessary to take into account not only differences of v_{mean} but also discrepancies between measured and modelled Weibull distributions and their influence on different turbine types. However, this procedure is labour intensive and could fill another thesis.
The second possibility, the influence of wind speed on available wind energy E_{wind} for extraction by a wind turbine is therefore used to interpret the differences between measured and modelled v_{mean}. It can be described by Equation 8.1 where P_{wind} is the power of the wind and t the time the wind is blowing with the wind speed (u) (Emeis, 2013).

$$E_{wind} = P_{wind}t = 0.5\rho A u^3 t \tag{8.1}$$

It can be seen that E_{wind} increases by the cube of u. Physically, a wind turbine can convert to electric energy up to $\frac{13}{27}$ of P_{wind} according to the "Betz limit" (Betz, 1926), although in reality they extract much less.
To illustrate the impact of v_{mean} on E_{wind}, the maximum difference between measured and modelled values at the sonic mast of the T-Location wind park will serve as an example. At this site $v_{mean} = 3.6ms^{-1}$ has been measured. The simulated value of Meteodyn run T3 that was scaled with the SODAR1 climatology is $1.5ms^{-1}$ higher. This means that the predicted E_{wind} is $\frac{5.1^3}{3.6^3} = 2.8$ times higher than it actually is at this site which would result in a severe overestimation of available wind energy. For the J-Location wind park the highest Meteodyn error of v_{mean} results in a 1.8 fold misjudgement of E_{wind}. On the contrary, the highest values from the S-Location site only result in a 1.35 fold misestimation of E_{wind} while the runs S4 and S5 reproduced measurements almost perfectly for both masts. The terrain at the J-Location site appears to be problematic for CFD models as all J-Location and also WindSim runs resulted in high errors. Meteodyn runs T1 and T4 yielded acceptable results for the T-Location wind park.
The validity of TI_{mean} can be analysed from the absolute differences between measured and modelled values at three heights at the 81m mast of the T-Location wind park. On the one hand, at $40m$ a.g. relative errors between 29.1% and 15.3% have been found (Fig. 7.1). At the other hand, errors were found to be much smaller at $60m$ and $80m$ a.g. Bechmann *et al.* (2011) found a mean relative error of 36.4% for predictions of k made by a group of six CFD models with a one equation turbulence closure scheme. Their lowest error was 34.2%. The relation between k and TI is given in Equation 6.3. Bourgeois *et al.* (2010) found relative errors of between 0.0% and 36.4% in complex terrain in Bosnia and Herzegovina. In Bourgeois *et al.* (2009) relative errors of between 0.0% and 66.7% are reported for a site in Croatia. The

relative modelling errors found in Meteodyn runs seem to be high but are still lower than values in other studies. The wrong estimation of turbulence intensity can result in a misclassification of the wind turbine class according to IEC 61400-1:2005(E) documented in IEC (2005). This would result in a faster degradation of the turbine rotor. The difference in TI between two turbulence classes is 2%. At hub height absolute differences between measured and modelled values of TI_{mean} are smaller than 2%. Therefore Meteodyn TI_{mean} predictions can still be seen as valid because they are good at hub height although they do not perform well at lower heights.

8.3 Meteodyn vs. WindSim

At the T-Location site, WindSim performed best for the cross checking in terms of number of predictions with the lowest difference. This becomes obvious by counting the red marked values in Table 7.2. Meteodyn runs T1 and T4 are also relatively close to predicted values. By looking at the differences in $Prod_{moy}$ between Meteodyn and WindSim with wake effect (Tab. 7.4), it can be said that even though WindSim performed better for the cross checking, the worse results of Meteodyn v_{mean} predictions do not have a big influence on $Prod_{moy}$. Meteodyn run T1 predicts approximately $300 MWhy^{-1}$ more than WindSim. For comparison: the annual total electricity consumption per capita in the EU was roughly $5MWh$ in 2010 (Bertoldi *et al.* , 2012). The cross checking results of the S-Location site are best for Meteodyn runs S4 and S5 (Tab.7.6). This is supported by looking at the vertical profiles in Figures 7.6 (a) and (b). At the J-Location site Meteodyn run J2 shows the best results for the cross checking closely followed by WindSim and Meteodyn runs J1 and J3. Nevertheless, none of the models were able to predict measurements very well. This can also be seen by looking at the modlled vertical profiles of v_{mean} in Figure 7.9. Especially at 50m mast2, even for run J2 they do not match measured profiles.
WindSim and Meteodyn cross checking results have to be seen under three limiting aspects. Firstly, the WindSim simulations are partly much older than Meteodyn simulations which were finished in 2015. The WindSim S-Location case study was finished in 2008, J-Location in 2011 and T-Location in 2014. Due to the ongoing development of the WindSim model, results could be better when the simulations would be ran again. Secondly, the goodness of CFD modelling results also depends on the user's modelling experience (Bechmann *et al.* , 2011). This was certainly much higher for the WindSim simulations. Besides from the differences in physical equations implemented in the models, furthermore the input data proceeding differs between Meteodyn and WindSim. For example, they require roughness and topography input data sets of different extent. Terrain smoothing methods and computational mesh generation is also not the same in Meteodyn and WindSim.
Considering these restrictions and the small number of case studies the comparison of the two models does not seem very reliable. Nevertheless, the models are designed for the same tasks and produce the same variables. Therefore, a concluding statement is tentatively made: Based on the cross checking results of v_{mean} discussed in this thesis, Meteodyn is seen as the slightly better choice for wind field simulations in complex terrain. Furthermore, the documentation of Meteodyn is much more detailed than the one of WindSim. It gives the user more insight into the model's physics and the possibility to estimate the uncertainty of the results.

8.4 Differences of $Prod_{moy}$ in Meteodyn and WindSim

The predictions of $Prod_{moy}$ for the S-Location wind park illustrates the points discussed in Section 8.2. Even if differences in v_{mean} at a particular site are small (like in WindSim and Meteodyn run S1), the impact on $Prod_{moy}$ can be large. The differences between $Prod_{moy}$ without wake effect in the Meteodyn runs and WindSim amount to approximately $2000 MWhy^{-1}$ (Tab. 7.8). On the one hand, this can be explained by differences in modelled values of the Weibull parameters (not shown in this work) while on the other hand, it may be explained by the differing fitting methods of the input and modelled climatology data to the Weibull distribution. In Figure 8.1 the Weibull distributions as fitted by WindSim and Meteodyn of the 100m mast1 and 100m mast2 climatologies of the S-Location site are shown.

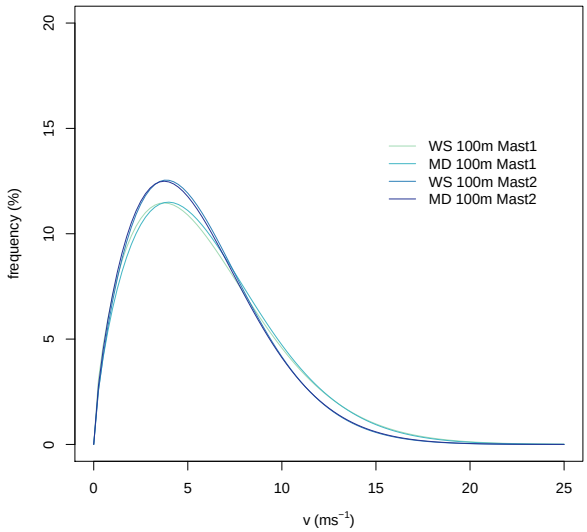

Fig. 8.1: Weibull distributions of the climatologies of 100m mast1 and 100m mast2 as fitted by Meteodyn and WindSim.

If these Weibull distributions were valid in hub height of an Enercon E82 wind turbine (power curve can be found in Figure 5.4) for $\rho = 1.225$, the difference in $Prod_{moy}$ would be approximately $50MWh$ and $3MWh$ between WindSim and Meteodyn for the 100m mast1 and 100m mast2 climatologies respectively. In Meteodyn, Weibull distributions are fitted with the maximum likelihood method (Meteodyn, 2015). The WindSim documentation does not report the method which was used.

For $Prod_{moy}$ with wake effect the difference is smaller because the wake effects are bigger at most turbines in all Meteodyn runs compared to WindSim for the S-Location wind park. The reason for that lies in the different formulations of c_k (see Table 3.1) which result in differences for c_{wake} (Eq. 3.1) between Meteodyn and WindSim. Figure 8.2 shows c_{wake} in Meteodyn and WindSim where $d_{rotor} = 82m$, $c_t = 0.45$ (valid for wind velocities around $5ms^{-1}$) and $z_{hub} = 100m$ are properties of an Enercon E82 wind turbine. x is set to $500m$. The Meteodyn curve is dependent on TI_{rotor}. It has values of around 0.15 for all turbines. The WindSim curve is dependent on z_0 which normally has low values between 0.01 and 0.1 near wind turbines because they are not located in forests or near other obstacles that could induce higher values for z_0. For the S-Location wind park this is the case for most of the cells near the turbines. There are only some single cells in the roughness data set that have higher values at some distance of the turbines. They are assumed not to have a big impact on ambient z_0 around the wind turbines. Therefore

the interval where c_{wake} is lower for Meteodyn than for WindSim is valid for the S-Location wind park resulting in larger wake effects in Meteodyn.

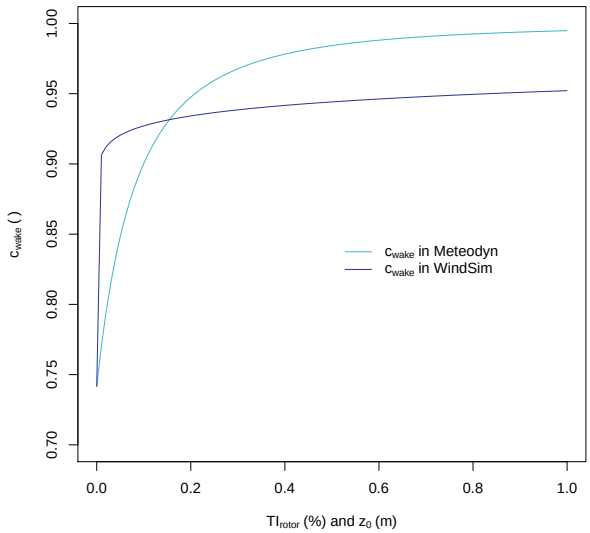

Fig. 8.2: c_{wake} in Meteodyn and WindSim at $500m$ distance of an Enercon E82 wind turbine of the S-Location wind park for $d_{rotor} = 82m$, $c_t = 0.45$, $z_{hub} = 100m$ and $x = 500m$.

8.5 Differences of v_{moy} between Meteodyn and WindSim

Differences in v_{moy} are smallest around the wind turbines in all WindSim and Meteodyn runs shown in this work. One reason for that is that the wind turbines are located at elevated sites with relatively homogeneous roughness values. A second reason is that the input location of the reference climatology for the simulation was always near the wind turbines except for turbines WT6–WT8 of the J-Location case study.

The aim of Meteodyn run T4 was to eliminate errors that could arise as a consequence of too small roughness and topography data sets. Actually runs T1–T3 show much higher differences compared to WindSim than run T4 although the extent of the input data was comparable in Meteodyn runs T1–T3 and WindSim (Fig. 4.2). This could be a hint that indeed, for very complex terrain, it is necessary to use bigger data sets in Meteodyn than in WindSim. The Meteodyn help facility does not give recommendations about the necessary extent of the input data.

The differences between Meteodyn and WindSim v_{moy} vary for the different Meteodyn runs of the T-Location case study. One pattern that appears in all difference plots are the negative values north of the mountain peak (higher v_{moy} in WindSim)(Fig. 7.3). The pattern of differences is not surprising because this region combines several terrain properties that are difficult to handle in CFD models. The area lies in between two narrow elongated hills with steep slopes and a very inhomogeneous surface. The comparison of Figures 4.3 and A.2 indicates the hills may be covered with debris and grass. As the dominating wind direction is SSW at this site, the trough is located in the lee of the mountain peak. It is likely that this is an area of enhanced recirculation and turbulence. Although CFD models are designed to handle such flow structures, the largest model errors can be found at the lee of hills and near steep slopes. Comparing a group of CFD models with a two equation turbulence closure (as WindSim belongs to) and a one equation turbulence closure (as Meteodyn belongs to) Bechmann *et al.* (2011) conclude

that the mean error of the first group is lower in the lee of a hill. At the luv side both groups performed well. This might be a hint that WindSim results are better in the lee of the mountain but it cannot be said for sure because no measurements are available in this area.
Another terrain structure that seems to be difficult to handle are steep forested slopes as can be found in the south east of the refinement area of the T-Location wind park and in the north western part of the refinement area of the S-Location wind park (Fig. 4.5).
WindSim predicted much lower values of v_{moy} than the different Meteodyn runs for more than half of the refinement area at the J-Location wind park site. These differences are mainly found north of the steep slope that divides the site. This terrain structure in combination with the dominating north-westerly wind direction (Fig. 5.3) leads to a disagreement of v_{moy} downstream of the scarp face in the two models. At the position of masts where the disagreement between the models is relatively low compared to the surrounding area, it is known from the cross checking that none of the models are able to reproduce measurements. It is therefore expected that if measurements would be available in the regions where WindSim and Meteodyn show big discrepancies, the modelling errors could even be bigger. In contrast to the T-Location wind park the models differ around the wind turbine locations in the J-Location wind park. A much higher resolution of the refinement area could possibly improve v_{moy} predictions.

8.6 TI_{moy} in Meteodyn and WindSim

Before any differences between Meteodyn and WindSim fields of TI_{moy} can be explained it has to be discussed whether they show the same variable and are therefore comparable at all. As already shown in Equations 6.2 and 6.3 there is a difference between the models' internal calculation of the variable TI_{moy}. It is not documented how to export the variable u_z, v_z and w_z in Meteodyn although it is calculated. Therefore it was not possible to remove w_z and recalculate TI_{moy} for Meteodyn according to the WindSim TI_{moy} in Equation 6.3.
The assumption that w_z can be neglected was made based on the following considerations. In a stable or neutral boundary layer in horizontal non-divergent flow mean w_z is approximately zero. In a convective boundary layer w_z has positive values in thermal updrafts near the surface and negative values higher up (Nieuwstadt and van Dop, 1982). As there is no heat conservation equation implemented in Meteodyn this phenomenon is not captured. In thunderstorms strong up- and downdrafts can occur but weather phenomena can also not be simulated in Meteodyn. Therefire, in a CFD model w_z only experiences substantial deviations from zero in recirculation zones and on steep slopes when the flow is forced to follow the surface structure. These effects decay with distance from the surface and should be negligible $80m$ a.g., which is the height at which TI_{moy} fields are compared between Meteodyn and WindSim. Based on this point of view, TI_{moy} should be comparable between Meteodyn and WindSim after the division of Equation 6.2 by $\sqrt{\frac{4}{3}}$ as explained in Section 6.6.
Another problem is that TI_{moy} is calculated from wind speeds higher than $10ms^{-1}$ which results in lower values for TI_{moy} than for the whole spectrum of wind speeds. As the WindSim help facility does not report such adjustments it is assumed that TI_{moy} is valid for the whole spectrum of wind speeds. This is seen as the main reason why WindSim TI_{moy} in Figure 7.5 (e) shows higher values than Meteodyn (Fig. 7.5 (a)-(d)). As long as it is not possible to export

Meteodyn TI_{moy} valid for the whole wind speed spectrum or adjust WindSim values according to the Meteodyn procedure, a comparison of TI_{moy} between the models is not meaningful.
The excluded regions in Figure 7.5 (e) showed $TI_{moy} > 40\%$ because these values were assumed to be overestimated. This threshold was made based on the maximum value of $TI = 34.95\%$ (valid for wind speeds $> 0ms^{-1}$) that was measured at $82m$ a.g. at the 81m mast and from findings in literature. Bourgeois *et al.* (2009) and Bourgeois *et al.* (2010) measured with a SODAR at $80m$ a.g values of 19% and 22% respectively, for the mean turbulence intensity plus one standard deviation. Their observations have been made at sites with complex topography for wind speeds higher than $4ms^{-1}$.
The four Meteodyn runs show varying patterns of TI_{moy} which are analysed in the following. As expected a zone of enhanced TI_{moy} is located in the lee of the mountain in all runs but with different intensity. As already explained in Section 8.5 there must be a recirculation zone at this location. In run T2 the forest model was activated which is the explanation for the higher TI_{moy} in the north-western and south-western as well as north-eastern corners of the refinement area. The isolated high TI_{moy} anomaly in the south of SODAR1 is located in the lee of a small forest north east of the anomaly. These patterns are also visible in runs T1 and T3 but much weaker. Run T4 does not show much variance of TI_{moy} for the refinement area. Measured $10min$ standard deviations in $80m$ a.g were fed into the model in runs T2–T4 for the location of the 81m mast. This was not done in run T1. TI_{moy} minima which can be seen very close to the 81m mast in Figures 7.5 (b) and (d) cannot be found in Figure 7.5 (a). In Figure 7.5 (c) the minimum is weaker. This anomaly decays at a distance of about $100m$ to the mast. It seems that the additional input data in runs T2–T4 only influenced TI_{moy} in the near neighbourhood of the mast.

8.7 Cost and benefits of the stability adjustment

For the stability adjustment in Meteodyn it is necessary to run the simulation for all wind direction sectors for different stability classes. This means that for three to four stability classes as in the J-Location case study it takes three to four times as much computation time as for one Meteodyn run of the other two case studies. The profiles of v_{mean} at the two 50m masts of the J-Location site are best matched for the higher stability classes (Fig. 7.9). As there was poor evidence that the mean atmospheric stratification is stable for all wind direction sectors this stability class was not chosen. At elevated, partly forested sites, near neutral atmospheric stratification is assumed because of a well mixed boundary layer. There was no data available to prove neither this assumption nor what the modelled vertical wind profiles suggest. For each wind direction sector the stability class which best fits measurements at $100m$ a.g. have been chosen instead (Fig. 7.10 and Tab. 7.9). As a consequence the directional mean profiles of v_{mean} in Figure 7.11 show worse results compared to the profiles of the highest stability class in Figure 7.9.
In the case where there would have been no stability adjustment, all profiles in Figure 7.11 would only show the profiles of stability class 2 in Figure 7.9 and A.11. The modelled profiles with stability class 2 match measured profiles slightly worse than the profiles in Figure 7.11 where a different stability class was chosen for each sector.
Therefore it is concluded that the time consuming procedure of the stability adjustment is

not worth the effort for the J-Location site. The stability adjustment only results in slight adjustments of v_{mean}. Is is much more important that the input surface roughness data set is reliable. It is assumed that the roughness was underestimated by the model as the vertical profiles of v_{mean} are shifted towards higher values compared to measured profiles. For runs J1 and J3 it would have been better to activate the forest model. In run J3 the measured and modelled profiles are closer (Fig. 7.9 (c) and (d). For this run the forest model is activated but modelled v_{mean} is still overestimated.

8.8 Cost and benefits of the forest model

The forest model was activated in Meteodyn runs T2, S3-S5 and J2. This improved the cross checking results compared to the other Meteodyn runs in the respective case studies in all runs except run T2. The terrain complexity (RIX) was highest at the T-Location site. One possible explanation might be that the errors were mainly induced due to the steep slopes at the site which could not be altered by the forest model. Another reason for the forest model not having an improving effect on the cross checking values, is certainly that there was less forest than at the J-Location and S-Location sites. The activation of the forest model made necessary that the smoothing was altered for some wind direction sectors to get convergent simulations. Therefore it cannot be said for sure that the improvement of the results only happened due to use of the forest model.

The activation of the forest model does not mean additional computational efforts. If the user wants to modify the forest density for different roughness classes this involves some additional work as the roughness data set has to be split into single data sets, each only including the cells where the forest density will be altered. This was only done at the S-Location site in Meteodyn run S5. It was not easy to choose the forest density classes without knowledge about the real vegetation densities at the site. The Meteodyn help facility gives no information what is seen a forest of "low" or "high" density. The cross checking results of runs S4 and S5 are similarly good. The vertical profiles of v_{mean} of runs S4 and S5 hardly show differences between the masts. It is therefore concluded that it is sufficient to set the forest density to normal for the complete roughness data set.

An activation of the forest model is necessary when there are some forested areas. If the model is not activated vertical profiles of v_{mean} are shifted to higher values as can be seen at the 100m mast2 in runs S1 and S2 in Figure 7.6 (b). The profiles of runs S1 and S2 also show a much smaller height gradient which is a result of the underestimation of the surface roughness. The difference between runs S1 and S2 and the other Meteodyn runs was small at the 100m mast1 where there was less forest cover than at the 100m mast2. Here the measured profile and the profiles of runs S3–S5 showed even larger values than Meteodyn run S1.

9. Conclusions

Meteodyn has been used to simulate the three-dimensional flow fields of three potential wind park sites of different terrain complexity in Switzerland. For each wind park several runs were conducted, not only to test different model settings but also to improve the simulation results compared to data of measurement campaigns which have been performed by the Bernese company Meteotest in the past. The improvement process was important because Meteodyn simulations were expected to be compared to WindSim simulations of the same sites to decide which model is more appropriate for the use in wind resource assessment especially in the very complex terrain of potential wind park sites in Switzerland. The WindSim simulations have been conducted by Meteotest prior to this work by more experienced CFD model users. Although this process was necessary, it also resulted in some limitations of this work. It was not easy to find reasons for the differences between the single runs of one wind park site without systematic sensitivity studies, which would have been very work intensive. Nonetheless based on the three WindSim runs and the twelve Meteodyn runs the following conclusions can be made.

The best and worse cross checking results showed relative errors of 0.00% and -38.5% while there was at least one run per wind park site that produced very good or acceptable results. Furthermore, simulated vertical wind profiles matched measured ones quite well except at 50m mast2 in the J-Location wind park. Therefore it can be said that Meteodyn can be used for simulating the flow in very complex (Swiss) terrain.

The T-Location wind park shows the most complex terrain among the three sites in this work. There WindSim reproduced better the measurements than all Meteodyn runs. For the S-Location site all of the Meteodyn runs but one, which was slightly worse, performed better than WindSim compared to measurements. At the J-Location site one of the Meteodyn runs fitted measurements the best, the other two were worse than WindSim. Although this wind park is located in the least complex terrain in terms of the ruggedness index, its very steep forested slopes dividing the area, induced modelling problems in WindSim and Meteodyn.

The fields of the mean annual wind speed (v_{moy}) showed differences between $-1.9ms^{-1}$ and $1.6ms^{-1}$ between Meteodyn and WindSim. Close to the measurement sites and wind turbines these differences were much smaller. This region is the most important for wind resource assessment so that the higher differences especially on steep slopes, at or in the luv of forest sites, in troughs or in the lee of mountains are of secondary importance.

Due to differences in v_{moy} and the parameters of the Weibull distributions between the models, WindSim and Meteodyn also predicted different values of the expected mean annual energy yield ($Prod_{moy}$). For the J-Location wind park the differences without wake effect are relatively small. They are bigger with wake effect. For the T-Location and S-Location wind park differences with wake effect are smaller than without wake effect. This occurred because of the different wake models in Meteodyn and WindSim. Within ranges of turbulence intensity at the position of the rotor and the roughness length (z_0), which are predominant near the wind turbines, the wind

speed reduction coefficient shows lower values in Meteodyn than in WindSim. This resulted in a bigger speed reduction in the wake in the Meteodyn runs. The differences are bigger or smaller with wake effect than without wake effect, dependent on the sign of the differences without wake effect. Among all runs of al case studies, for S-Location run S3 the highest difference was found for $Prod_{moy}$ without wake effect. It was approximately $2500 MWhy^{-1}$ lower in WindSim than in Meteodyn. This energy difference would be enough to meet the annual electricity demand of 500 average European households.

The computation-time demanding stability adjustment tilts vertical wind profiles and will therefore always improve cross checking results because the user can choose the profile that best fits measurements. However, without measurements to justify the choice of stability class at the site, this practice only results in the hedging of model results towards the measured data without physical explanation.

The mean annual turbulence intensity (TI_{moy}) and v_{moy} in Meteodyn (and WindSim) show local anomalies with enhanced or lowered values, respectively in areas of high z_0 (=forest or other high vegetation). As cross checking values and vertical wind profiles improved for the runs where the forest model was activated compared to measurements it is assumed that TI_{moy} is underestimated and v_{moy} is overestimated without the model in Meteodyn. The Meteodyn help facility does not tell the user that the forest model should not be switched off but the findings of this thesis showed that it should always be activated.

10. Outlook

To get rid of the limitation which results from using simulations that were performed with an old WindSim version but the newest Meteodyn version, the models could be compared again at the same sites. WindSim runs would then have to be performed in the latest model version and a final optimized Meteodyn run including all findings of this thesis would have to be conducted. The model settings responsible for the good results could not be find for all case studies in this thesis. Systematic sensitivity studies concerning mesh resolution, size of the variable *radius* and number of wind direction sectors could help to find the settings with the biggest influence on simulation results. This would be a very time intensive work.
In one case study it was assumed that the steep forested slope, which divides the area was responsible for the unsatisfactory cross checking results. This problem could probably be solved by enhancing the resolution of the refinement area. It was not done in this work due to CPU limitations. Problems in CFD models that evolve from coarse grid resolution could soon be solved by growing CPU resources of computers, anyway. This will also make the use of LES CFD models, which are still very computation time intensive, more affordable. In the near future, LES CFD models could replace RANS CFD models. As the unsatisfactory results at the steep forested slopes could also be a result of the steady state assumption in RANS CFD models, LES CFD models could be more suitable at this site.
There was no data available to determine the atmospheric stability for the case studies of this work. If it could be proven that indeed the atmosphere is often stable at the sites there would be a physical explanation for the improved vertical wind profiles compared to measurements for high stability classes. Conducting an additional long measurement campaign to determine the atmospheric stability at the sites, would be an expensive solution. Using mesoscale reanalysis data as reported in Albrecht *et al.* (2014) is probably the better choice.
The wind park sites of this work have been chosen because they are located in very complex terrain and measurement data for at least two sites was available. One important limitation to evaluating the simulated fields of v_{moy} and TI_{moy} in this work was the lack of measurements. The biggest differences between the models occurred at steep forested slopes and in the lee of mountains. As these areas are not interesting for wind turbine placement, no mast measurements have been made there. Nevertheless it would have been useful to have a data base to answer the question if both models failed in predicting the flow in these problematic areas or if one of them performed better. To answer this question the models could be compared by using the publicly available data from the field campaigns of the Bolund Experiment described in Bechmann *et al.* (2011) and Berg *et al.* (2011) or of Askervein Hill described in Taylor and Teunissen (1983) and Taylor and Teunissen (1985) where data of more measurements locations is available.

Acknowledgements

This Master thesis was written in cooperation with the Wind Energy Group of Meteotest (Bern), which operates independently in the field of wind resource assessment in Switzerland and other European countries. Meteotest uses WindSim since 2001 for wind resource assessments. This Master Thesis provides a base of decision for Meteotest to decide which CFD software should preferably be used in the future.
As this thesis contains material concerning ongoing wind park projects, site names and coordinates are altered and partly blackened in the online version of this master thesis.

I want to thank Meteotest for the great opportunity of writing a thesis about an applied research topic and the great birthday cheese.

I also want to thank...

...my supervisors Dr. Saskia Bourgeois and Prof. Dr. Olivia Romppainen-Martius for always encouraging me in asking questions and for giving advice during the last year.

...my advisor Dr. Paul Froidevaux for his useful hints about the structure and scientific style of my thesis.

...Sarah Koller who patiently answered my numerous questions about the wind park projects conducted by Meteotest.

... Tanja Humar-Mägli for preparing and converting data for me.

... Adrian Schossig and Stéphanie Arcusa for proofreading my thesis.

... my family and friends for all kinds of support during the five years of my university time.

List of Figures

List of Tables

Bibliography

Albrecht, C., Delaunay, D., Grötzner, A., Kohlert, M., and Pauscher, L. 2014. Atmospheric Stability: General Classificatin and Simulation in Meteodyn WT. *European Wind Energy Association Annual Event 2014, Barcelona.*

Arritt, R. W. 1987. The Effect of Water Surface Temperature on Lake Breezes and Thermal Internal Boundary Layers. *Bound.-Layer Meteor.*, **40**, 101–125.

Ayotte, K. W. 2008. computational Modelling for Wind Energy Assessment. *J. Wind Eng. Ind. Aerodyn.*, **96**, 1571–1590.

Barthelmie, R. J., Rathmann, O., Frandsen, S. T., Hansen, K., Politis, E., Prospathopoulos, J., Rados, K., Cabezon, D., Schlez, W., Phillips, J., Neubert, A., Schepers, J. G., and van der Pijl, S. 2007. Modelling and Measurements of Wakes in Large Wind Farms. *J. Phys. Conf. Ser.*, **75**, 1–9.

Barthelmie, R. J., Hansen, K., Frandsen, S. T., Rathmann, O., Schepers, J. G., Schlez, W., Phillips, J., Rados, K., Zervos, A., Politis, E. S., and Chaviaropoulos, P. K. 2009. Modelling and Measuring Flow and Wind Turbine Wakes in Large Wind Farms Offshore. *Wind Energ.*, **12**, 431–444.

Bechmann, A., Sørensen, Berg, J., Mann, J., and Réthoré, P.-E. 2011. The Bolund Experiment, Part II: Blind Comparison of Microscale Flow Models. *Bound.-Layer Meteor.*, **141**, 245–271.

Berg, J., Mann, J., Bechmann, A., Courtney, M. S., and Jørgensen, H. E. 2011. The Bolund Experiment, Part I: Flow Over a Steep, Three-Dimensional Hill. *Bound.-Layer Meteor.*, **141**, 219–243.

Bertoldi, P., Hirl, B., and Labanca, N. 2012. *Energy Efficiency Status Report 2012 - Electricity Consumption and Efficiency Trends in the EU-27.* Luxembourg: Publications Office of the European Union.

Betz, A. 1926. *Wind-Energie und ihre Ausnutzung durch Windmühlen.* Göttingen: Vandenhoeck and Ruprecht.

Bourgeois, S., Cattin, R., Winkelmeier, H., and Locker, I. 2009. CFD Modeling of the Vertical Wind Profile and the Turbulence Structure above Complex Vertical Terrain and Validation with SODAR and LIDAR Measurements. *European Wind Energy Conference 2009, Marseille.*

Bourgeois, S., Winkelmeier, H., and Meissner, C. 2010. Turbulence Intensity and High Wind Speeds above Complex Terrain: Measurements and CFD-Modelling. *DEWEC German Wind Energy Conference 2010, Bremen.*

Bowen, A. J., and Mortensen, N. G. 1996. Exploring the Limits of WA^{s}P the Wind Atlas Analysis and Application Program. *Proceedings of the European Union Wind Energy Conference, Gøteborg*, 584–587.

Brower, M. C. 2012. *Wind Resource Assessment. A Practical Guide to Developping a Wind Project.* Hoboken: John Wiley and Sons Inc.

Büttner, G., Kosztra, B., Maucha, G., and Pataki, R. 2012. *Implementation and Achievements of CLC2006.* Tech. rept. European Environment Agency (EEA).

Castro, F. A., Palma, J.M.L.M, and Silva Lopes, A. 2008. Simulation of the Askervein Flow. Part 1: Reynolds Averaged NavierStokes Equations ($k - \epsilon$ Turbulence Model). *Boundary-Layer. Meteorol.*, **107**, 501–530.

Cattin, R., Schaffner, B., Buzzi, M., and Kunz, S. 2002. Wind modeling in mountainous terrain: validation by SODAR. *DEWEC German Wind Energy Conference 2002, Wilhelmshaven.*

Christiansen, M. B., and Hasager, C. B. 2005. Wake Effects of Large Offshore Wind Farms Identified from Satellite SAR. *Remote Sens. Environ.*, **98**, 251–268.

Dierer, S., Mägli, T., and Cattin, R. 2008. *Windenergie-Projekt* [redacted]*, Kanton Freiburg. Windgutachten und Ertragsprognosen.* Bern: Meteotest.

Draxl, A., and Mayr, G. J. 2011. Meteorological Wind Energy Potential in the Alps using ERA40 and Wind Measurement Sites in the Tyrolean Alps. *Wind Energ.*, **14**, 471–489.

Dyer, A. J., and Hicks, B. B. 1970. Flux-gradient relationships in the Constant Flux Layer. *Quart. J. Roy. Meteor. Soc.*, **96**, 715–721.

EEA. 2015. *Corine land cover 2006 (CLC2006) 100 m - version 12/2009 of the Euorpean Environment Agency.* `http://www.eea.europa.eu/data-and-maps/data/corine-land-cover-2006-clc2006-100-m-version-12-2009`. Access: 2015-02-18.

Eidsvik, K. J. 2005. A Syste, Model for Wind Power Estimation in Mountainious Terrain. Prediction of Askervein Hill Data. *Wind Energ.*, **8**, 237–249.

El Kasmi, A., and Masson, C. 2010. Turbulence Modeling of Atmopheric Boundary Layer Flow over Complex Terrain: a Comparison of Models at Wind Tunnel and Full Scale. *Wind Energ.*, **13**, 689–704.

Emeis, S. 2013. *Wind Energy Meteorology. Atmospheric Physics for Wind Power Generation.* Berlin: Springer.

Federal Ministry for the Environment, Natures Conservation, Building and Nuclear Safety (BMUB). 2002. Erste Allgemeine Verwaltungsvorschrift zum Bundes-Immissionsschutzgesetz (Technische Anleitung zur Reinhaltung der Luft - TA Luft). *GMBl*, **25–29**, 511–605.

Frandsen, S. T. 2007. Turbulence and Turbulence-generated Structural Loading in Wind Turbine Clusters. *Risø Technical Report*, R–1188(EN).

Garratt, J. R. 1999. *The Atmospheric Boundary Layer.* New York: Cambridge University Press.

Gobbi, M. F., and Dorweiler, R. P. 2012. Simulation of Wind Over a Relatively Complex Topography: Application to the Askervein Hill. *J. of the Braz. Soc. of Mech. Scl. and Eng.*, **34**, 493–500.

González, J. S., Payán, M. B., Santos, J. M. R., and González-Longatt, F. A. 2014. Review and Recent Developments in the Optimal Wind-turbine Micro-siting Problem. *Renew. Sust. Energ. Rev.*, **30**, 133–144.

Google. 2015a. *Satellite Image of the Region around the* [redacted] *Wind Park*. `https://maps.google.de`. Access: 2015-02-17.

Google. 2015b. *Satellite Image of the Region around the* [redacted] *Wind Park*. `https://maps.google.de`. Access: 2015-02-17.

Google, and DigitalGlobe. 2015. *Satellite Image of the Region around the* [redacted] *Wind Park*. `https://maps.google.de`. Access: 2015-02-17.

Gravdahl, A. R. 1998. Meso Scale Modelling with a Reynolds Averaged Navier-Stokes Solver. Assessment of Wind Resources along the Norwegian Coast. *Proceedings of the 31th IEA Experts Meeting State of the Art on Wind Resource Estimation, Risø, Denmark*.

Hurley, P. J. 1997. An Evaluation of Several Turbulence Schemes for the Prediction of Mean and Turbulent Fields in Complex Terrain. *Bound.-Layer Meteor.*, **83**, 43–73.

IEC. 2005. *International Standard IEC 61400-1:2005(E)- Wind Turbines Part1 1: Design Requirements*. Internation Electrotechnical Comisson.

Jarvis, A., Reuter, H. I., and Guevara, E. 2008. *Hole-filled seamless SRTM data V4 of the International Centre for Tropical Agriculture (CIAT)*. `http://srtm.csi.cgiar.org`. Access: 2014-12-15.

Jones, W. P., and Launder, B. E. 1972. The Prediction of Laminarization with a Two-equation Model of Turbulence. *Int. J. Heat Mass Transfer.*, **15**, 301–314.

Katic, I., Højstrup, J., and Jensen, N. O. 1986. A Simple model for cluster efficiency. *EWEC'86. Proceedings.*, **1**, 407–410.

Kim, H. G., and Patel, V. C. 2000. Test of Turbulence Models for Wind Flow over Terrain with Separation and Recirculation. *Bound.-Layer Meteor.*, **94**, 5–21.

Koller, S., and Bourgeois, S. 2011. *Windenergie-Projekt* [redacted]. *Windgutachten - aktualisierter Schlussbericht.* Bern: Meteotest.

Koller, S., Bourgeois, S., and Cattin, R. 2014. *Windgutachten für den Standort* [redacted]. *Datenanalyse und Modellierung mit Ertragsprognosen*. Bern: Meteotest.

Landberg, L., Myllerup, L., Rathmann, O., Lundtang Petersen, E., Hoffmann Jørgensen, B., Badger, J., and Gylling Mortensen, N. 2003. Wind Resource Estimation–An Overview. *Wind Energ.*, **6**, 261–271.

Launder, B. E., and Spalding, D. B. 1974. The Numerical Computation of Turbulent Flows. *Comput. Method. Appl. M.*, **3**, 269–289.

Leroy, J. 1999. *Wind Field Simulations at Askervein Hill*. Tech. rept. VECTOR AS, Tønsberg.

Maurizi, A., M., Palma J. M. L., and Castro, F. A. 1998. Numerical Simulation of the Atmospheric flow in a Mountainous Region of the North of Portugal. *J. Wind Eng. Ind. Aerodyn.*, **74-76**, 219–228.

Meteodyn. 2012. *Technical Note Meteodyn WT*. Nantes: Meteodyn.

Meteodyn. 2015. *Meteodyn WT Help Facility and On-Line Documentation*. Nantes: Meteodyn.

meteodyn.com. 2014. *Homepage of The CFD Software for Wind Resource and Production Assessment of Wind Farms in Complex Terrain of Meteodyn - Meteorology and Dynamics*. `http://meteodyn.com/en/logiciels/cfd-wind-modelling-software-meteodynwt/`. Access: 2014-10-19.

Moreno, P., Gravdahl, A., and Romero, M. 2003. Wind Flow over Complex Terrain: Application of Linear and CFD Models. *European Wind Energy Conference 2003, Madrid.*

Nieuwstadt, F. T. M., and van Dop (eds). 1982. *Atmospheric Turbulence and Air Polution Modelling*. Dordrecht: D. Reidel Publishing Company.

Palma, J. M. L. M., Castro, F. A., Ribeiro, L. F., Rodrigues, A. H., and Pinto, A. P. 2008. Linear and Nonlinear Models in Wind Resource Assessment and Wind Turbine Micro-siting in Complex terrain. *J. Wind Eng. Ind. Aerodyn.*, **96**, 2308–2326.

Politis, E. S., Prospathopoulos, J., Cabezon, D., Hansen, K. S., Chaviaropoulos, P. K., and Barthelmie, R. J. 2012. Modeling Wake Effects in Large Wind Farms in Complex Terrain: the Problem, the Methods and the Issues. *Wind Energ.*, **15**, 161–182.

Probst, O., and Cárdenas, D. 2010. State of the Art and Trends in Wind Resource Assessment. *Energies*, **3**, 1087–1141.

Quaschning, V. 2013. *Regenerative Energiesysteme: Technologie–Berechnung–Simulation*. München: Hanser Verlag.

Sanderse, B., van der Pijl, S.P., and Koren, B. 2011. Review of Computational Fluid Dynamics for Wind Turbine Wake Aerodynamics. *Wind Energ.*, **14**, 799–819.

SFSO, Swiss Federal Statistical Office. 2013. *Arealstatistik Schweiz–Nomenklatur Arealstatistik Bodennutzung (NOLU04)*. Tech. rept.

Stathopoulos, T. 2002. The Numerical Wind Tunnel for Industrial Aerodynamics: Real or Virtual for the New Millenium? *Wind Struct.*, **5**, 193–208.

Stull, Roland B. 1988. *An Introduction to Boundary Layer Meteorology*. Dordrecht: Kluwer Academic Publishers.

Sumner, J., Watters, C. S., and Masson, C. 2010. CFD in Wind Energy: The Virtual, Multiscale Wind Tunnel. *Energies*, **3**, 989–1013.

Swisstopo, Federal Office of Topography. 2005. *DHM25 das Digitale Höhenmodell der Schweiz*. Tech. rept.

Swisstopo, Federal Office of Topography. 2007. *VECTOR25 das Digitale Landschaftsmodell der Schweiz*. Tech. rept.

Taylor, P. A., and Teunissen, H. W. 1983. *Askervein '82: Report on the Sept./Oct. 1982 Experiment to Study Boundary Layer Flow over Askervein*. Tech. rept. MSRS-83-8. Meteorological Services Research Branch Atmospheric Environment Service, Ontario.

Taylor, P. A., and Teunissen, H. W. 1985. *The Askervein Hill Project: Report on the Sept./Oct. 1983 Main Field Experiment*. Technical Report MSRB-84-6. Meteorological Services Research Branch Atmospheric Environment Service, Ontario.

Troen, I. 1990. A High Resolution Spectral Model for Flow in Complex Terrain. *Ninth Symposium Turbulence Diffusion 1990, Roskilde*, 417–420.

WindSim. 2013. *WindSim Built-in Software Description*. Tønsberg: WindSim AS.

WindSim. 2014. *Homepage of the CFD Software WindSim of WindSim AS*. `https://www.windsim.com`. Access: 2014-11-19.

Wood, N. 1995. The Onset of Separation in Neutral, Turbulent Flow over Hills. *Bound.-Layer Meteor.*, **76**, 137–164.

Wyngaard, J. C. 2010. *Turbulence in the Atmosphere*. New York: Cambridge University Press.

Yakhot, V., and Orszag, S. A. 1986. Renormalization Group Analysis of Turbulence. I. Basic Theory. *SIAM J. Sci. Comput.*, **1**, 3–51.

Yakhot, V., Orszag, S.A., Thangam, S., Gatski, T.B., and Speziale, C.G. 1992. Development of Turbulence Models for Shear Flows by a Double Expansion Technique. *Phys. of Fluids A*, **4**, 1510–1520.

Yamada, T. 1983. Simulations of Nocturnal Drainage Flows by a q^2l Turbulence Closure Model. *J. Atmos. Sci.*, **40**, 91–106.

Appendix

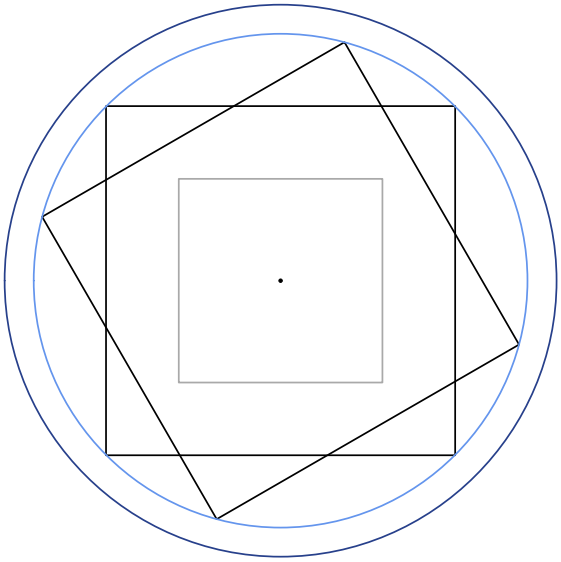

Fig. A.1: Computational domain in Meteodyn depending on the variable *radius*. Dark-blue and light-blue circles represent the extent of the input land surface roughness and topography data sets. The black rectangles give the extent of the computational mesh for two different inflow directions. The grey rectangle has the size of the maximum possible area for the output two-dimensional data sets (Meteodyn (2015); figure altered)

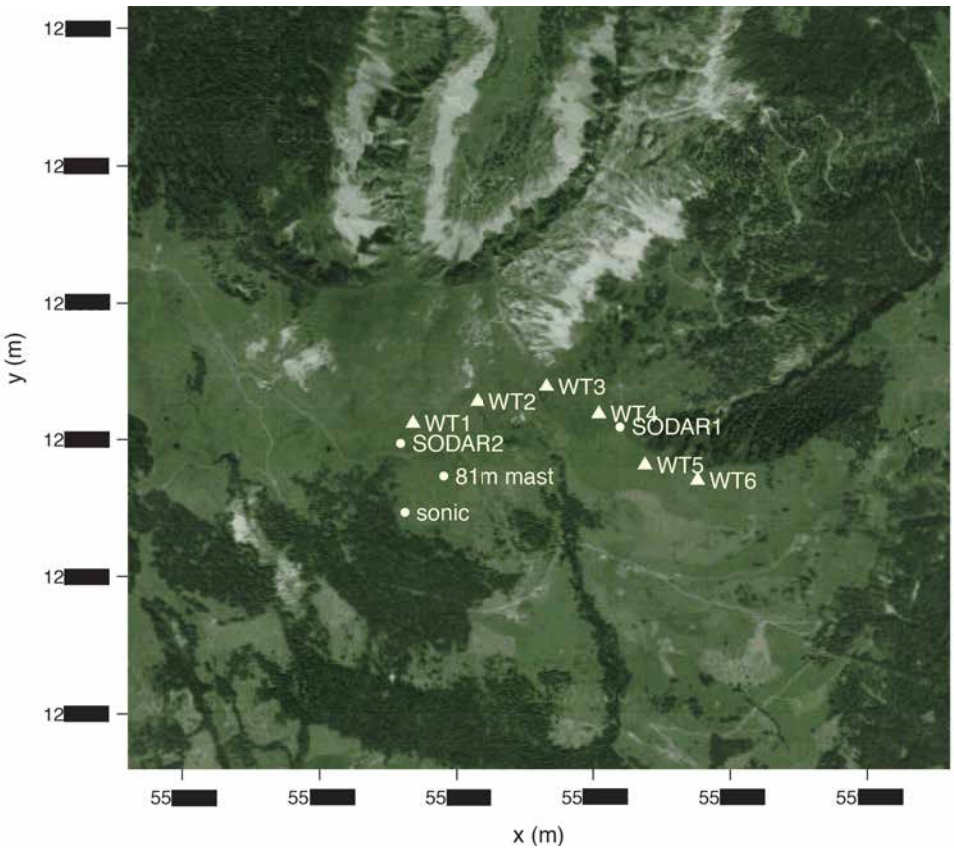

Fig. A.2: Satellite image of the refinement area of the T-Location wind park. Positions of measurement devices and wind turbines are indicated with circles and triangles, respectively (Google and DigitalGlobe, 2015).

Tab. A.1: Surface cover classes and corresponding roughness lengths in m as used in the T-Location, J-Location and S-Location simulations (EEA, 2015; SFSO, 2013).

V25 class	**CORINE class**	**description**	**roughness length (m)**
Z_Wald	25	forest	1.50
Z_SumWa	25	swamp in forest	1.50
Z_GerWa	25	boulder in forest	1.50
Z_WaldO	24	open forest	1.00
Z_SumWaO	24	swamp in open forest	1.00
Z_GerWaO	24	boulder in open forest	1.00
Z_Siedl	2	residential area	1.00
Z_StauDa	9	dam	1.00
Z_StauMa	9	massive (concrete) dam	1.00
Z_BaumS	22	tree nursery	0.50
Z_Gebue	29	shrubbery	0.50
Z_GerGeb	29	boulder with shrubbery	0.50
Z_ObstAn	16	fruit shrubbery/trees	0.50
Z_Fels	31	rock	0.20
Z_Reben	15	vineyards	0.20
Z_HaPist	6	tract with solid surface	0.10
Z_SumGeb	27	swamp and shrubbery	0.10
Z_SteBru	7	stone pit	0.05
Z_KiGrub	7	gravel pit	0.05
Z_LeGrub	7	clay pit	0.05
Z_Glet	34	glacier	0.05
Z_GerHle	34	boulder on glacier	0.05
Z_Geroel	32	boulder	0.02
Z_GsPist	18	grass tract	0.02
Z_Fluss	40	river	0.02
Z_See	41	lake	0.02
Z_Uebrig	18	remaining area	0.02

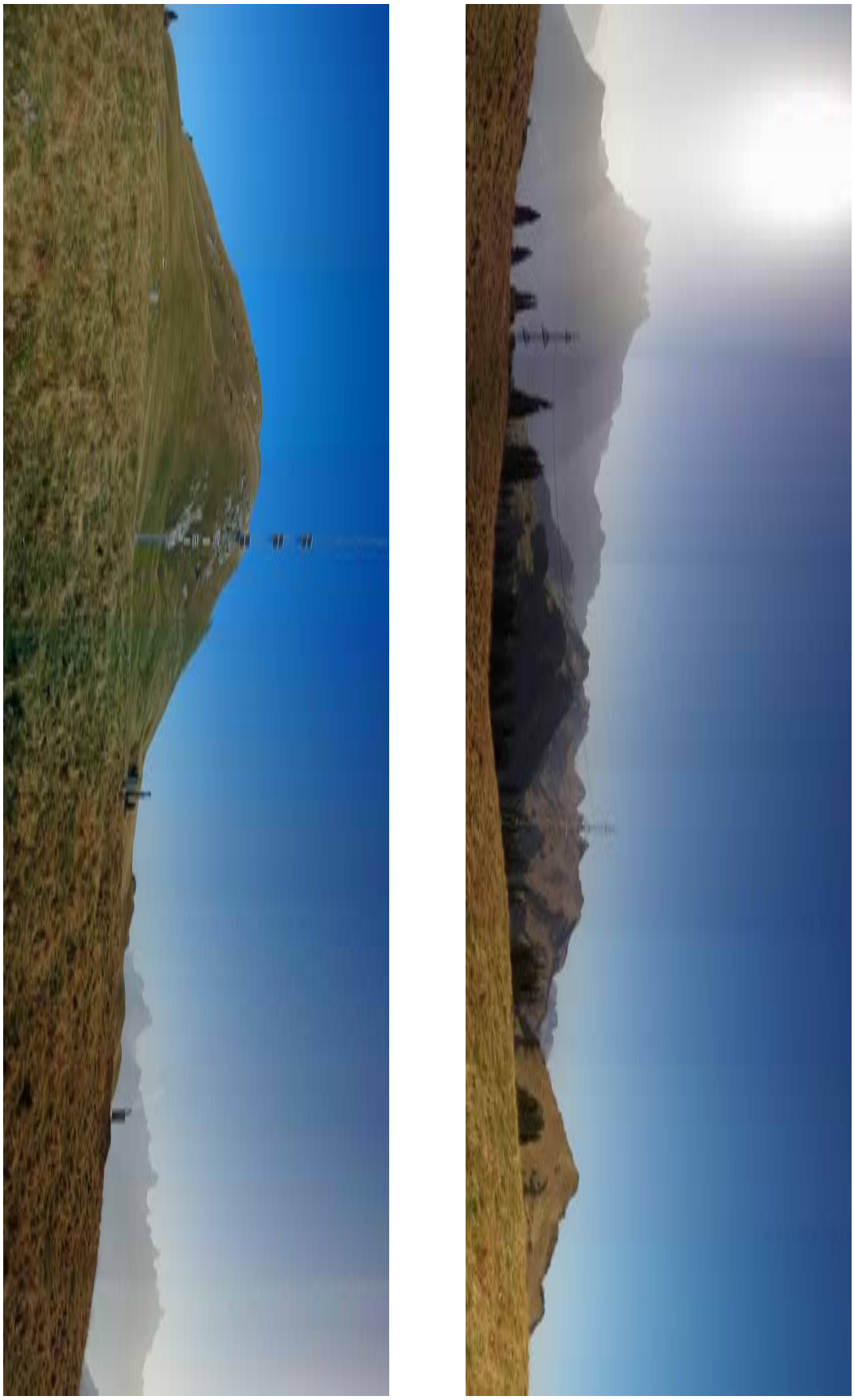

Fig. A.3: Panorama photo of the site of the planned T-Location wind park taken in northward (left) and southward direction (right) (Koller *et al.* , 2014).

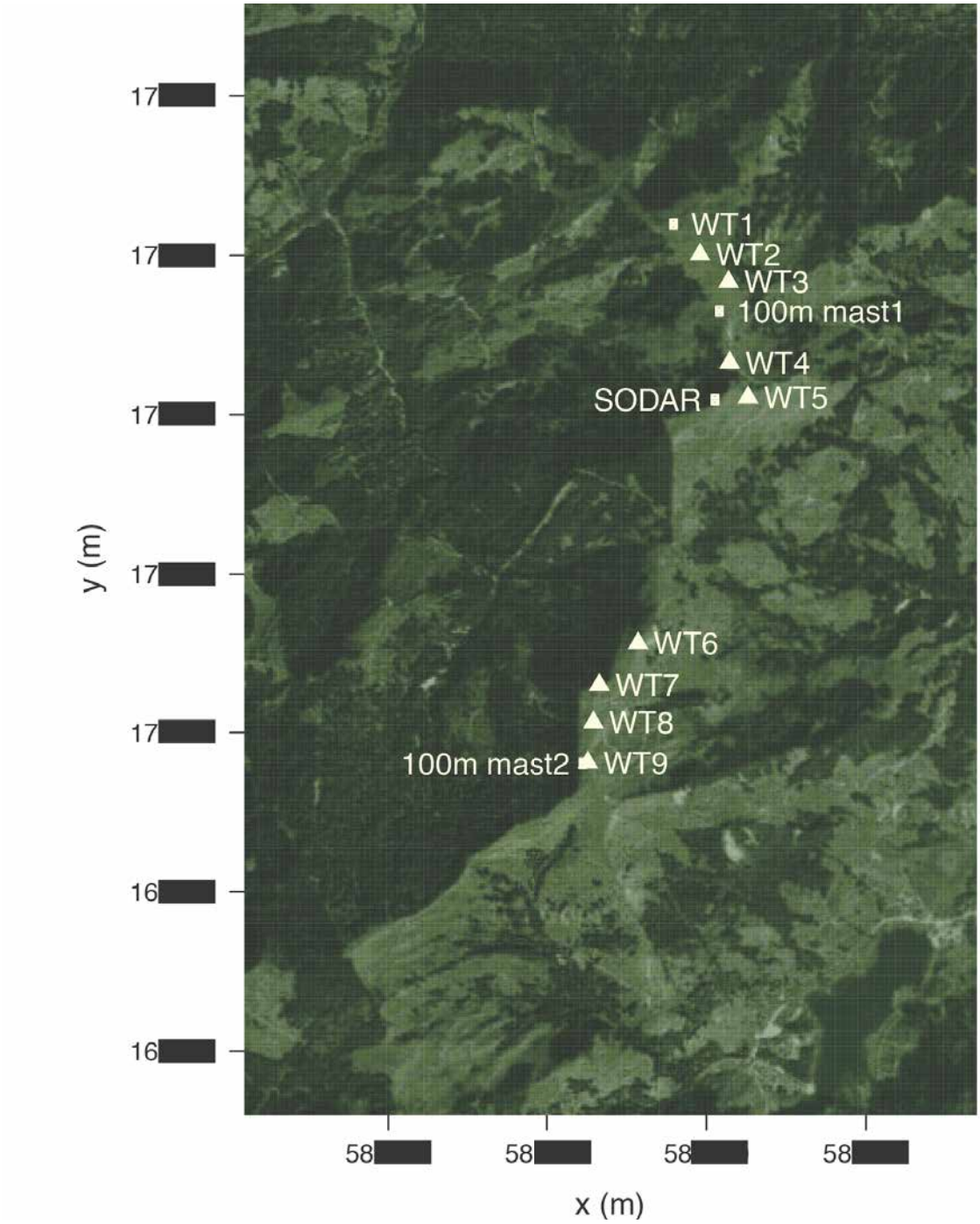

Fig. A.4: Satellite image of the refinement area of the S-Location wind park. Positions of measurement devices and wind turbines are indicated with circles and triangles, respectively (Google, 2015a).

Fig. A.5: Panorama photo of the site of the planned S-Location wind park (at position of 100m mast1) taken in eastward (left) and westward direction (right) (Dierer *et al.* , 2008).

Fig. A.6: Panorama photo of the site of the planned S-Location wind park (at position of 100m mast2) taken in eastward (left) and westward direction (right) (Dierer *et al.* , 2008).

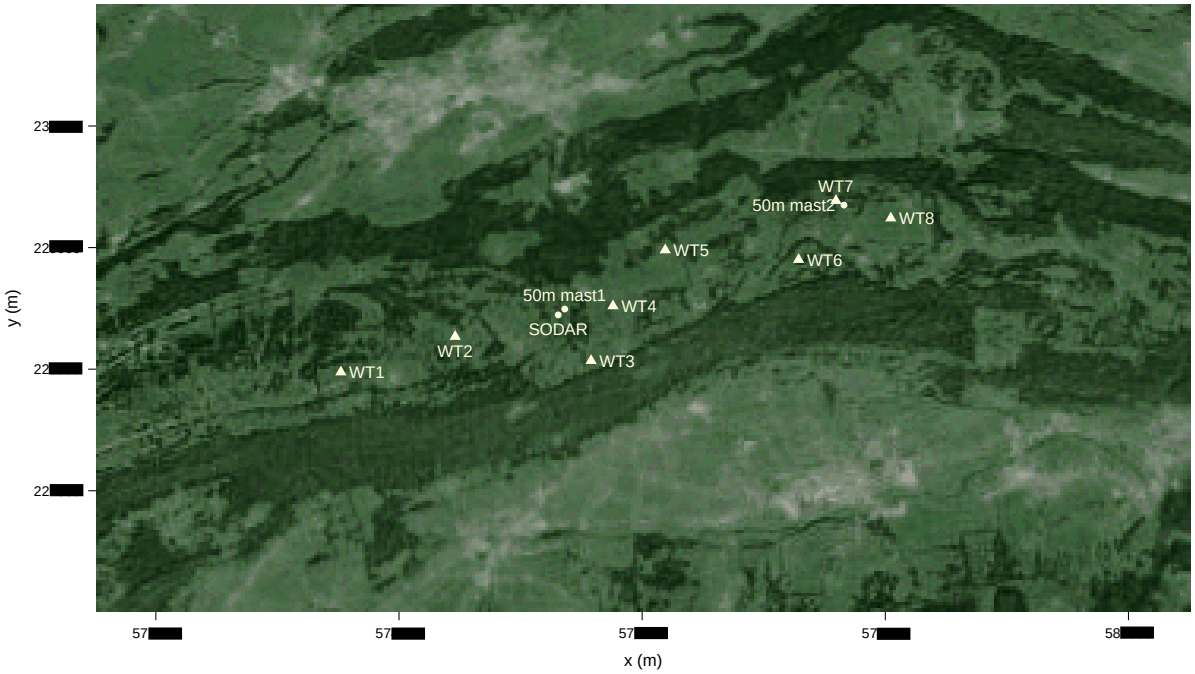

Fig. A.7: Satellite image of the refinement area of the J-Location wind park. Positions of measurement devices and wind turbines are indicated with circles and triangles, respectively (Google, 2015b).

Fig. A.8: Panorama photo of the site of the planned J-Location wind park (at position of 50m mast1) taken in eastward (left) and westward direction (right) (Koller and Bourgeois, 2011).

Fig. A.9: Panorama photo of the site of the planned J-Location wind park (at position of 50m mast2) taken in north-eastward (left) and south-eastward direction (right) (Koller and Bourgeois, 2011).

Tab. A.2: Description of the measurement devices of the 81m mast at the T-Location wind park site (Koller *et al.* (2014); table altered).

device	**parameter**	**direction of boom (°)**	**height a.g. (m)**	**heated**
Thies anemometer First Class Advanced	v	300	82	no
Vaisala WAA252	v	120	82	yes
Vector Instruments wind vane W200p	dd	0	78	yes
Thies anemometer First Class Advanced	v	300	60	no
Thies wind vane First Compact	dd	0	58	no
Thies anemometer First Class Advanced	v	300	40.25	no
Vaisala WAA252	v	120	40	yes
hygro-thermic Sensor	T_a, RH	–	10	no
air pressure sensor AB60	p	–	5	no

Tab. A.3: Description of the measurement devices of the 100m mast1 at the S-Location wind park site (Dierer *et al.* (2008); table altered).

device	**parameter**	**direction of boom (°)**	**height a.g. (m)**
Thies anemometer First class	v centre	100	
Vaisala WAA252	v	226	98.5
Thies wind vane Classic .012	dd	48	98.5
Thies anemometer First Class	v	234	86
Thies anemometer First Class	v	228	66
Thies wind vane Classic .012	dd	51	66
Galltec hygro-thermic sensor KPK1/6-ME	T_a, RH	–	48
Vaisala air pressure sensor PTB100B	p	–	5

Tab. A.4: Description of the measurement devices of the 50m mast1 at the J-Location wind park site (Koller and Bourgeois (2011); table altered).

device	**parameter**	**height a.g. (m)**
Young wind monitor	v, dd	48.1
anemometer NRG #40 Max	v	47.1
wind vane NRG 200P	dd	47.1
anemometer NRG #40 Max	v	39.5
anemometer NRG #40 Max	v	31.5
wind vane NRG 200P	dd	31.5
Rotronic hygro-thermic sensor	T_a, RH	3.0

Tab. A.5: Minimum and maximum values of the difference in v_{moy} between Meteodyn runs T1-T4 and WindSim in the refinement area of the T-Location wind park.

statistic	$\boldsymbol{v_{moy}}$ **(ms^{-1})**				$\boldsymbol{TI_{moy}}$ **(%)**			
	T1	T2	T3	T4	T1	T2	T3	T4
minimum	−1.3	−1.9	−1.9	−1.3	−26.8	−23.9	−26.6	−27.4
maximum	0.6	0.8	1.0	0.5	3.1	18.0	8.3	−2.0

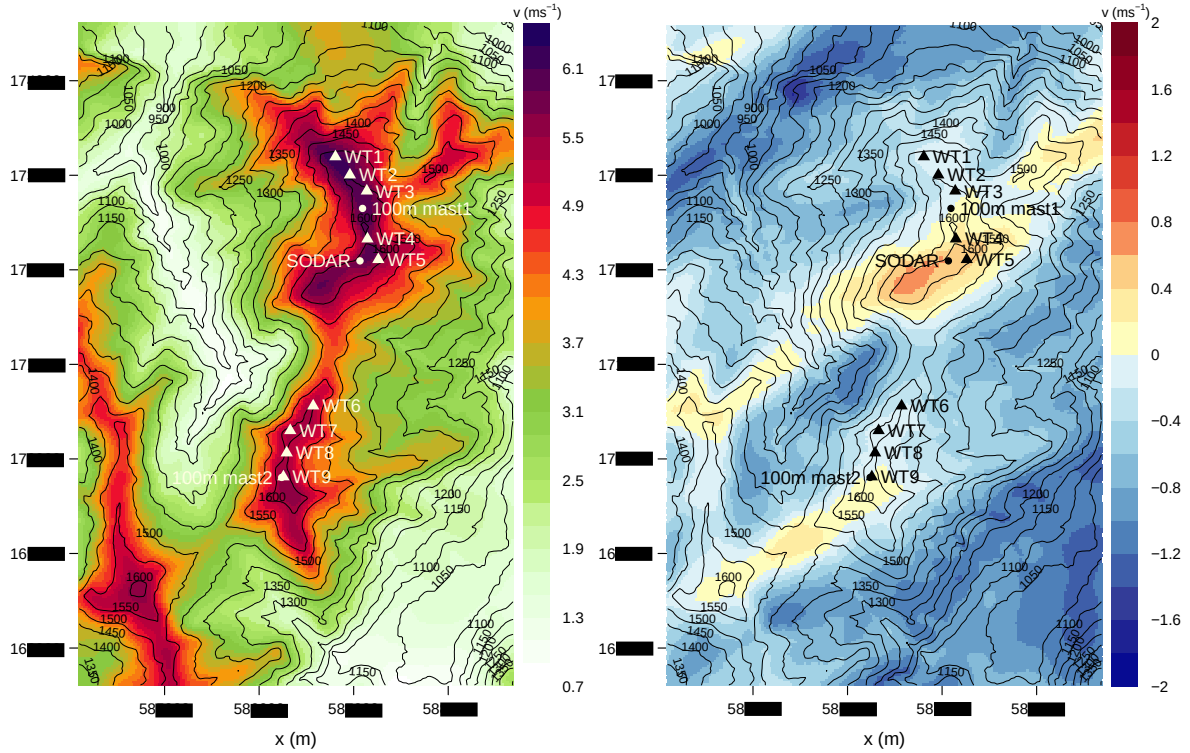

(a) Meteodyn S5 **(b)** S5–WindSim

Fig. A.10: v_{moy} of Meteodyn run S5 (a) and differences in ms^{-1} calculated as Meteodyn–WindSim in $100m$ a.g. for the refinement area of the S-Location wind park site in ms^{-1} (shaded). The triangles and circles indicate the position of the wind turbines and measuring sites, respectively. The black lines are height contour lines with an equidistance of $50m$.

Tab. A.6: Minimum and maximum values of the difference in v_{mean} between Meteodyn runs S1-S5 and WindSim in the refinement area of the S-Location wind park.

statistic	**S1**	**S2**	**S3**	**S4**	**S5**
minimum (ms^{-1})	−1.2	−1.0	−1.5	−1.6	−1.6
maximum (ms^{-1})	1.6	1.3	0.7	0.7	0.7

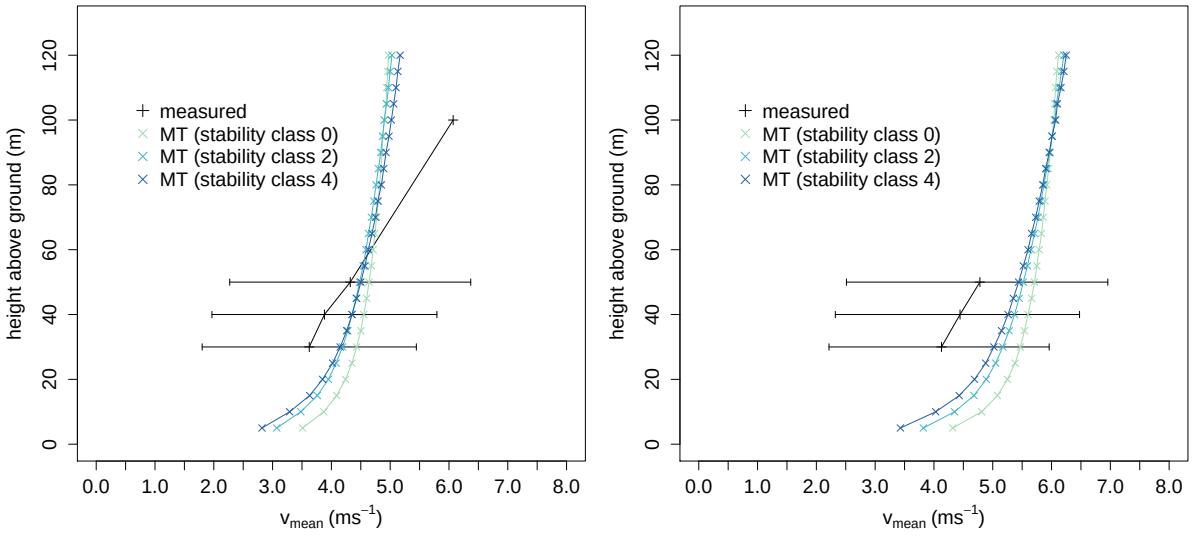

(a) 50m mast1 (J3) **(b)** 50m mast2 (J3)

Fig. A.11: Vertical wind profiles as measured (with one standard deviation whiskers) and simulated by Meteodyn run J3 at the 50m mast1 where the 50m mast2 climatology was the reference (a) and at the 50m mast2 where the 50m mast1 climatology was the reference (b).

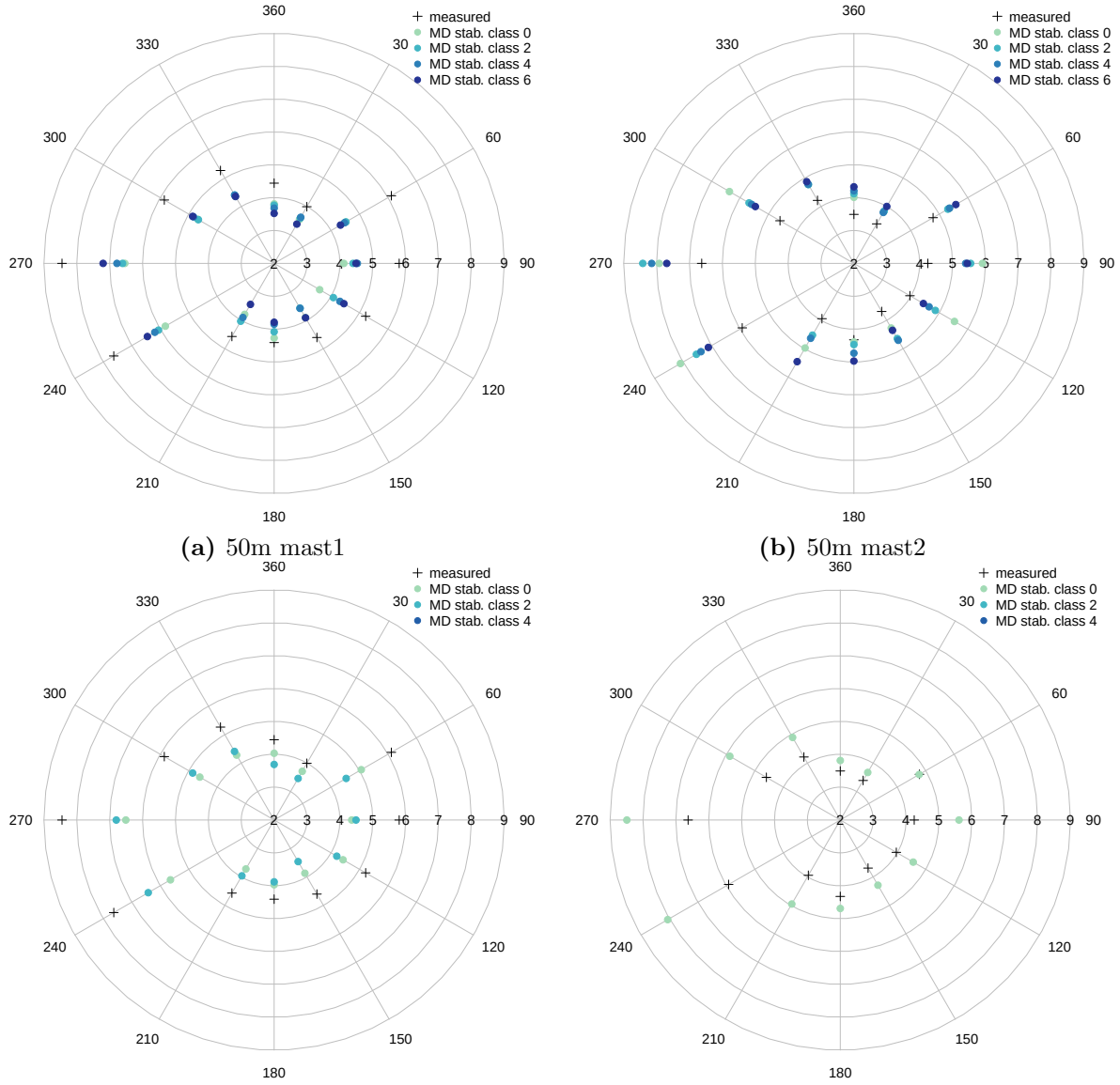

(a) 50m mast1 **(b)** 50m mast2

(c) 50m mast1 **(d)** 50m mast2

Fig. A.12: Measured and simulated (Meteodyn run J1 and J3) directional mean wind speed in $100m$ a.g. at the 50m mast1 where the 50m mast2 climatology was the reference (a, c) and in $50m$ a.g. at the 50m mast2 where the 50m mast1 climatology was the reference (b, d).

Tab. A.7: Minimum and maximum values of the difference in v_{mean} between Meteodyn runs J1–J2 and WindSim in the refinement area of the J-Location wind park.

statistic	**J1**	**J2**	**J3**
minimum (ms^{-1})	−0.7	−0.8	−0.3
maximum (ms^{-1})	1.1	1.0	1.0

Declaration

under Art. 28 Para. 2 RSL 05

Last, first name:	Daus, Regina Maria
Matriculation number:	09-054-115
Programme:	M.Sc. Climate Sciences Bachelor ☐ Master ☒ Dissertation ☐
Thesis title:	Wind Field Simulation in Complex Terrain Validation and Comparison of Two Computational Fluid Dynamics Models
Thesis supervisor:	Prof. Dr. Olivia Romppainen-Martius and Dr. Saskia Bourgeois

I hereby declare that this submission is my own work and that, to the best of my knowledge and belief, it contains no material previously published or written by another person, except where due acknowledgement has been made in the text. In accordance with academic rules and ethical conduct, I have fully cited and referenced all material and results that are not original to this work. I am well aware of the fact that, on the basis of Article 36 Paragraph 1 Letter o of the University Law of 5 September 1996, the Senate is entitled to deny the title awarded on the basis of this work if proven otherwise. I grant inspection of my thesis.

Bern, August 5, 2015

Signature